UNIVERSIDADE FEDERAL DE MINAS GERAIS

Instituto de Ciências Exatas – ICEX

Programa de Pós–Graduação em Física

TÍTULO: Traffic Model with an Absorbing Phase Transition

Mauro Lucio Lobão Iannini

Belo Horizonte

2017

Mauro Lucio Lobão Iannini

TÍTULO: Traffic Model with an Absorbing Phase Transition

Tese apresentada ao Programa de Pós-Graduação do Departamento de Física do Instituto de Ciências Exatas da Universidade Federal de Minas Gerais como requisito para obtenção do grau de Doutor em Física.

Orientador: Ronald Dickman

Belo Horizonte
2017

Agradecimentos

A minha esposa Carmen, pelas incontáveis vezes que pacientemente respeitou o tempo que precisei para desenvolver esse trabalho.

Ao meu filho Nathan, pelos preciosos momentos que desfrutamos entre os intervalos de trabalho.

Ao meu orientador Ronald Dickman que, além da imensa colaboração, acreditou no trabalho e soube pacientemente esperar pelos frutos que hoje colhemos.

À CAPES pelo apoio finaceiro a esse projeto.

"I have not failed. I've just found 10,000 ways that won't work."
"Opportunity is missed by most people because it is dressed in overalls and looks like work."

Thomas Edison

Abstract

The contribution of Nagel and Schreckenberg (NaSch) model in study of traffic models is remarkable. First of all it is the first model based on cellular automata, the update rules is quite simple but one of them has a special importance: the randomization process. This step introduces a stochastic parameter, the probability p, in the system capable of reproduce some features quite common in real traffic, e.g., the transition between free flow to jammed state. In original NaSch model the randomization process produces a lot of unusual behaviours, for instance we have the exaggerate decelerations due the addition of randomization process to the slowing down one. We propose a slight modification in randomization step that produces two kinds of driver's behaviours: The stochastic and deterministic. The first one, as an original model, the drivers can deceleration in the randomization process with probability p. The second one cannot. Despite of simplicity, this new model produces interesting results as phase transition, hystereses and absorbing state. The plane $p - \rho$ is divided in three different regions. The first one represents an absorbing state, all conductors have deterministic behaviour. The second one the state which both sort of behaviours coexists and the system never evolves to absorbing state and the third one, in which the state of a system depends on its initially configuration; some distributions can evolve to absorbing states and others cannot.

Resumo

A contribuição do modelo de Nagel e Schreckenberg (NaSch) no estudo dos modelos de tráfego é notável. Inicialmente foi o primeiro modelo baseado em autômatos celulares com regras de atualização bastante simples. Uma delas tem uma importância especial: o processo de randomização. Essa etapa introduz um parâmetro estocástico, a probabilidade p, no sistema capaz de reproduzir algumas características bastante comuns no tráfego real, por exemplo, a transição entre o fluxo livre para o estado congestionado. No modelo NaSch original, o processo de randomização produz muitos comportamentos incomuns, por exemplo, desacelerações exageradas devido à adição do processo de randomização ao processo de adaptação. Propomos uma ligeira modificação no passo de randomização que produz dois tipos de comportamentos do condutor: O estocástico e o determinístico. O primeiro, como no modelo original, os motoristas podem desacelerar no processo de randomização com probabilidade p. O segundo não está sujeito à desaceleração nessa etapa. Apesar da simplicidade, este novo modelo produz resultados interessantes como transição de fase, histerese, estado absorvente. O plano $p - \rho$ é dividido em três regioês distintas. A primeira representa um estado absorvente, todos os condutores têm comportamento determinístico. A segunda, o estado em que ambos os tipos de comportamentos coexistem e o sistema nunca evolui para estado absorvente e a terceira, na qual o estado do sistema depende da sua configuração inicial: algumas distribuições podem evoluir para estados absorventes e outras não.

List of Figures

Table of contents

Chapter 1

Traffic Models

The ideas and techniques of statistical physics are being used currently to study several aspects of complex systems many of which are different from the known domain of physical systems. Physical, chemical, earth, biological and social sciences are examples of this trend. Biological evolution of species, formation and growth of bacterial colonies, folding of proteins, flow of vehicular traffic and transactions in financial markets are just a few examples of the extent of these applications. Most of these systems are interesting not only from the point of view of Natural Sciences for fundamental understanding of how Nature works but also from the points of view of applied sciences and engineering for the potential practical use of the results of these investigations.

For a long time physicists have been trying to understand the fundamental principles governing the flow of vehicular traffic using theoretical approaches based on statistical physics. The approach of a physicist is usually quite different from that of a traffic engineer. Physicists have been trying to develop a model of traffic by incorporating only the most essential elements needed to describe the general features of typical real traffic (minimal principles). The theoretical analysis and computer simulation of these models not only provide deep insight into the properties of the model such as phase transition, metastable states, absorbing phases but also help us to understanding the complex phenomena observed in real traffic. Below we present a brief resume of the main existing class of traffic models. In traffic models different approaches have been used in order to model traffic flows using methods from physics. There are several ways to distinguish these theories, e.g., macroscopic or microscopic, deterministic or stochastic, discrete or continuous, etc. In this section we present the main approaches used in traffic study.

1.1 Hydrodynamic models

The first macroscopic description of traffic model was proposed by Lighthill and Whitham (1955). The fluid-dynamic model has its principles based on the assumption that the number of vehicles does not change, i.e., no vehicles are entering or leaving the freeway. Another feature is that the traffic is considered as a compressible fluid. The conservation of the vehicle number leads to the continuity equation:

$$\frac{\partial \rho(x,t)}{\partial t} + \frac{\partial Q(x,t)}{\partial x} = 0.$$

In this equation, we have two functions $\rho(x,t)$ and $Q(x,t)$, unless they are related to each other we need more information to solve it. An alternative possibility is to assume that

$Q(x,t)$ is determined primarily by the local density $\rho(x,t)$ so that $Q(x,t)$ can be treated as a function of only $\rho(x,t)$. Consequently, the number of unknown variables is reduced to one as, according to this assumption, the two unknowns $\rho(x,t)$ and $Q(x,t)$ are not independent of each other.

The Lighthill–Whitham–Richards theory is based on the assumption that:

$$Q(x,t) = q(\rho(x,t)), \tag{1.1}$$

where $q(\rho)$ is a function of ρ. Such a relation is known as a fundamental diagram. An additional hypothesis about $q(\rho(x,t)$ is needed for solving it, in this case a phenomenological relation extracted from empirical data or derived from more microscopic considerations should be introduced. With the hypothesis in Eq. (1.1) the x-dependence of $Q(x,t)$ arises only from the x-dependence of $\rho(x,t)$ at the same time $Q(x,t) = \rho(x,t)v(x,t)$ and the x-dependence of $v(x,t)$ arises only from the x-dependence of $\rho(x,t)$. In this way, using Eq. (1.1) the equation of continuity can be expressed as:

$$\frac{\partial \rho(x,t)}{\partial t} + \frac{dq}{d\rho}\frac{\partial \rho(x,t)}{\partial x} = 0 \tag{1.2}$$

with

$$\frac{dq}{d\rho} = v(x,t) + \rho(x,t)\frac{dv}{d\rho}.$$

The Eq. (1.2) is nonlinear because, in general, $dq/d\rho$ depends on ρ. If $dq/d\rho$ were a constant v_0, independent of ρ, Eq. (1.2) would become linear and the general solution would be of the form:

$$\rho(x,t) = f(x - v_0 t), \tag{1.3}$$

where f is an arbitrary function of its argument. Such a solution describes a density wave motion, as an initial density profile would get translated by a distance $v_0 t$ in a time interval t without any change in its shape. If we define a wave as a signal that is transferred from one part to another with a known velocity of propagation, then the solutions of the form Eq. (1.3) can be regarded as a density wave. There are several similarities between the density wave and the known mechanical waves like, e.g., acoustic or elastic waves. But the acoustic or elastic waves are solutions of linearized partial differential equations, whereas the Eq. (1.2) is nonlinear, and hence, $dq/d\rho$ is ρ-dependent. Waves of the type described by Eq. (1.2) are called kinematic waves to emphasize their purely kinematic origin, in contrast to the dynamic origin of the acoustic and elastic waves. We will present an important use of the kinematic waves in the following section.

1.2   Three phases theory

In the traffic literature there is a phenomenological description presented by Kerner [1]. In this description each state is represented by a point in the phase space defined by the flux and density coordinates. Empirically the flux is measured by the ratio between the number of vehicles passing through a fixed detector and a set time interval (minutes, hours etc.). The density on the other hand corresponds to the number of vehicles per unit of length. The use of only a fixed detector does not allow to find the density of direct form, once known the flux, the density is found by the relation:

$$\rho = \frac{q}{\overline{v}} \quad \text{with} \quad \overline{v} = \frac{1}{m} \sum_{i=1}^{m} v_i. \tag{1.4}$$

Where v_i represents the velocity of a vehicle i, $\overline{v}$ is the mean velocity and q is the flux. However, there are special cases where this formulation can fail. It should be noted that the vehicle density ρ is related to vehicles on a freeway section of a given length whereas the vehicle speed is measured at the location of the detector only and is averaged over the time interval Δt. In addition, low vehicle speeds can usually be measured to a lower accuracy than higher vehicle speeds. As a result, at higher vehicle densities (lower average vehicle speed), the vehicle density estimated via Eq. (1.4) can lead to a considerable error in comparison with the real vehicle density. For this reason, empirical data for higher vehicle densities (more than 70 vehicles/km) are not usually considered. There are also other cases why the estimation of the density via Eq. (1.4) can lead to a considerable error at higher vehicle densities. In particular, this can occur when the vehicle speed and flux are strongly spatially inhomogeneous. Thus, the averaging of the vehicle speed through Eq. (1.4) gives a temporal averaging of the speed at the detector location made during some time interval. If traffic flow is spatially inhomogeneous, this temporal averaging of the speed can give a very different average speed in comparison with a spatial averaging of the vehicles speed made at a given instant on a freeway section of a given length [1].
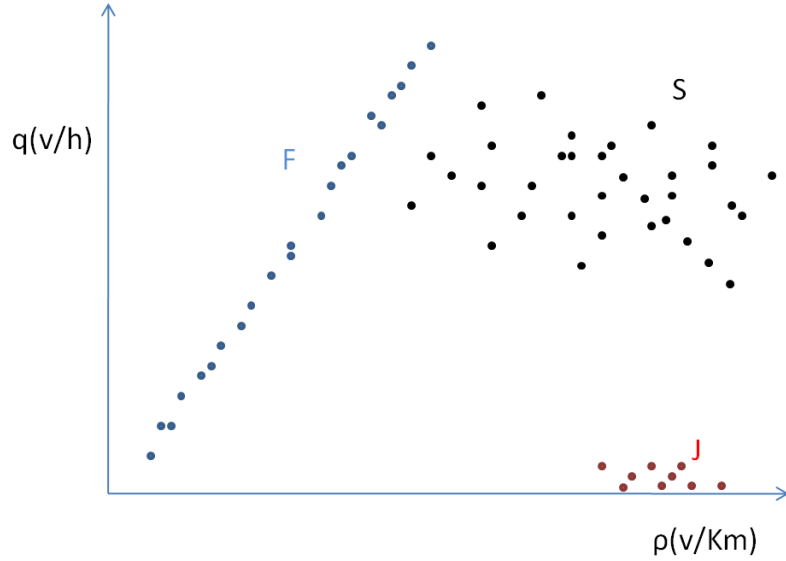
Figure 1.1: Illustrative figure representing flux as a function of density. Note the location of the three phases.

The states originated by the empirical data analysis are grouped in the $q - \rho$ plane into three distinct regions: free flow (F), synchronous flow (S) and wide moving jam (J). Free flow is characterized by weak interactions between the vehicles; the mean speed corresponds to the limit established by the freeway. The relationship between flux and density is practically linear and the slope of the line (builded by the points in the region F) corresponds to the maximum velocity. Synchronized flow is characterized by the

---

[1]For a more detailed description of the measurements made by the detector and the restrictions imposed by the use of this technique consult Kerner [1] pp. 15 to 17.

existence of interaction between the vehicles so that the average speed is lower than that of free flow. The main characteristic of this region is the apparent absence of a functional relationship between flow and density. The points are scattered irregularly over a large region of the $q - \rho$ plane. The region J, in turn, is marked by successive decelerations and accelerations (stop and go traffic) of vehicles when entering and exiting the congestion fronts. Generally the extension of this region is significant, but the main differences between it and the synchronized flow are the high concentration of vehicles and the low average speed developed (negligible flux). We can see these states in Fig. 1.1. Before studying the propagation of waves in these phases we have to introduce some basic concepts. The distance between two consecutive vehicles is $1/\rho$, the "time" distance $1/q$ and the average speed q/ρ. In the transitions between two states we will consider, in order to simplify the analysis, that the vehicles are at the same speed and equally spaced. The distance, the time interval and the vehicles speed are defined according to the state in which they are. The figure 1.2 presents three possible transitions between states. Fig.
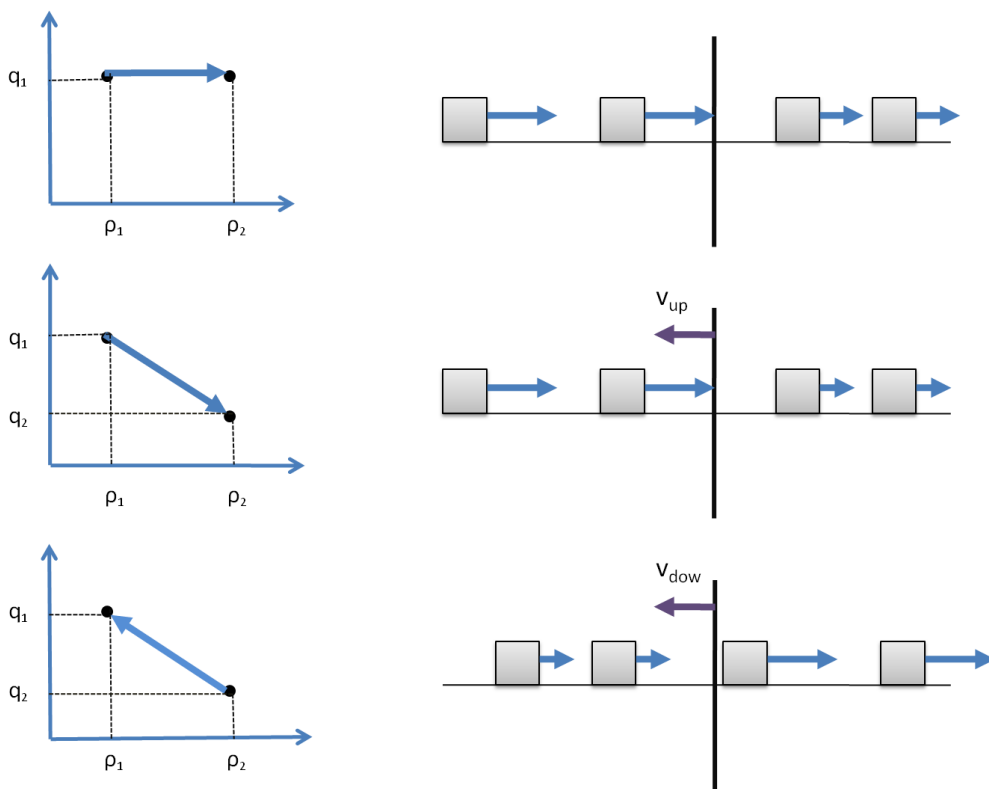
Figure 1.2: Illustrative figure representing three state transitions. The first represents a transition where the flow is preserved. In the second and third transitions the flow decreases and increases respectively.

1.2 shows the vertical lines in three different situations, each line represents the front of the shock wave[2]. When the shockwave propagation reduces the vehicles speed, we call it an *upstream front*, when increases, *downstream front*. For simplicity we will consider the acceleration (or deceleration) of vehicles instantaneously at the moment they are reached by such fronts. The first transition is characterized by keeping the flux constant, consequently the wavefront is fixed and does not move because the fluxes are equal on both sides of the front. In the second transition the vehicles depart from a state where

---

[2]We define shock waves as a sudden change of the vehicles velocity due to traffic conditions. In relation to the freeway frame, the shock wave can be at rest or in motion

the flux is greater to another where the flux is smaller. In this case the upstream front should move towards the region where the flux is higher, because on the wave front frame the input flow must be equal to the output one. In the third transition, the downstream front moves toward the region where the flux is lower.
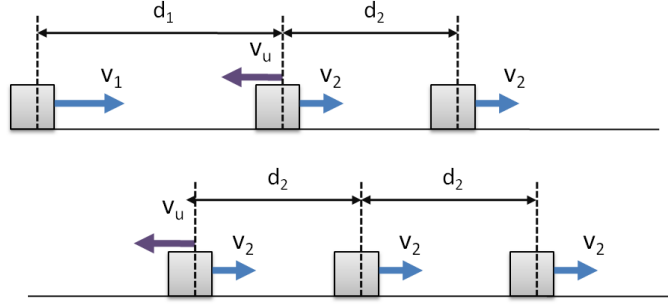
Figure 1.3: Illustrative figure represented the propagation speed of the wave.

The meaning of the slope of the line joining the two states can be understood through Fig. 1.3. In the first illustration, the wavefront is located on the second vehicle (from right to left) and moves toward the third one, located on the left of the front. After the time interval t the wavefront is on the third vehicle causing immediate slowdown from v_1 to v_2 and its distance for the second vehicle from d_1 to d_2. At this point the distances traveled by the relative motion between $[v_{up}, v_2]$ are:

$$(v_1 + v_{up})t = d_1 \quad \text{e} \quad (v_2 + v_{up})t = d_2.$$

Isolating t and remembering that $d = \frac{1}{\rho}$,

$$\rho_1(v_1 + v_{up}) = \rho_2(v_2 + v_{up}),$$

using $q = \rho v$

$$v_{up} = \frac{q_2 - q_1}{\rho_1 - \rho_2}.$$

The slope of the line joining the states represents the velocity of the wavefront. This analysis comes from wave kinematic theory. The three phases theory uses these results to study vehicle behaviour in two distinct regions of S phase.

The steady propagation of the downstream front in a wide moving jam has mean velocity v_g and can be represented in the flow-density plane by a line. This line is called "the line J". The slope of the line J is equal to the velocity v_g of this front. The left coordinates of the line J are related to the parameters of free flow (ρ_{min}, q_{out}) exhibited by vehicles that have accelerated from the standstill inside the jam. The right coordinates of the line J, $(\rho_{max}, 0)$, are related to the vehicle density inside the jam ρ_{max} where the vehicle speed v is zero. These features have further been found in empirical studies of wide moving jam propagation by Kerner and Rehborn. The velocity of the upstream fronts (1) and (2) are defined by the slope of the respective lines. Thus $v_1^{up} > v_g^{down} > v_2^{up}$ and for this reason the states located above the line J are subject to transition $S \to J$ while the states located below are not. A better explanation is given by Fig. 1.4, the arrows at the right represent the empirical downstream velocity (v_{down}) and the arrows at the left represent the upstream velocity of the states 1 (upper arrow) and 2 (bottom arrow) respectively.
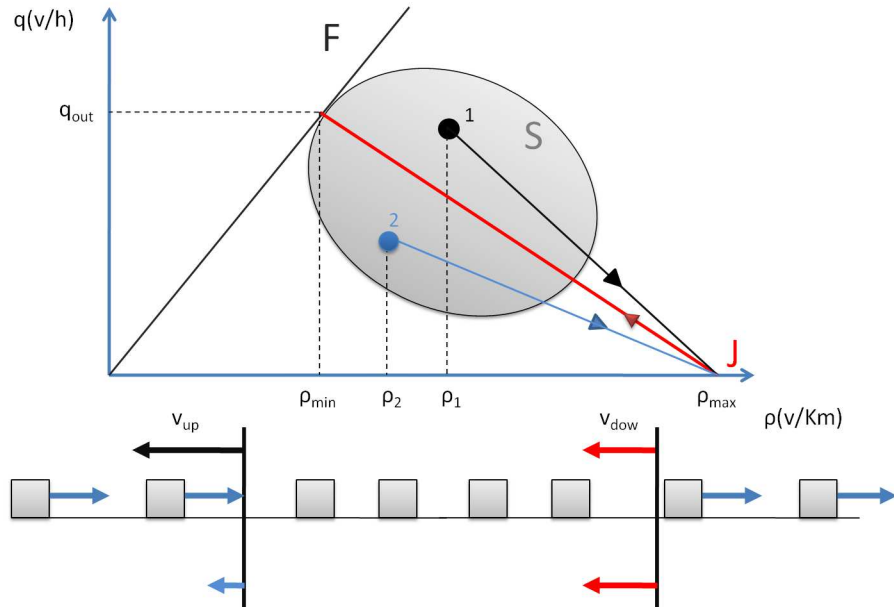
Figure 1.4: Illustrative figure represented the upstream and downstream fronts in two distinct regions of region S.

We can see that in state (1) owing to $v_1^{up} > v^{down}$ the wave responsible for jam formation is faster than the wave responsible for free flow. Thus the possible state reached by the system is in the region J. But in the state (2) the jam formation is not possible, owing to $v_2^{up} < v^{down}$ the downstream front will reach the upstream one. The complete study of the three phase theory can be found in [1] as well as the transitions between the phases and other traffic features.

1.3 Dynamical models

The dynamical model is based on the equation of motion of each vehicle. This equation has as an assumption the fact that each driver of a vehicle responds to a stimulus from other vehicles in some specific way. The response is expressed in terms of acceleration, which is the only direct controllable quantity for a driver. Generally, the stimulus and the sensitivity may be a function of the positions of vehicles, their time derivatives, and so on. This function is decided by supposing that the drivers of vehicles obey postulated traffic regulations at all times in order to avoid accidents. In the dynamical model we have two kinds of stimulus: in the earliest dynamical models the difference in the velocities of the n-th and $(n+1)$-th vehicles was assumed to be the stimulus for the n-th vehicle. In other words, it was assumed that every driver tends to move with the same speed as that of the corresponding leading vehicle so that

$$\ddot{x}_n = \frac{1}{\tau}\big[\dot{x}_{n+1}(t) - \dot{x}_n(t)\big],$$

where $1/\tau$ is related with the driver's sensitivity. Other dynamical models take into account the driver's own velocity and the distance to the vehicle ahead. All drivers have the common sensitivities and the length of vehicle is negligible. We assume that each

vehicle has legal velocity V [3] and that each driver of a vehicle responds to a stimulus from the vehicle ahead of him. The drivers can control the acceleration in such a way that they can maintain the legal safe velocity according to the motion of the preceding vehicle. Then the dynamical equation of the system is obtained via:

$$\ddot{x}_n = a\big[V(\Delta x_n) - \dot{x}_n\big], \qquad (1.5)$$

where

$$\Delta x_n = x_{n+1} - x_n,$$

for each vehicle number n $(n = 1, 2, ..., N)$. N is the total number of vehicles, a is a constant representing the driver's sensitivity (which has been assumed to be independent of n), and x is the coordinate of the nth vehicle. The dots denote differentiation with respect to time t. We assume here that the legal velocity $V(\Delta x)$ of vehicle number n depends on the following distance of the preceding vehicle number $n + 1$. When the headway becomes short the velocity must be reduced and becomes small enough to prevent crashing into the preceding vehicle. On the other hand, when the headway becomes longer the vehicle can move with higher velocity, although it does not exceed the maximum velocity. Thus, V is a function having the following properties: a monotonically increasing function, and $V(\Delta x)$ has an upper bound $V_{max} \equiv V(\Delta x \to \infty)$. Further, this model has periodic boundary conditions: vehicles move on a circuit with length L and the $(N+1)$th vehicle is identical to the first vehicle. Depending on choice of V and the headway Δx, the system can be stable or unstable.

In Fig. 1.5 the trajectories of a specific vehicle (the 50th vehicle) are shown in two different cases: the stable and unstable trajectories. In the stable case, the vehicle moves with constant velocity, i.e., the distance increases linearly. On the other hand, in the unstable case we observe a vehicle moving backward $(v < 0)$. This always happens whenever the solution of this model is in the unstable region. As long as we take the models of a single lane, this means a collision of two successive vehicles. The above behavior indicates that, instead of congestion, such traffic accidents occur everywhere. Then, by choosing an appropriate legal velocity function, we can modify the model so that a vehicle never moves backward. In [2] another function is proposed with intention of preventing it. In addition to the models presented in this section we have to take into account kinetic models. In such models traffic is treated as a gas of interacting particles where each particle represents a vehicle. The different versions of the kinetic theory of vehicular traffic have been developed by modifying the kinetic theory of gases. Due to the extensive study in this kind of model, we published an article entitled "Kinetic theory of vehicular traffic", in which we present the key features in the chapter 4.

---

[3]the term "legal velocity" was introduced in [2], although we think that the term "safety or desirable velocity" is more appropriate
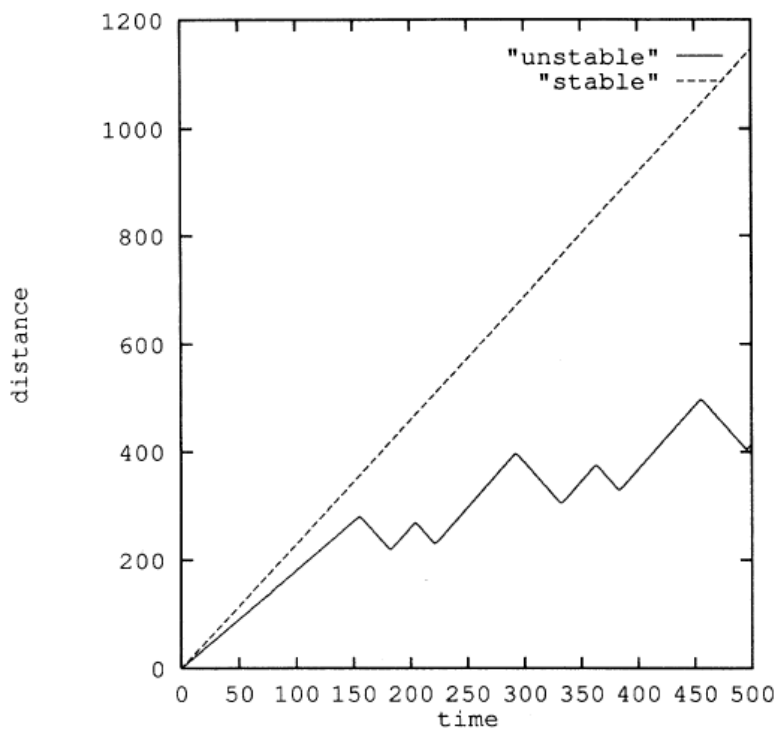
Figure 1.5: Trajectories of a vehicle (the 50th vehicle) in two typical cases. The stable case defined by $L = 200$ and $N = 100$ (dotted line) and the unstable case defined by $L = 50$ and $N = 100$ (solid line).

Chapter 2

NaSch Model

2.1 Model

The NaSch model(NS) was the first traffic model based on a cellular automaton [3]. The model is defined on a one-dimensional lattice of length L, with periodic boundaries, representing a single-lane freeway. Each site of the lattice can be in one of the $v_{max} + 2$ states: It may be empty, or it may be occupied by one car having an integer velocity between zero and v_{max}. Time, space, and velocity are discretized. The process starts with an initial distribution of N vehicles ($N \leq L$). The state of system is updated at each iteration according to the following steps: Acceleration, deceleration, randomization and displacement. Each iteration, between two consecutive times (t and $t + 1$) consists of 4 steps according to the NS update rules: (t_1, t_2, t_3 and $t + 1$). Note that the three initial steps do not represent vehicle movement but only intermediate steps required for defining the final speed just before the displacement step. The update rules are:

1. **Acceleration**
   The velocity of each vehicle with $v < v_{max}$ is increased by one unit. If a vehicle already possesses the maximum velocity before this step, its velocity remains unchanged.
   $$v_j(t_1) = \min[v_j(t) + 1, v_{max}].$$
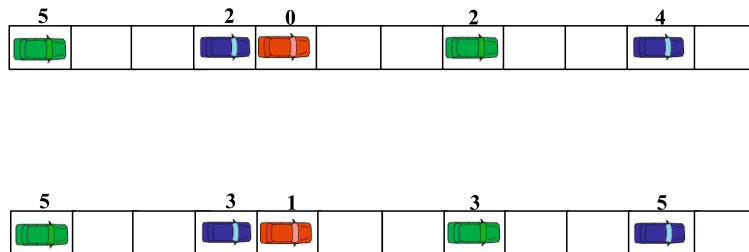
Figure 2.1: An example of acceleration step. The figure shows the vehicles configuration before (upper) and after (lower) the acceleration step. Note that the vehicles accelerate independent of the possibility of displacing with the new velocity.

2. **Slowing Down**
   All vehicles with $v_j(t_1) > d_j$ reduce their speed to $v_j(t_2) = d_j$. Here, d_j is defined as a number of empty cells between the car j and $j+1$. Thus

$$v_j(t_2) = \min[d_j(t), v_j(t_1)].$$
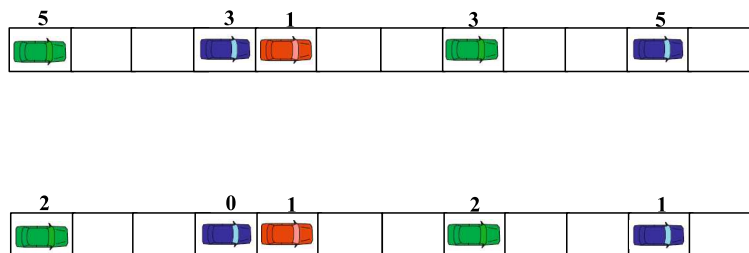
Figure 2.2: An example of slowing down step. The figure shows the vehicles configuration before (upper) and after (lower) the slowing down step. Now the vehicles can adjust their velocities according to the distance (headway) in relation to the forward vehicle.

3. **Randomization**
   This step introduces stochasticity in the model; without it the model would be deterministic and the stationary state reached quickly. In this step each vehicle reduces its speed by one unit with probability p or maintains it with probability $1 - p$. Vehicles with $v = 0$ are not subject to this step.

$$
\begin{aligned}
v_j(t_3) &= \max[v_j(t_2) - 1, 0], \quad \text{with probability } p \\
v_j(t_3) &= v_j(t_2), \qquad\qquad\quad\; \text{with probability } 1 - p.
\end{aligned}
$$
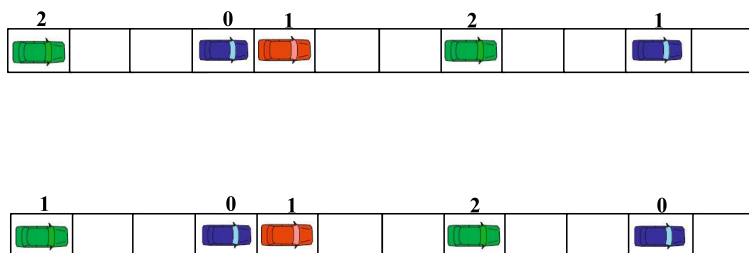
Figure 2.3: An example of randomization step. The figure shows the vehicles configuration before (upper) and after (lower) the randomization step. This step introduces substantially modification in macroscopical traffic behaviour due the introduction of individual behaviour (controlled by parameter p). In some cases drivers decelerated (at random), in others do not.

4. **Displacement**

This step represents the displacement of the vehicles according to the velocity previously established.

$$v_j(t+1) = v_j(t_3).$$
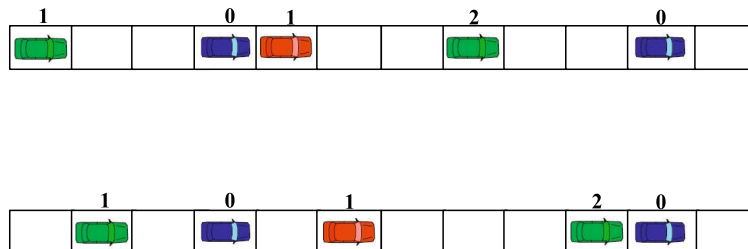
Figure 2.4: An example of displacement. The figure shows the vehicles configuration before (upper) and after (lower) the displacement step. This step represents the final step in which the vehicles displace according to the velocity defined in the previous step.

The randomization step is an essential component for the reproduction of the main features presented in real traffic, e.g., the transition between free flow to jammed state, start-and-stop waves, and shocks (due to driver overreaction). This step in the model can be compared with the unpredictable reaction of the drivers in front of traffic conditions though in the NS model the probability p is independent of the traffic conditions, e.g., the density of vehicles on the lattice.

In Fig. 2.5 we present the graph flux as a function of density (also known as the fundamental diagram) for $p = 0.1$, 0.5 and 0.9. We observe the presence of two branches; the first one corresponds to the free flow regime where the vehicles almost do not interact themselves due to the large distances between them. In this condition the second step in the NS update rules practically does not apply. Let us set $v_{max} = 5$ and the states

$$|0\rangle = \begin{pmatrix} 1 \\ 0 \\ 0 \\ 0 \\ 0 \\ 0 \end{pmatrix} \quad \text{............} \quad |5\rangle = \begin{pmatrix} 0 \\ 0 \\ 0 \\ 0 \\ 0 \\ 1 \end{pmatrix},$$

for velocities (the value in the line n corresponds to the probability of finding a vehicle with velocity $n - 1$). The stochastic matrix for a single vehicle is:

$$T = \begin{pmatrix} p & 0 & 0 & 0 & 0 & 0 \\ 1-p & p & 0 & 0 & 0 & 0 \\ 0 & 1-p & p & 0 & 0 & 0 \\ 0 & 0 & 1-p & p & 0 & 0 \\ 0 & 0 & 0 & 1-p & p & p \\ 0 & 0 & 0 & 0 & 1-p & 1-p \end{pmatrix}.$$

Let P_t be the probability distribution of velocities at the time t. The relation between P(t) and P(t-1) is given by:

$$P_t = TP_{t-1}.$$

Given the P_0, P_t can be found via:

$$P_t = T^t P_0.$$

After a little algebraic work (for further details, see chapter 7), we have:

$$\lim_{t \to \infty} P_t = \begin{pmatrix} 0 \\ 0 \\ 0 \\ 0 \\ p \\ 1-p \end{pmatrix}.$$

After the vehicle attains the stationary state, the mean velocity is:

$$\overline{v} = p(v_{max} - 1) + (1-p)v_{max} \qquad \therefore \qquad \overline{v} = v_{max} - p,$$

and the flux q is

$$q = \rho(v_{max} - p). \tag{2.1}$$

This analysis cannot be used for higher densities since it does not take into account the interactions between the vehicles. When we consider these interactions the problem cannot be solved in this way. We will see in section 2.3 a first analytic approach (mean-field theory) to this problem. Although the equation (2.1) cannot be used for higher densities, it explains the slight difference between the slopes in the first branch according to the probability p. The second branch corresponds to jammed state in which the interactions between the vehicles are more frequent. In this regime the presence of start-and-stop waves and driver overreaction is common. The overreaction can be explained due to overlap of two successive decelerations; the first one due to the second step in the NS update rules, the vehicles reduce their velocities due the small distance between them. The second one is related to the randomization step, with probability p the vehicle may reduce, in addition to the first deceleration, its velocity by one more unit.

In the NS model two special values ($p = 0$ and $p = 1$) produce deterministic behaviour in the system. In both cases the randomization step does not apply (in the first case the vehicles never reduce their velocity while in second one, always reduce). For $p = 0$ and $\rho \leq \rho_c{}^1$ ($\rho_c = 1/(v_{max} + 1)$) the system always evolves to absorbing state in which all vehicles attain the maximum velocity while for $\rho > \rho_c$ the system evolves to a stationary state with $\overline{v} = (1 - \rho)/\rho$. For $p = 1$ and $\rho \leq 1/3$ few initial states can evolve to a stationary state with $\overline{v} \neq 0$ since if a vehicle stops it never moves again. For $\rho > 1/3$ the system, in a certain moment, attains the absorbing state with $\overline{v} = 0$.

---

[1]For the deterministic case, ρ_c is the critical density
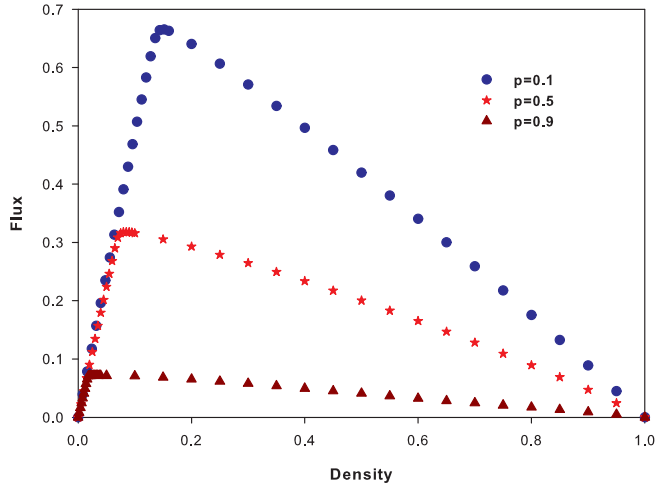
Figure 2.5: Fundamental diagram using Monte Carlo simulation for probabilities $p = 0.1$, 0.5, and 0.9.

2.2 Scaling behaviour

In this section we will study the phase transition in the NS model. A special case in the Ns model arises when $p = 0$. In addition to its deterministic behaviour we can assert that there is a continuous phase transition at the point ρ_c. In the following subsections we discuss some quantities that support this assertion.

2.2.1 Singularity

In Fig. 2.6 the fundamental diagram, for $p = 0$, exhibits a sharp change at ρ_c; this singularity is characterized by a discontinuity in the first derivative. For $p \neq 0$ this change is smooth, as can be seen in Fig. 2.5.
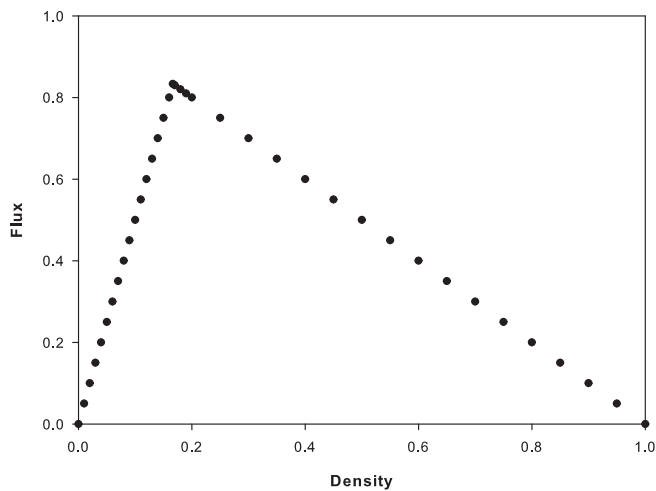
Figure 2.6: Fundamental diagram for $p = 0$.

With the intention to study in more details the criticality in this case we should

look for an appropriate order parameter to describe the singularity shown in Fig. 2.6. The natural candidate is the fraction of jammed vehicles, e.g., vehicles with velocities smaller than v_{max}. Unfortunately in the deterministic model this fraction and any related quantities depend on the initial spatial distribution. So we propose an order parameter M defined by:

$$M = 1 - \frac{q}{\rho v_{max}}.$$

For $p = 0$ and $\rho > \rho_c$,

$$\overline{v} = \frac{1 - \rho}{\rho}.$$

Remembering that $q = \rho \overline{v}$, we have

$$q = 1 - \rho \ \ \mathbf{and} \ \ v_{max} + 1 = \frac{1}{\rho_c},$$

so that M is given by

$$M = \begin{cases} 0 & (\rho \leq \rho_c) \\ \frac{1}{v_{max}} \frac{\rho - \rho_c}{\rho \rho_c} & (\rho > \rho_c). \end{cases}$$

For $p = 0$ the graph M as a function of ρ is shown in Fig. 2.7.
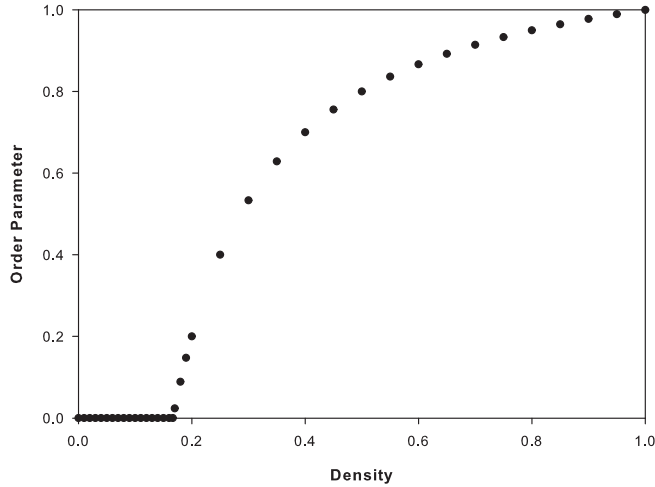
Figure 2.7: Order parameter for $p = 0$. Note the singularity at $\rho = \rho_c$.

2.2.2 Density of nearest-neighbor pairs

The density of nearest-neighbor pairs is given by:

$$m = \frac{1}{L} \sum_{i=1}^{L} n_i n_{i+1},$$

with $n_i = 0$ for an empty cell and $n_i = 1$ for a cell occupied by a car (irrespective of its velocity). In the case $p = 0$, below the critical density ρ_c this order parameter vanishes since every car has, at least, v_{max} empty sites in front and propagates with $v = v_{max}$. In Fig. 2.8 a sharp transition occurs at $\rho_c = \frac{1}{v_{max}+1}$. For densities below this point m
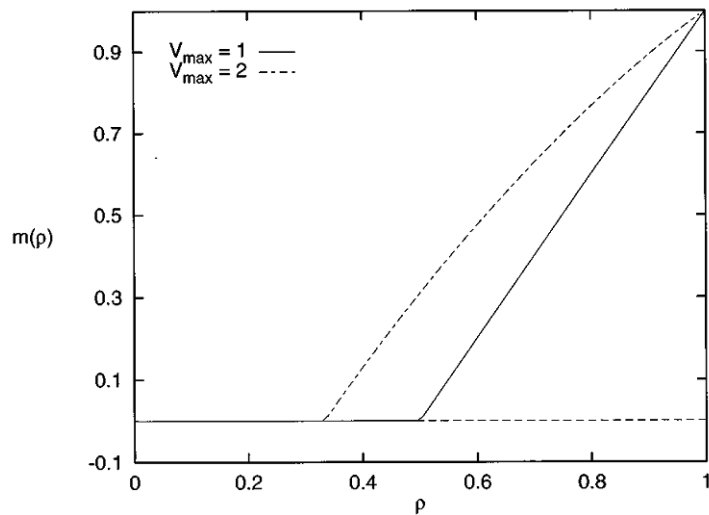
Figure 2.8: Figure extracted from Ref. [4], p. 1311: order parameter as a function of density for $p = 0$. Below the density $\rho_c = \frac{1}{v_{max}+1}$ m vanishes exactly.

vanishes exactly.

The Fig. 2.9 shows that the order parameter does not exhibit a sharp transition for $p > 0$. Although m becomes rather small for small densities it is always different from zero. This situation is quite similar to the behaviour of order parameter in finite systems and there is no phase transition for $p > 0$.
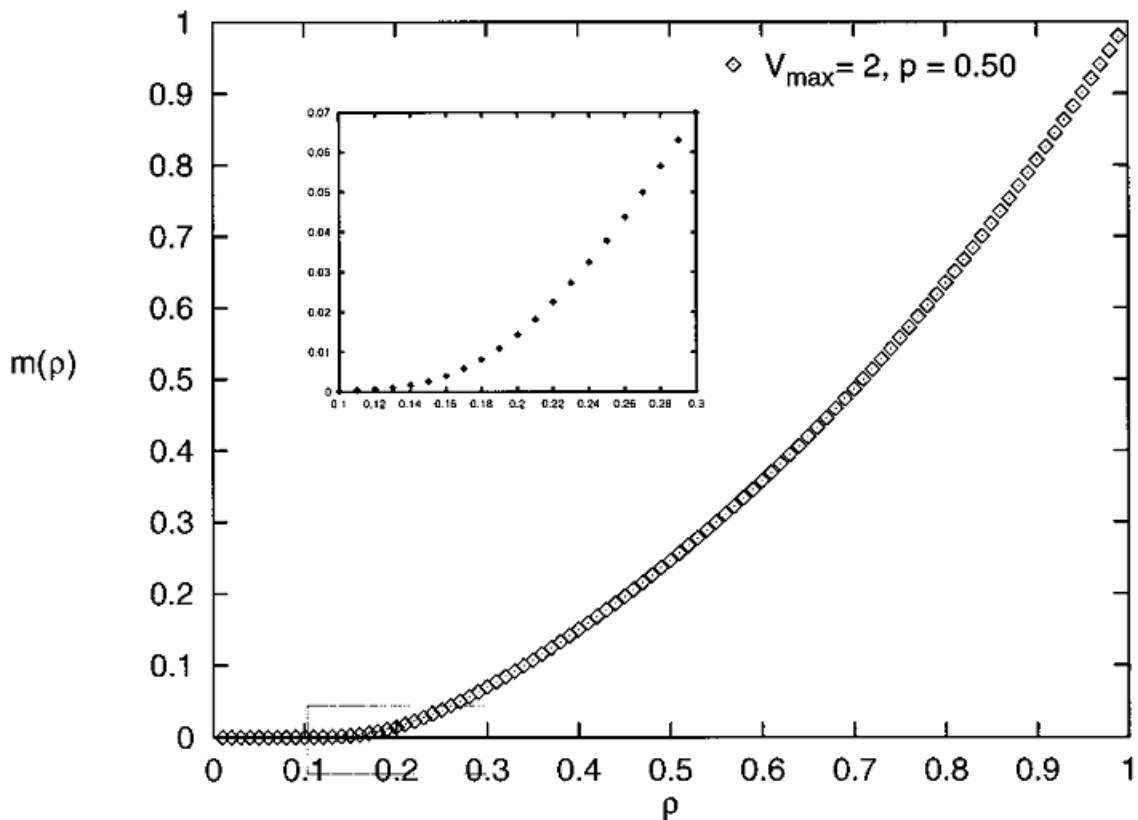
Figure 2.9: Figure extracted from Ref. [4], p. 1311: order parameter as a function of density for $p > 0$. It does not vanish exactly for $\rho < \rho_c$, but converges smoothly to zero even for small values of the probability.

2.2.3 Spatial Correlations

A key feature of continuous phase transition is a diverging correlation length at criticality and a corresponding algebraic decay of the correlation function. Using lattice gas variables the density-density correlation function is given by

$$G(r) = \frac{1}{L} \sum_{i=1}^{L} n_i n_{i+r} - \rho^2.$$

Considering the deterministic case ($p = 0$) in the vicinity of the transition density one observes a decay of the amplitude of $|G(r)|$ for larger values of the distance between the sites as shown in Fig. 2.10. Precisely at ρ_c the correlation function is given by

$$G(r) = \begin{cases} \rho_c - \rho_c^2 & r = 0, \ v_{max} + 1 \ ... \ n(v_{max} + 1) \\ -\rho_c^2 & \text{otherwise.} \end{cases}$$

At the transition point the system attains the absorbing state with the only possible state: all vehicles have $v = v_{max}$ and there are exactly v_{max} empty cells in front each vehicle. Considering small, but finite, values of p the correlation function has the same structure as in the deterministic case, but the amplitude, rather than decaying algebraically, decays exponentially for all values of ρ.

The decay of the amplitude determines the correlation length for a given pair of (p, ρ), which is finite for all densities with $p > 0$. The maximal value of the correlation length ξ_{max} determines the transition density. As shown in the Fig. 4.7, the maxima value of the correlation length, as a function of p, diverges at $p \to 0$.

2.2.4 Relaxation time

An expected feature of a second order transition is the divergence of the relaxation time at the transition point. In this work we use two distinct but related definitions of the relaxation time. The first, used in the literature [5] is relaxation time and the second one is called stationary time. One will see that both diverge at the transition point. The relaxation time is defined based on the expected behaviour of the system according to the function $v \propto e^{-t/\tau}$:

$$\tau = \int_0^\infty [\min(v^*(t), < \overline{v_\infty} >) - < \overline{v(t)} >] dt. \tag{2.2}$$

v, t and τ are dimensionless. $v^*(t)$ denotes the average velocity in the acceleration phase $t \to 0$ for low vehicle density $\rho \to 0$. Because the vehicles do not interact with each other, $v^*(t) = (1 - p)t$ holds in this regime. So the relaxation time is obtained by summing up the deviations of the average velocity $< \overline{v_\infty} >$ from the values of a system with one single vehicle that can move without interactions with other cars $\rho \to 0$. One finds a maximum of the relaxation, for the case $p = 0$, at the density of maximum flux. The criterion for criticality is power-law dependence of τ and σ on system size according to:

$$\tau_m(L) \propto L^z, \quad \sigma(L) \propto L^{\frac{-1}{\nu}}.$$

$\tau_m(L)$ is the maximum value of $\tau(\rho)$ in a ring of size L and $\sigma(L)$ is the width in the middle of the curve as a function of size L. We can see the dependence of these quantities on
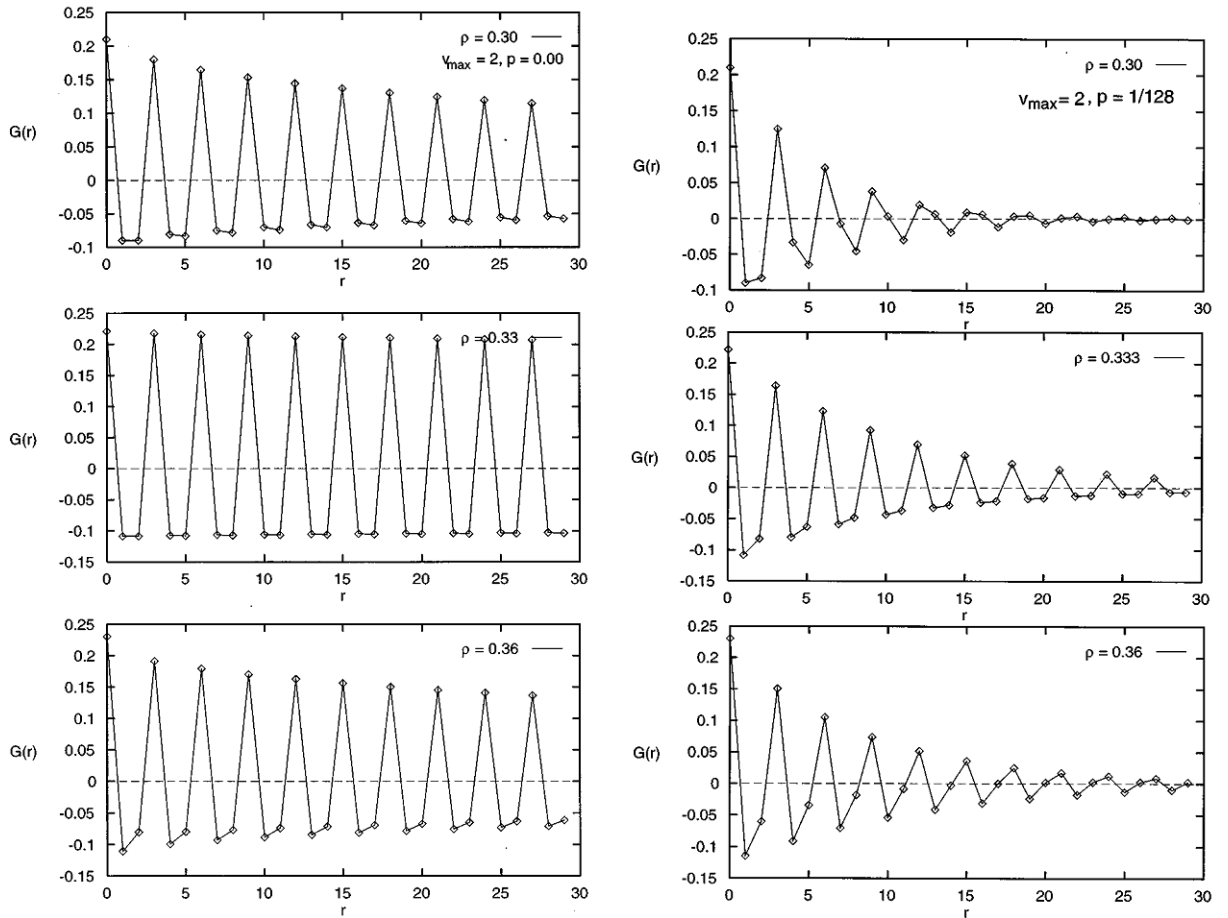
Figure 2.10: Figure extracted from Ref. [4], p. 1311 and 1312. (Left) Correlation function in the vicinity of the phase transition for the deterministic limit. At $\rho = \rho_c$ the amplitude is independent of the distance r. In the vicinity of ρ_c the correlation function decays algebraically. (Right) Correlation function for $p > 0$. The amplitude of the correlation function decays exponentially for all values of ρ.

systems of size L in Fig. 2.12. For the deterministic case the exponents are $z = 0.53 \pm 0.04$ and $v = 2.01 \pm 0.05$ [4].

As we can see in Fig. 2.13, for $p \neq 0$ neither quantities $\tau_m(L)$ and $\sigma(L)$ have the same behaviour of the determinist case. In our work we define a quantity related to the relaxation time which we call the stationary time. This is the time that a system starting from a random initial distribution with $v = 0$ takes to attain the mean velocity of the stationary state. In the stationary state, the mean velocity of the system at a certain time fluctuates around its mean (taken during a meaningful interval of time), but in the limit of big sizes this fluctuation amplitude tends to zero. So we define the stationary time the time that the system reaches, for the first time, the expected mean velocity of the stationary state. For an improved estimate we take the mean stationary time over a sample of 200 independent realizations, each with a different initial condition.

For $p = 0$ the stationary state is well-defined and the mean velocity is:

$$\overline{v} = \begin{cases} v_{max} & (\rho \leq \rho_c) \\ \frac{1-\rho}{\rho} & (\rho > \rho_c). \end{cases} \tag{2.3}$$

In Fig. 2.14 the stationary time clearly diverges at ρ_c. A qualitative explanation can help us to clarify this behaviour: at small densities, the vehicles have large spaces
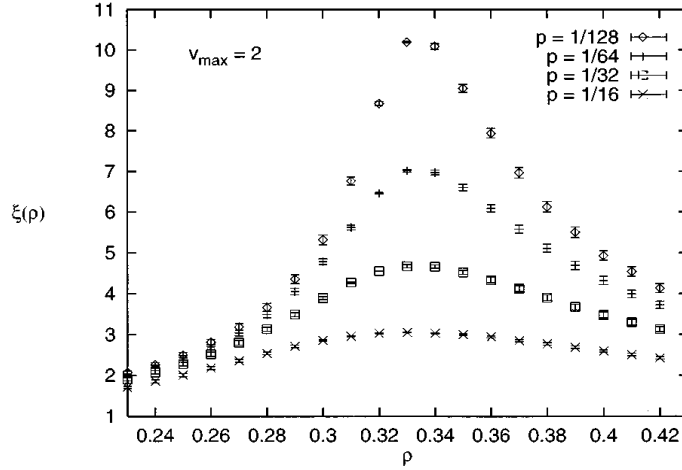
Figure 2.11: Figure extracted from Ref. [4], p. 1313: correlation length versus density for several p values. Note that, at the critical point $\rho_c = 1/3$, the maximal value of the correlation length diverges for $p \to 0$.
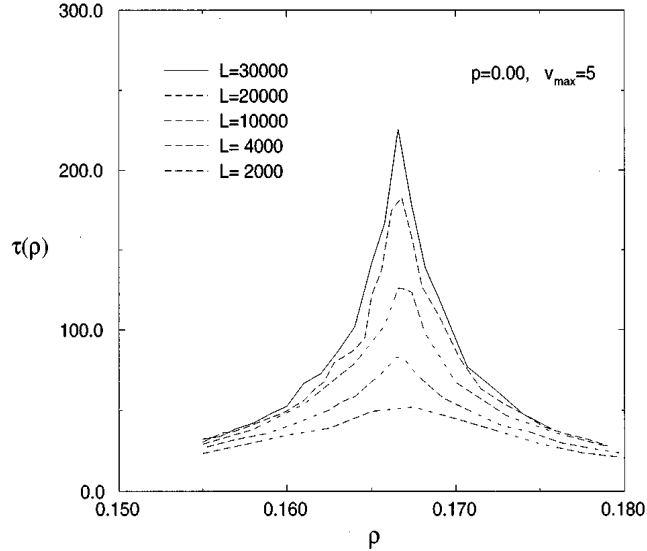
Figure 2.12: Figure extracted from Ref. [4], p. 1310: relaxation time versus density for different sizes L of the lattice. These results are studied for $v_{max} = 5$ and $p = 0$.

between them, so it requires little time to attain the maximum velocity and the system can attain the stationary state in different ways depending on the initial distribution. For $\rho = \frac{1}{v_{max}+1}$ the space between the vehicles is just sufficient to accommodate all vehicles with maximum velocity. So we have one way to fit all vehicles and depending on the initial distribution, the system requires more time to reach the stationary state.

The behaviour for $p \neq 0$ is different. First of all the point, in which the stationary time is maximum, is located at a smaller density than that marking the point of maximum flux. Second the stationary time seems not to diverge with the system size. In Fig. 2.15 both features are shown. Note that the point where the stationary time is maximum does not coincide with the point with maximum flux. Another difference in relation to the deterministic model is the behaviour of the stationary time in the vicinity of the critical point. For $p = 0$ the divergence of the stationary time at the critical point is clear but for

18
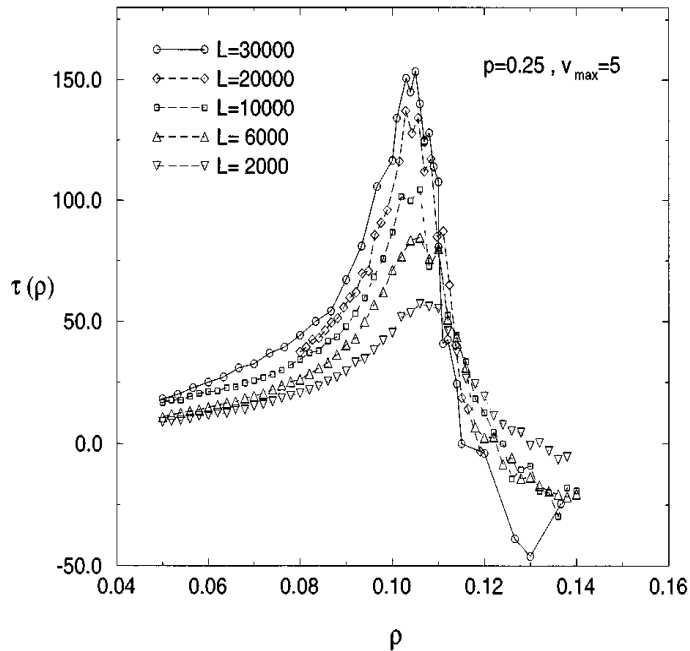
Figure 2.13: Figure extracted from Ref. [4], p. 1310: relaxation time versus density for different sizes L of the lattice. These results are studied for $v_{max} = 5$ e $p = 0.25$.

the probabilistic case the stationary time is maximum at a certain point, but it does not seem to diverge. Due to this, we prefer to label this point as Mst (Maximum stationary time) instead of labeling as critical point. The scaling analysis of the Mst with lattice size shows that the growth of Mst is insignificant and suggests that the stationary time does not diverge in the limit of infinite lattice sizes.

For $p > 0$ another indication for the absence of critical behaviour is the well established fact that the density of maximum flux $(\rho(q_{max}))$ and the transition density (ρ_c) are different for $p \neq 0$. Correlations obviously favor states with higher flux (see, e.g., Fig. 2.10). So it would be expected that the state with the strongest correlations is also the state with the highest flux, as in the deterministic case. Therefore it would be strange if the system exhibits a second order phase transition with diverging correlation length at $\rho_c \neq \rho(q_{max})$.

2.2.5   Discussion about criticality in NS model

The addition of the probability p in NS model destroys the criticality whatever the quantity chosen (flux, spatial correlation etc.). Analogous behavior is also found in the Ising chain in a transverse field. The transverse field Γ is the control parameter and corresponds to the density ρ in the NS model whereas the temperature T corresponds to the noise parameter p. Some authors [4] believe that this correspondence can be used to predict scaling laws. Further the NS model does not have absorbing states whose existence is essential to establish continuous transition between active and inactive states.

Some authors[4, 6] proposed different kinds of order parameters. The idea is to use quantities related with the fraction of jammed vehicles, e.g., the fraction of standing cars, the cars with velocity below $v_{max} - 1$ etc. This attempt is based on a possible transition described by a sharp change in free flow to congested one. The problem is finding an appropriate definition (parameter) for these regimes. For example the definition used by
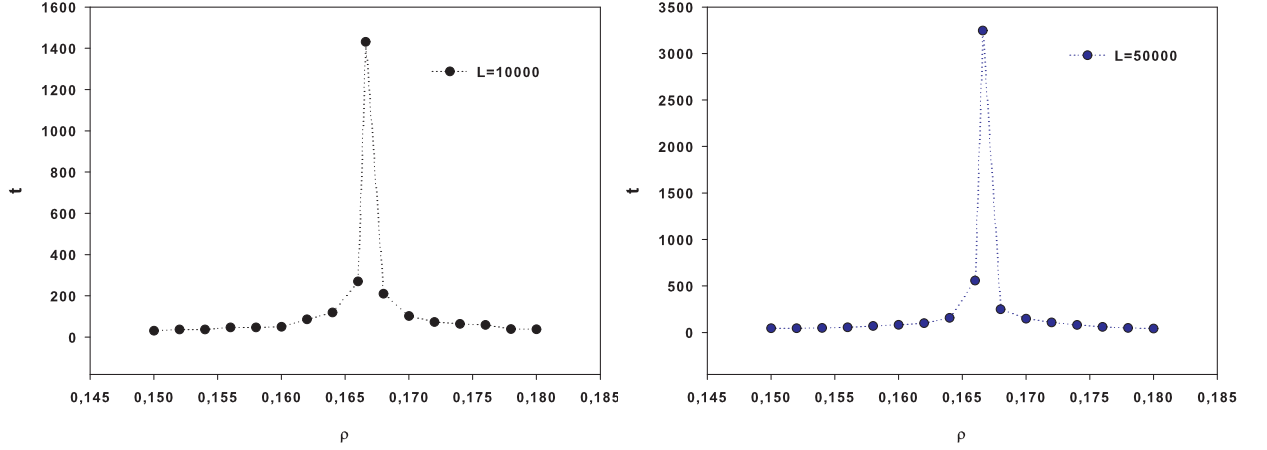
Figure 2.14: Stationary time for $p = 0$ and sizes $L = 10000$ and 50000. Note that the divergence of stationary time at the critical density ρ_c.
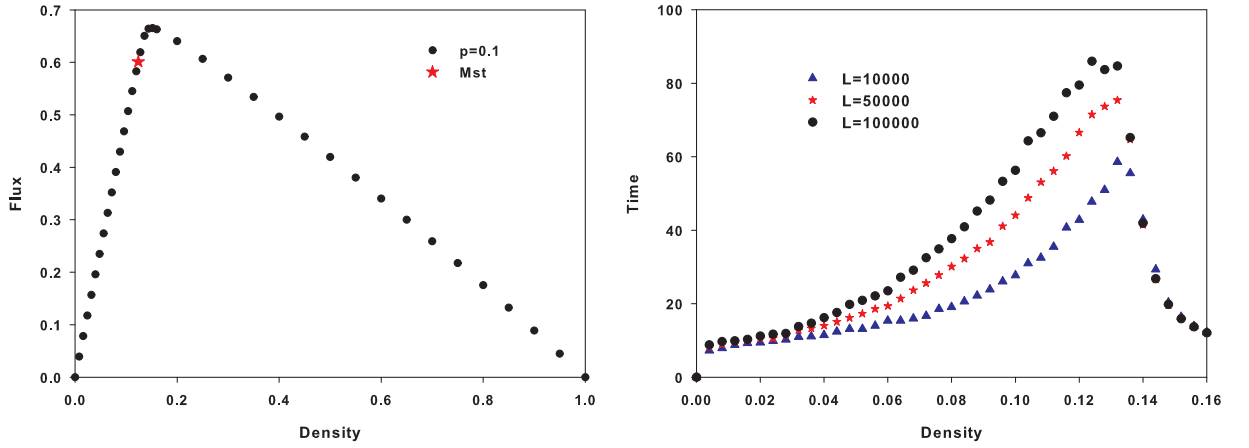
Figure 2.15: On the left, graph flux versus density for $p = 0.1$. On the right, maximum stationary time for different lattice sizes.

[6] is:

$$\bar{M}_i = 1 - \frac{1}{2T\bar{\rho}_i} \sum_{t=t_0+1}^{t_0+T} l_i(t),$$

and

$$\bar{\rho}_i = \frac{1}{T} \sum_{t=t_0+1}^{t_0+T} n_i(t).$$

The second expression represents the density of cars on site i over a time period T; t_0 is the relaxation time (usually $t_0 = 10L$) and $n_i(t)$ is zero if the cell i is empty and one if it is occupied at time t. In the first expression; $l_i(t)$ is one if at time $t-1$ the cell i is occupied (empty) and at time t it is empty (occupied); $l_i(t)$ is zero if at both times the cell i is occupied or empty. This choice of parameter is created based on that a jammed regime means that all cars are grouped in long clusters. For $p = 0$, like other quantities discussed previously, $\bar{M} = 0$ at $\rho \leqslant \rho_c$ and $\bar{M} \neq 0$ at $\rho > \rho_c$. Here i is omitted because in stationary state none of these parameters will be position dependent. A simple analysis

20

in the order parameter allows us to conclude that $\bar{M}_i = 0$ only if all vehicle that occupied the cell i at the time $t-1$ moves to the other cells in the next time. This means that the vehicles never stop due the interaction between them (jammed formation), but we know that even for small densities these interactions always occur. Finally, according to the simple argument shown in [7], quantities related to the fraction of vehicles cannot be used to identify a possible phase transition in NS model.

2.3 Mean-field theory

The exact solution of NS model is found in two special cases: For deterministic case $p = 0$ (already discussed) and for $p > 0$ with $v_{max} = 1$ [8]. The other cases the exact solution is unknown but an approximate solution via mean-field theory can help to understand some aspects of the model. In this section we will use the method developed by Nagel et al. in [8]. The first attempt consists in supposing the probability independence in the form $p(1, 2..n) = p(1)p(2)....p(n)$, where $p(i)$ denotes the probability that an event occurs at the site i and $p(1, 2, 3)$ denotes the probability that event n ($n = 1, 2, 3$) occurs simultaneously at the sites i, $i + 1$ and $i + 2$. Instead of focusing on probabilistic evolutions of positions and velocities of each vehicle in lattice, we focus on the probabilistic evolutions of sites. Let the probability of a site $i(i = 1, 2..L)$ is empty at time t be $d(i, t)$ and the probability of being occupied by a vehicle with velocity α be $c_\alpha(i, t)$. In this way the normalization condition implies:

$$d(i, t) + c_0(i, t) + c_1(i, t) + c_2(i, t) + c_3(i, t) + ... + c_{v_{max}}(i, t) = 1.$$

Let $c(i, t)$ be the probability of site i at the time t to be occupied by a vehicle, so $c(i, t) = \sum_{j=0}^{vmax} c_j(i, t)$ and the normalization condition can be written as:

$$d(i, t) + c(i, t) = 1.$$

We use the same notation of sub-steps established in update rules, i.e., acceleration (t_1), slowing down (t_2), randomization (t_3) and displacement ($t + 1$). The temporal evolution of the probabilities can be described by the following sets of equations in each of the sub-steps.

<div align="center">

Acceleration step

</div>

Following the acceleration substep all vehicles have $v > 0$, since this process does not take into account if a vehicle can move with its updated velocity without colliding with the car ahead. After this substep, probability of finding a vehicle with $v = v_{max}$ is the sum of the probabilities of velocities v_{max} and $v_{max} - 1$, just prior to acceleration, so:

$$\begin{aligned}
&c_0(i, t_1) = 0, \\
&c_\alpha(i, t_1) = c_{\alpha-1}(i, t) \qquad (0 < \alpha < v_{max}), \\
&c_{v_{max}}(i, t_1) = c_{v_{max}}(i, t) + c_{v_{max}-1}(i, t).
\end{aligned}$$

<div align="center">

Slowing down step

</div>

The probability $c_\alpha(i, t_2)$ has its origin in the evolution of the following probabilities

$$c_0(i, t_2) = c(i + 1, t_1) \sum_{\beta=1}^{v_{max}} c_\beta(i, t_1) + c_0(i, t_1)$$

$$c_\alpha(i, t_2) = c(i + \alpha + 1, t_1) \prod_{j=1}^{\alpha} d(i + j, t_1) \sum_{\beta=\alpha+1}^{v_{max}} c_\beta(i, t_1) + c_\alpha(i, t_1) \prod_{j=1}^{\alpha} d(i + j, t_1) \qquad (0 < \alpha < v_{max})$$

$$c_{v_{max}}(i, t_2) = \prod_{j=1}^{v_{max}} d(i + j, t_1) c_{v_{max}}(i, t_1). \qquad (2.4$$
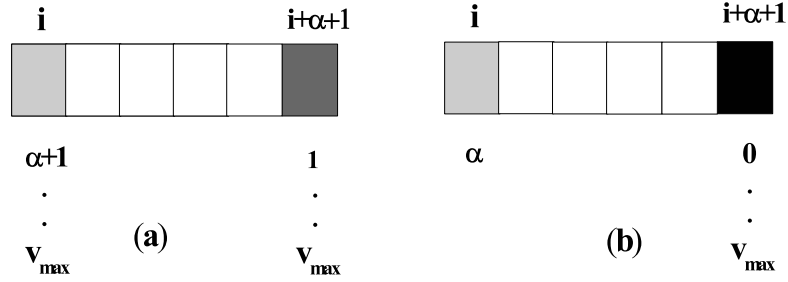
Figure 2.16: Figure contains all possible configurations at the stage t_1 capable of engendering the state $v = \alpha$ at the site i at the stage t_2 . The values above the sites indicate the position and the values below all possible velocities. Recall that $\sum_1^{v_{max}} = c$ and $\sum_0^{v_{max}} = 1$

To understanding the terms used in Eq. 2.4 we refer to the diagram in Fig. 2.16. The first term on the right of $c_0(i, t_2)$ and $c_\alpha(i, t_2)$ arises by considering that all vehicles with $v \geq \alpha + 1$ are located at the site i and, in the site $i + \alpha + 1$ there is a vehicle (no matter what speed it has). In this way the vehicles at the site i will have, after the slowing down process, velocity α. The second term arises when the vehicle located at site i has α or more empty sites in front of it, no matter if in the site $i + \alpha + 1$ has a vehicle or not. The expression for $c_{v_{max}}(i, t_2)$ reflects the requirement that the vehicle already had the maximum velocity at t_1 and has at least v_{max} empty sites in front of it.

Randomization step

The equations at the randomization step are:

$$c_0(i, t_3) = c_0(i, t_2) + pc_1(i, t_2),$$
$$c_\alpha(i, t_3) = qc_\alpha(i, t_2) + pc_{\alpha+1}(i, t_2) \qquad (0 < \alpha < v_{max}),$$
$$c_{v_{max}}(i, t_3) = qc_{v_{max}}(i, t_2).$$

The expression for $c_0(i, t_3)$ reflects the requirement that, in the previous step, the vehicle already had $v = 0$ due to slowing down process or had $v = 1$ and decelerated due to randomization one. The probability $c_\alpha(i, t_3)$ depends on the probabilities $c_\alpha(i, t_2)$ and $c_{\alpha+1}(i, t_2)$. With probability q the vehicles with velocity α (represented by the term $c_\alpha(i, t_2)$) will not reduce its speed and with probability p the vehicles with velocity $\alpha + 1$ (represented by the term $c_{\alpha+1}(i, t_2)$) will reduce.

Displacement step

In this step the probability $c_\alpha(i, t_3)$, defined according the three previous sub-steps, is passed along to the cell $i + \alpha$. So

$$c_\alpha(i + \alpha, t + 1) = c_\alpha(i, t_3) \quad (0 \le \alpha \le v_{max}).$$

Grouping the equations, we have

$$c_0(i, t+1) = c_0(i, t)[c(i+1, t) + pd(i+1, t)] + [c(i+1, t) + pd(i+1, t)c(i+2, t)] \sum_{\beta=1}^{v_{max}} c_\beta(i, t),$$

$$c_\alpha(i, t+1) = \prod_{j=1}^{\alpha} d(i - \alpha + j, t) \left[qc_{\alpha-1}(i - \alpha, t) + \left[qc(i+1, t) + pd(i+1, t) \right] c_\alpha(i - \alpha, t) \right.$$

$$\left. + \left[qc(i+1, t) + pd(i+1, t)c(i+2, t) \right] \sum_{\beta=\alpha+1}^{v_{max}} c_\beta(i - \alpha, t) \right] \quad (0 < \alpha < v_{max} - 1),$$

$$c_{v_{max}-1}(i, t+1) = \prod_{j=1}^{v_{max}-1} d(i - v_{max} + 1 + j, t) \left[qc_{v_{max}-2}(i - v_{max} + 1, t) + \left(qc(i+1, t) + pd(i+1, t) \right) \right.$$

$$\left. \left(c_{v_{max}-1}(i - v_{max} + 1, t) + c_{v_{max}}(i - v_{max} + 1, t) \right) \right],$$

$$c_{v_{max}}(i, t+1) = q \prod_{j=1}^{v_{max}} d(i - v_{max} + j, t) \left[c_{v_{max}-1}(i - v_{max}, t) + c_{v_{max}}(i - v_{max}, t) \right].$$

From $c_\alpha(i, t+1)$, the probability $c_\alpha(i, t+2)$ can be obtained doing the same steps developed to find $c_\alpha(i, t+1)$ from $c_\alpha(i, t)$, but for the obvious reason this procedure is impractical. The stationary state can be obtained by other means, e.g., numerical solution. Instead of looking for time-dependent solution, we study just the stationary states, when the distributions c and d become spatial independent

$$c(i + \alpha) = c(i) \quad \text{and} \quad d(i + \alpha) = d(i) \quad \text{for all } \alpha,$$

so the equations are simplified to read,

$$c_0 = c_0 \left(c + pd \right) + \left(1 + pd \right) c \sum_{\beta=1}^{v_{max}} c_\beta,$$

$$c_\alpha = d^\alpha \left[qc_{\alpha-1} + \left(qc + pd \right) c_\alpha + \left(q + pd \right) c \sum_{\beta=\alpha+1}^{v_{max}} c_\beta \right] \quad (0 < \alpha < v_{max} - 1),$$

$$c_{v_{max}-1} = d^{v_{max}-1} \left[qc_{v_{max}-2} + \left(qc + pd \right) \left(c_{v_{max}-1} + c_{v_{max}} \right) \right],$$

$$c_{v_{max}} = qd^{v_{max}} \left[c_{v_{max}-1} + c_{v_{max}} \right].$$

Another way of expressing these equations is rewrite them as a function of c, p and d (for further detail see the chapter 7). So

$$
\begin{aligned}
c_0 &= \frac{c^2(1+pd)}{1-pd^2}, \\
c_1 &= qc^2 d\frac{1+d+pd^2}{(1-pd^3)(1-pd^2)}, \\
c_\alpha &= \frac{1+(q-p)d^\alpha}{1-pd^{\alpha+2}}dc_{\alpha-1} - \frac{qd^\alpha}{1-pd^{\alpha+2}}c_{\alpha-2}, \\
c_{v_{max}-1} &= \frac{1-qd^{v_{max}}}{1-d^{v_{max}-1}(q+pd)}qd^{v_{max}-1}c_{v_{max}-2}, \\
c_{v_{max}} &= \frac{qd^{v_{max}}}{1-qd^{v_{max}}}c_{v_{max}-1}.
\end{aligned}
$$

With the intention of evaluating these approximation, we compare in Fig. 2.17 these results with those obtained by computational simulation (Monte Carlo method).
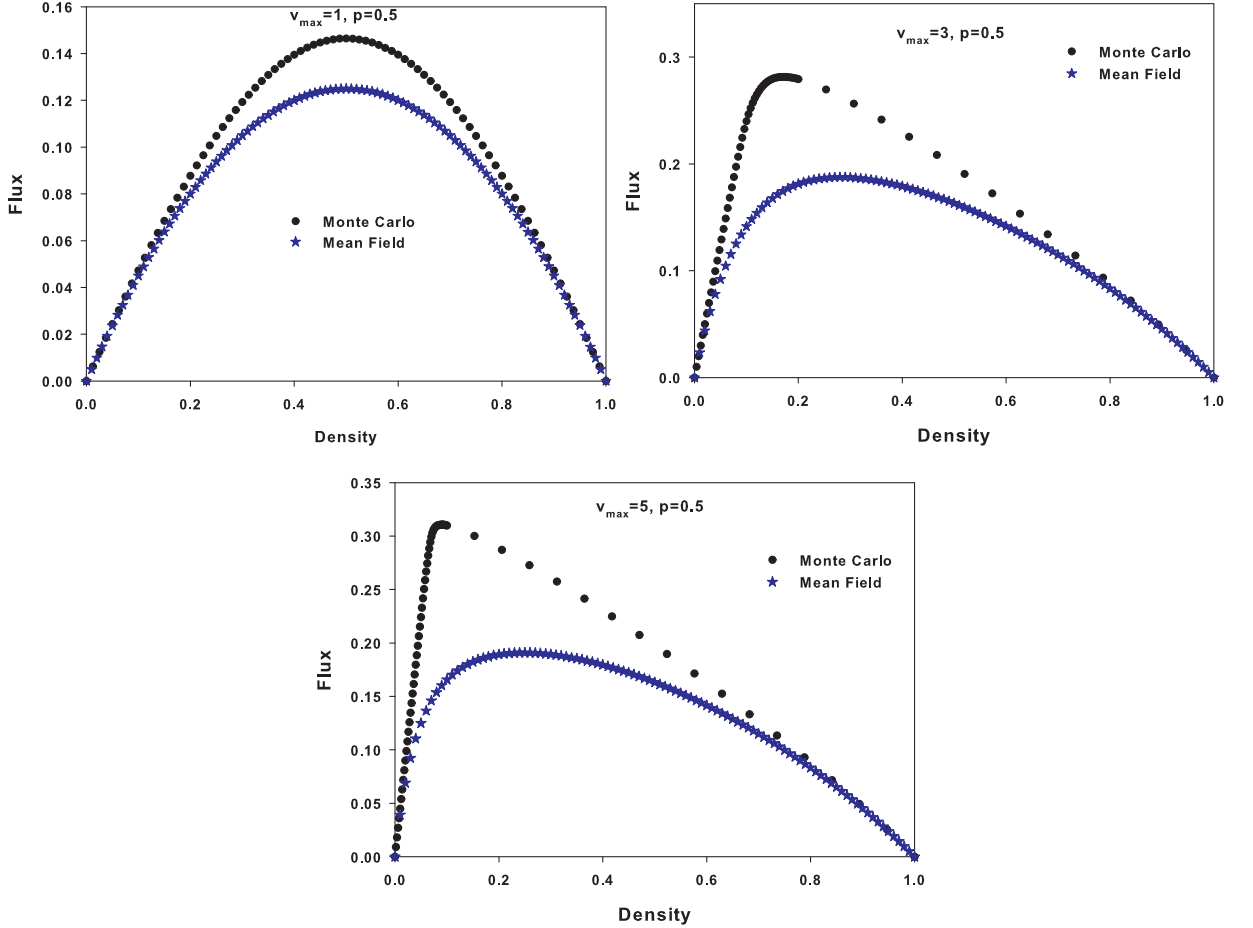
Figure 2.17: Comparison between the Monte Carlo method and the 1-cluster mean field theory for the velocities $v_{max} = 1$, 3 and 5. We use $p = 0.5$ for all cases.

This simple mean-field result yields, compared with the Monte Carlo simulation, small values for the flux. This fact can easily be understood since the reduction to a single car problem ignores all spatial correlations of the vehicles. Vehicles, for instance, with high

velocities tend to be equidistant and can therefore maintain a high velocity with a larger probability than in the mean-field system where is so much more difficult to accelerate and stay at high velocities over a certain time.

2.3.1 N-cluster approximation

In order to improve the simple mean-field theory of the preceding section we have to take into account correlations between neighboring sites. We divide the lattice into segments or clusters of length n ($n = 1, 2...$) such that two neighboring clusters have $n-1$ sites in common. The probability of finding a cluster in the stationary state $(\sigma_1, ..., \sigma_n)$ will be denoted by $P_n(\sigma_1, ..., \sigma_n)$. Due to the translational invariance of the stationary state of the system with periodic boundary conditions, one does not have to specify the actual location of n-cluster and the first cell of the cluster will be numbered by 1. In the 1-cluster approximation we have $v_{max} + 2$ possible states and in order to simplify the calculations we apply the four update rules in the order slowing down, randomization, displacement and acceleration instead of the order defined previously. This has the advantage that after one update cycle one ends up with the acceleration step and therefore no car has velocity $v = 0$. It follows that every site j is in one of the $v_{max} + 1$ states where now 0 denotes an empty site. So we eliminate one variable d of the equation system, but we have to take into account for the flux calculation that $v = v_{max}$ comes as a result of the acceleration step applied in $v_{max} - 1$ and v_{max} (the last one does not accelerate). The probability of finding a state c^n is:

$$P\left(c^{(n)}\right) = \sum_{c^{(n+2v_{max})}} W\left(c^{(n+2v_{max})} \to c^{(n)}\right) P\left(c^{(n+2v_{max})}\right).$$

The term $c^{(n+2v_{max})}$ denotes the state constituted by the set of the states of $n + 2v_{max}$ cells. The first cell is labeled by $1 - v_{max}$ and the last one $n + v_{max}$, thus $c^{(n+2v_{max})} = (1 - v_{max}, ..., n + v_{max})$. This additional extension of the cluster occurs since all vehicles which can drive into or out of the cluster $c^{(n)} = (1, ..., n)$ within the next time step contribute to the transition rates W. So we have to take into account not only the given cluster, but also the v_{max} sites to its left (with the variables $(1 - v_{max}, ..., 0)$) and the v_{max} sites to its right (with the variables $(n + 1, ..., n + v_{max})$). The transition probability $W\left(c^{(n+2v_{max})} \to c^{(n)}\right)$ is given by the update rules of NS model. The probability $P\left(c^{(n+2v_{max})}\right)$ is given by:

$$P\left(c^{(n+2v_{max})}\right) = \prod_{i=1-v_{max}}^{0} P(c_i \mid \underline{c_{i+1}, ..., c_{i+n-1}}) * P\left(c_1, ..., c_n\right) * \prod_{i=1}^{v_{max}} P(\underline{c_{i+1}, ..., c_{i+n-1}} \mid c_{i+n}).$$

The conditional probability on the left-hand side is

$$P(c_i \mid \underline{c_{i+1}, ..., c_{i+n-1}}) = \frac{P_n(c_i, c_{i+1}, ..., c_{i+n-1})}{\sum_c P_n(c, c_{i+1}, ..., c_{i+n-1})},$$

and on the right-hand side is

$$P(\underline{c_i, ..., c_{i+n-2}} \mid c_{i+n-1}) = \frac{P_n(c_i, c_{i+1}, ..., c_{i+n-1})}{\sum_c P_n(c_i, ..., c_{i+n-2}, c)}.$$

To clarify this method, we present in the next section the 2-cluster approximation to solve NS model with $v_{max} = 1$ and $p = 0.5$.

2.3.2 2-cluster approximation

For the case $v_{max} = 1$ we have to add two cells to the cluster $c^{(2)}$, so:

$$P\left(c^{(2)}\right) = \sum_{c^{(4)}} W\left(c^{(4)} \to c^{(2)}\right) P\left(c^{(4)}\right).$$

Figure 2.18 shows all possible configurations for $c^{(4)}$ and their corresponding probabilities,

$\boxed{1\,0\,0\,\alpha}$ $\Rightarrow$	$\boxed{0\,0}$ p		
	$\boxed{1\,0}$ q	$\boxed{1\,0\,1\,0}$ $\Rightarrow$	$\boxed{1\,1}$ qp
			$\boxed{0\,0}$ qp
$\boxed{\alpha\,1\,0\,\alpha}$ $\Rightarrow$	$\boxed{1\,0}$ p		$\boxed{0\,1}$ p^2
	$\boxed{0\,1}$ q		$\boxed{1\,0}$ q^2
		$\boxed{0\,0\,0\,\alpha}$ $\Rightarrow$	$\boxed{0\,0}$ 1
$\boxed{\alpha\,1\,1\,0}$ $\Rightarrow$	$\boxed{1\,1}$ p	$\boxed{\alpha\,1\,1\,1}$ $\Rightarrow$	$\boxed{1\,1}$ 1
	$\boxed{1\,0}$ q	$\boxed{0\,0\,1\,1}$ $\Rightarrow$	$\boxed{0\,1}$ 1
$\boxed{0\,0\,1\,0}$ $\Rightarrow$	$\boxed{0\,1}$ p		$\boxed{0\,1}$ p
	$\boxed{0\,0}$ q	$\boxed{1\,0\,1\,1}$ $\Rightarrow$	$\boxed{1\,1}$ q
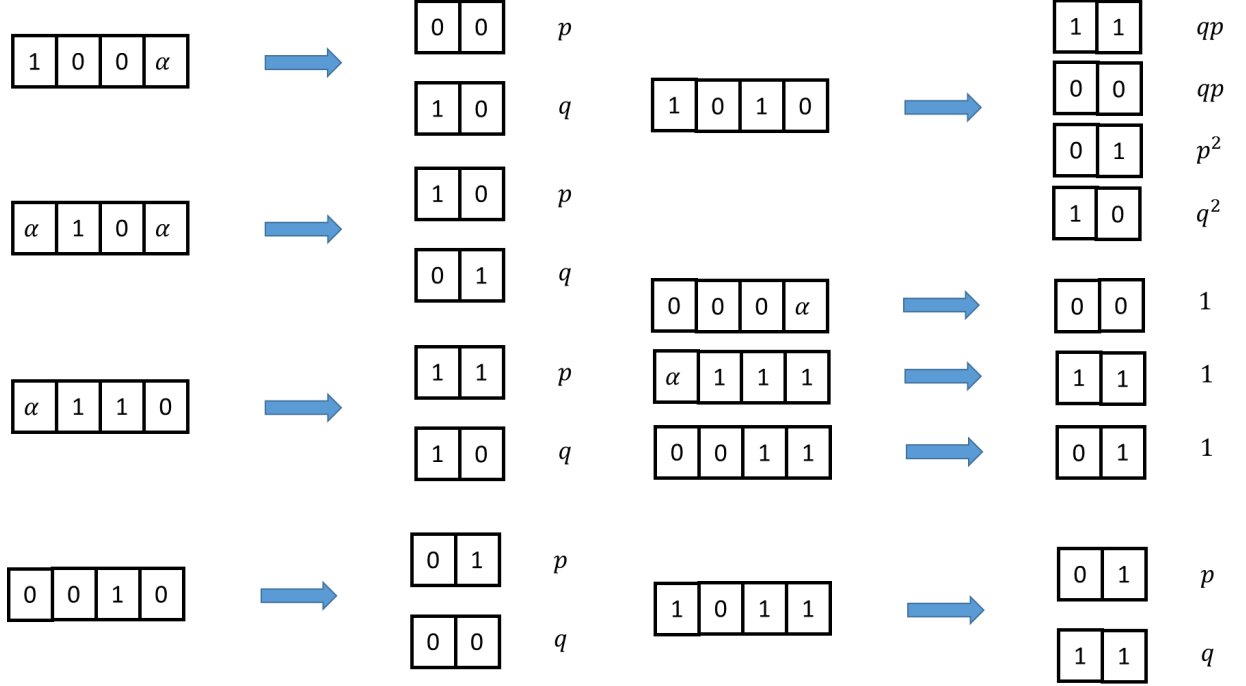
Figure 2.18: Figure showing all possible states of 4-cluster $(c^{(4)})$ and their corresponding probabilities of evolving to states $c^{(2)}$.

by using the update rules of NS model, to evolve to the clusters $c^{(2)}$. The symbol α within the cells means that independent of the state of this cell, the final state after the NS update rules is unchanged. So we can find the probabilities $P(1,0)$, $P(0,1)$, $P(1,1)$ e $P(0,0)$ via:

$$P(1,0) = qP(1,0,0,\alpha) + pP(\alpha,1,0,\alpha) + qP(\alpha,1,1,0) + q^2 P(1,0,1,0),$$
$$P(0,1) = qP(\alpha,1,0,\alpha) + pP(0,0,1,0) + p^2 P(1,0,1,0) + 1P(0,0,1,1) + pP(1,0,1,1),$$
$$P(1,1) = pP(\alpha,1,1,0) + qpP(1,0,1,0) + 1P(\alpha,1,1,1) + qP(1,0,1,1),$$
$$P(0,0) = pP(1,0,0,\alpha) + qP(0,0,1,0) + qpP(1,0,1,0) + 1P(0,0,0,\alpha),$$

using

$$P(a,b,c,d) = \frac{P(a,b)}{P(1,b)+P(0,b)} P(b,c) \frac{P(c,d)}{P(c,1)+P(c,0)},$$

and for determining the flux we need to find only $P(1,0)$; we have:

$$P(1,0) = \quad q\left[\frac{P(1,0)}{P(1,0)+P(0,0)} P(0,0) \frac{P(0,\alpha)}{P(0,1)+P(0,0)}\right] + p\left[\frac{P(\alpha,1)}{P(1,1)+P(1,0)} P(1,0) \frac{P(0,\alpha)}{P(0,1)+P(0,0)}\right]$$

$$+q\left[\frac{P(\alpha,1)}{P(1,1)+P(0,1)} P(1,1) \frac{P(1,0)}{P(1,0)+P(1,1)}\right] + q^2 \left[\frac{P(1,0)}{P(1,0)+P(0,0)} P(0,1) \frac{P(1,0)}{P(1,0)+P(1,1)}\right].$$

Due to the particle-hole symmetry $P(1,0) = P(0,1)$ (in a closed ring one must have the same number of $(0,1)$ and $(1,0)$ pairs, therefore occurring with the same probability). The relations $P(1,1) + P(1,0) = c$ and $P(0,0) + P(1,0) = 1 - c = d$ are related to the conservation of vehicles in the system. In this way $P(1,0)$ can be found easily by:

$$P(1,0) = q\frac{P(1,0)}{1-c}[1 - c - P(1,0)]1 + pP(1,0) + q[c - P(1,0)]\frac{P(1,0)}{c} + q^2\frac{P(1,0)}{1-c}P(1,0)\frac{P(1,0)}{c},$$

$$\frac{qcP(1,0)[1 - c - P(1,0)] + pc(1-c)P(1,0) + (1-c)q[c - P(1,0)]P(1,0) + q^2P^3(1,0) - c(c-1)P(1,0)}{c(1-c)} = 0,$$

$$qc[1 - c - P(1,0)] + pc(1-c) + q[1-c][c - P(1,0)] + q^2P^2(1,0) - c(c-1) = 0,$$

$$q^2P^2(1,0) + [-qc - q(1-c)]P(1,0) + qc(1-c) + pc(1-c) + qc(1-c) - c(1-c) = 0,$$

$$q^2P^2(1,0) - q(c+1-c)P(1,0) + c(c-1)[q + p + q - 1] = 0,$$

$$q^2P^2(1,0) - qP(1,0) + qc(c-1) = 0,$$

$$qP^2(1,0) - P(1,0) + c(c-1) = 0,$$

leading to

$$\boxed{P(1,0) = \frac{1 - \sqrt{1 - 4qc(1-c)}}{2q}.}$$

The flux depends only on $P(1,0)$. So the flux is determined by the evolution of the state $(1,0)$ to $(0,1)$ (according to the randomization step, it occurs with probability q), thus the flux is given by:

$$f = \frac{1}{2}\left[1 - \sqrt{1 - 4qc(1-c)}\right].$$

We can see in the Fig. 2.19 that the 2-cluster approximation comes close to the Monte
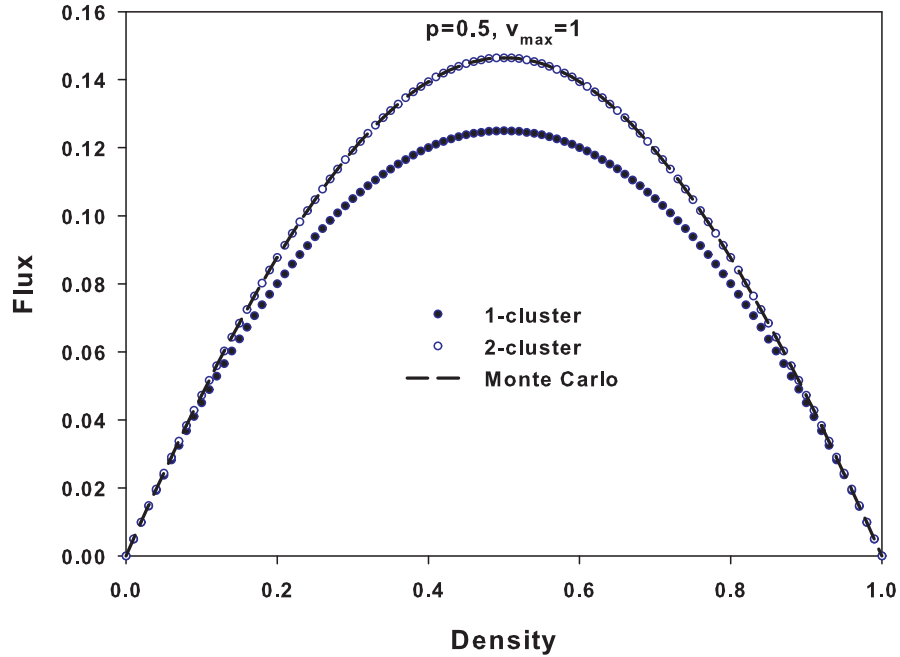
Figure 2.19: Graph comparing the 1-cluster (simple mean-field method), 2-cluster and Monte Carlo techniques for obtained the stationary flux in NS model.

Carlo simulation. In fact, going to the three- and higher-cluster approximations one finds

that the solution remains the same, indicating that this is the exact result. With this approximation it is possible to write down a closed system of equations for the n-cluster probabilities $P_n(\sigma_1, ..., \sigma_n)$. The number of the equations is given by $(v_{max}+1)^n$, the total number of possible configurations of n site variable with $v_{max}+1$ possible states (without change of the order of the update steps, one would have $(v_{max}+2)^n$ equations). In practice some of these equations turn out to be trivial so that the relevant number is less than $(v_{max}+1)^n$. Due to the exponential growth with respect to n one is, especially for larger v_{max}, restricted to only small cluster lengths n (for the realistic value of $v_{max} = 5$, one has, for the two-cluster approximation, already 36 equations).

In Ref. [9] a rather simple extension of MFT is accomplished. The key idea is a reduction of the configuration space by removing all states which cannot by reached dynamically. In the context of cellular automata these states are called Garden of Eden (GoE) states or paradisical states (because they cannot be revisited). Part of the difficulties come from the fact that one uses parallel dynamics. This introduces a non-local aspect into the problem since the whole lattice is updated at once. On the other hand, random-sequential dynamics is much simpler to treat analytically. For $v_{max} = 1$, for instance, simple mean-field theory gives already the correct steady state, i.e., there are no correlations. A simple example for $v_{max} = 1$ is the configuration $(\bullet, 1, 2)$ of two consecutive cells, where '$\bullet$' denotes an empty cell and the numbers correspond to the velocities of the cars. Cars move from left to right. Obviously the velocity is just the number of cells the car moved in the previous time step. Therefore, the configuration $(\bullet, 1, 2)$ could have evolved only from a state which has two cars in the leftmost cell. Since double occupations are not allowed in the present model, states containing $(\bullet, 1, 2)$ are dynamically forbidden, i.e., they are GoE states.

We will use pMF for $v_{max} = 1$ and compare with simple mean-field theory (1-cluster). The 1-cluster approximation yields the following set of equations:

$$c_0 = c(c + pdc), \tag{2.5}$$
$$c_1 = cd(qc + d). \tag{2.6}$$

By using pMF for $v_{max} = 1$, configurations like $(0,1)$ and $(1,1)$, i.e., a moving vehicle is directly followed by another car, are not allowed. This is not possible as can be seen by looking at the possible configurations at the previous timestep. The momentary velocity gives the number of cells that the car moved in the previous timestep. In both configurations the first car moved one cell. Therefore, it is immediately clear that $(0,1)$ is a GoE state since otherwise there would have been a doubly occupied cell before the last timestep. The configuration $(1,1)$ is also not possible since both cars must have occupied neighbouring cells before the last timestep too. Therefore, according to rule R2, the second car could not move. Comparing to the simple mean-field theory, only the first equation is modified. Note that only for c_0 the equations are different, for PMF theory the state (c, c) is not acceptable because this configuration can be broken down into the states $(1,0)$, $(1,1)$, $(0,0)$ and $(0,1)$. The states $(1,1)$ and $(0,1)$ are not allowed, so only $(1,0)$ and $(0,0)$ are possible states and we have to replace in Eq. (2.5) c^2 by cc_0. The new set of equations is:

$$c_0 = c(c_0 + pdc),$$
$$c_1 = cd(qc + d).$$

Due to the modification introduced in the first equation $c_0 + c_1 \neq c$. For this reason, one has to introduce a normalization constant $\eta = \frac{1}{c_0 + d}$ into the equations:

$$c_0 = \eta c(c_0 + pcd),$$
$$c_1 = \eta cd(qc + d).$$

Expanding the first equation and remembering that $c_1 = c - c_0$, we have:

$$c_1 = \frac{1 - \sqrt{(d-c)^2 + 4pcd^2}}{2}.$$

The flux is given by c_1 and we recover the exact solution for the case $v_{max} = 1$ found by a 2-cluster approximation. This result confirms the expectations mentioned above. One can see clearly that the difference between random-sequential and parallel dynamics is the existence of GoE states in the latter. After eliminating these GoE states, no correlations are left in the reduced configuration space.

Chapter 3

Other cellular automata models

We present in this section a brief discussion about other cellular automata models. Most of these models are slight modifications on the update rules of NS model. They are of interest because NS model is a minimal model in the sense that all the four steps are necessary to reproduce the basic features of real traffic; however, additional rules are needed to capture more complex situations, e.g., metastable states. Some basic rules of the NS model should be preserved in these new approaches. For example step 1 in the NS model reflects the general tendency of the drivers to drive as fast as possible without exceeding the maximum speed limit. Step 2 is intended to avoid collision between the cars. The randomization in step 3 accounts for the different behavioural patterns of the individual drivers, especially, nondeterministic acceleration as well as overreaction while slowing down; this is crucially important for the spontaneous formation of traffic jams. In addition, the use of a parallel updating scheme (instead of a random-sequential one) is crucial since it accounts for the reaction time and can lead to a chain of overreactions. As an example, suppose that a car slows down in the randomization step. If the density of cars is large enough this might force the following car also to brake in the deceleration step. In addition, if p is larger than zero, it might brake even further in step 3. Eventually this can lead to the stopping of a car, thus creating a jam. This simple mechanism of spontaneous jam formation is rather realistic and cannot be modeled by the random-sequential update.

In Fig. 3.1 we see the the spontaneous jam formation for $p \neq 0$ and its corresponding backward motion (this feature is not present for $p = 0$).

3.1   Changing the orders of substeps in the NS model

The effect of changing the substep order in the NS model is shown in Ref. [10]. The authors, initially, studied the following update rules:

1. **Acceleration**

$$v_j(t_1) = \min[v_j(t) + 1, v_{max}].$$

2. **Randomization**

$$v_j(t_2) = \max[v_j(t_1) - 1, 0] \quad \text{with probability } p,$$
$$v_j(t_2) = v_j(t_1) \qquad\qquad\quad \text{with probability } 1 - p.$$
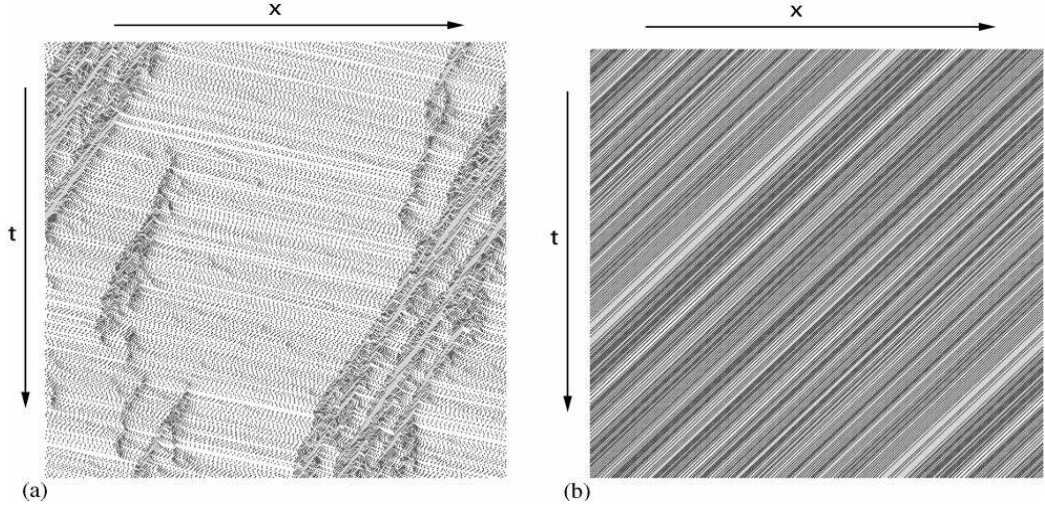
Figure 3.1: Figure extracted of Ref. [10]. Typical space-time diagram of the NS model for (a) $p = 0.25$ and $\rho = 0.2$, (b)$p = 0$ and $\rho = 0.5$.

3. **Deterministic deceleration**

$$v_j(t_3) = \min[d_j(t), v_j(t_2)].$$

4. **Displacement**

$$x_j(t+1) = x_j(t) + v_j(t_3).$$

The difference between this model and the NS model is in the anticipation of the randomization step in relation to the deceleration one. The fundamental diagram with the same simulation conditions as those of the NaSch model, is shown in Fig. 3.2. This figure indicates that the model leads to a higher value of maximum flux 40% higher than that obtained with the NaSch model. When compared to the NS model, this changing leads to a better approximation with the observed data in real traffic. In fact, when a driver finds a high vehicle density ahead, he will first delay at random and estimate whether he should decelerate or not by observing and evaluating his anticipation velocity and the headway between successive vehicles. If he finds his anticipation velocity will surpass the headway, he slows down. Due to the anticipation of the randomization step, braking times in the state of free flow will be reduced and more vehicles with the maximum velocity will cause an increase of capacity, while the fact that vehicles cannot maintain the maximum velocity at high density and, as well as the fluctuation of velocity leads to the spontaneous formation of jams and capacity drops. In contrast to the NaSch model, the modified version allows more vehicles to maintain a higher or even maximum velocity. This model is thus called the sensitive drive model or the SDNS model.

This model displays bistable states. They becomes clear if we start the system with two different initial conditions. One is the homogeneous distribution with the same headway; the other is the megajam consisting of one large compact cluster of standing vehicles. Thus we obtain the fundamental diagram with two branches as shown in Fig. 3.3. The results of the VDR model arise from introducing two delay probabilities dependent on velocity instead of the constant randomization in the NS model, while the same result in this model comes from interchanging the order of the deterministic deceleration and the stochastic one in the steps of the evolution rules.
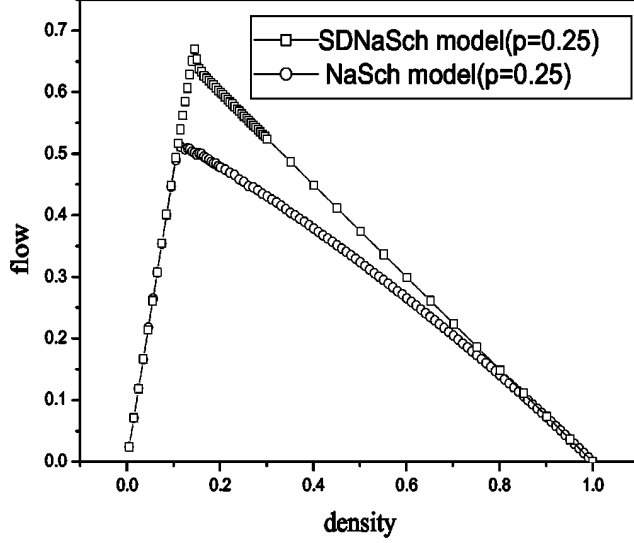
Figure 3.2: Figure extracted of Ref. [10]; the fundamental diagram of SDNS and NS model for $p = 0.25$.

When the density is in the range $\rho_1 < \rho < \rho_2$, the flux, in fundamental diagram, is discontinuous. The upper branch over the flux q_{jam} corresponds to the homogeneous traffic flow, which has larger flow with no jam due to the reduction of braking times in the sensitive driving. This case belongs to the free state and the flux reaches the maximum as $\rho \approx 0.18$. The lower branch corresponds to the traffic jam; the flux reduces rapidly because of the increase of the braking probability. It is evident that there is a hysteresis loop in the fundamental diagram. From the simulated results, we can get the following relations. In the regime of the upper branch as $0 < \rho < \rho_2$, the average velocity is that of the free-flow, $\overline{v_f} = (1 - p)v_{max} + p(v_{max} - 1) = v_{max} - p$, therefore the flux is:

$$q = \rho \overline{v_f} = \rho(v_{max} - p).$$

In the regime of the lower branch as $\rho_2 < \rho$, the average waiting time T_w of the first vehicles at the head of the megajam is given by $T_w = 1/(1 - p)$. The flux is

$$q = (1 - p)(1 - \rho).$$

From the above analysis, the number of vehicles in the state of deceleration between $0 < \rho < \rho_2$ decreases and the capacity of the road approaches more closely the empirical data than that predicted by the NS model due to the role of the stochastic delay prior to deterministic deceleration. The increase in the number of braking vehicles in $\rho_1 < \rho < \rho_2$ is due to the role of the stochastic delay and deterministic deceleration at the same time will frequently lead to the breakdown of flow and so to a traffic jam. Therefore, according to the authors of Ref. [10], the exchange of the order of the stochastic delay and deterministic deceleration has significant effect on traffic flow. Another change studied by these authors consists in changing the update rules as follows:

1. **Randomization**

$$v_j(t_1) = \max[v_j(t) - 1, 0], \quad \text{with probability } p,$$
$$v_j(t_1) = v_j(t), \qquad\qquad\quad \text{with probability } 1 - p.$$
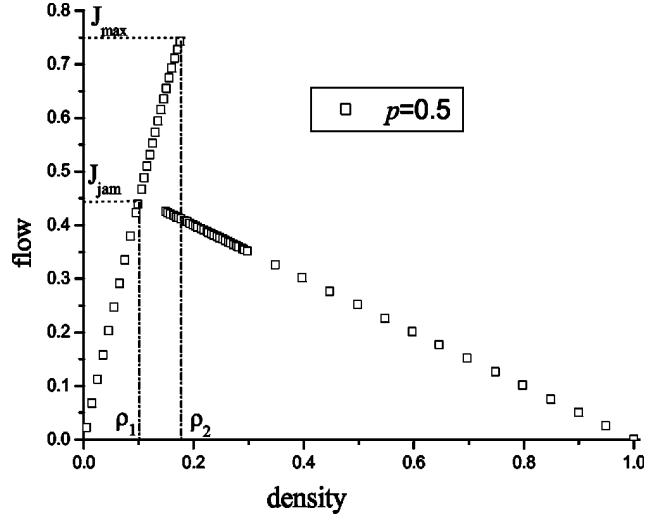
Figure 3.3: Figure extracted of Ref. [10]; the fundamental diagram via numerical simulation with two different initial conditions: uniform distribution state and inhomogeneous congestion $v_{max} = 5$, $L = 5 \times 10^3$, $p = 0.5$. The metastable state appears in $\rho_1 < \rho < \rho_2$.

2. **Acceleration**

$$v_j(t_2) = \min[v_j(t_1) + 1, v_{max}]$$

3. **Deterministic deceleration**

$$v_j(t_3) = \min[d_j(t), v_j(t_2)]$$

4. **Displacement**

$$x_j(t+1) = x_j(t) + v_j(t_3)$$
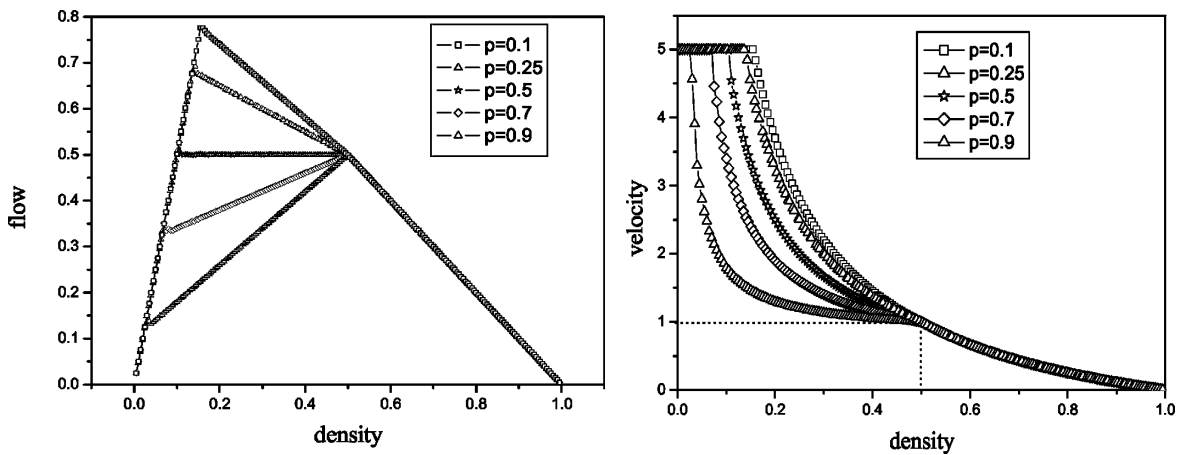
Figure 3.4: Figure extracted by Ref. [10]. The fundamental diagram is shown at the left and the graph velocity versus density at the right.

The fundamental diagram is shown in the left part of Fig. 3.4, and the corresponding velocity-density curve at the right. There are three different parts; $0 < \rho < \rho_1$, $\rho_1 < \rho < \rho_2$ and $\rho_2 < \rho < 1$ which correspond to three different phases, namely, free flow, low-speed

flow and jam. In this model we have an interesting situation; as the density ρ approaches 0.5, the velocity in low-speed flow approaches unity. The velocity is:

$$v = \begin{cases} v_{max} & \rho < \rho_1, \\ \frac{1}{2\rho} - \frac{(1-2\rho)(2p-1)}{\rho} & \rho_1 < \rho < \rho_2, \\ \frac{1}{\rho} - 1 & \rho \geq \rho_2. \end{cases}$$

Where $\rho_1 = \frac{1-p}{v_{max}+1-2p}$ and $\rho_2 = \frac{1}{2}$.

The NS model is updated in sequence R1-R2-R3 (corresponding to acceleration-deceleration-randomization), while the two models studied in Ref. [10] are R1-R3-R2 and R3-R1-R2. The update rules R2-R1-R3, R2-R3-R1, and R3-R2-R1 are discarded due the possibility of collisions between the vehicles.

3.2   VDR model

The velocity-dependent randomization (VDR) model [11] adds a simple slow-to-start rule to the NS model. Instead of using a unique deceleration probability p, these authors include a velocity dependence in this parameter, so that $p = p(v)$. For simplicity, they study the case:

$$p(v) = \begin{cases} p_0 & \text{if } v = 0 \\ p & \text{if } v > 0. \end{cases}$$

Since we are interested in hysteresis phenomena, we restrict ourselves to the case $p_0 \geq p$. Note that for $p_0 = p$ the NaSch model is recovered. The parameters used are: maximum velocity $v_{max} = 5$, braking probability $p = \frac{1}{64}$ for moving cars, $p_0 = 0.75$ for stopped cars, Ref. [11] reports numerical simulations of periodic systems with $L = 10000$ lattice sites. Fig. 3.5 shows the fundamental diagram of the VDR model. The average flux
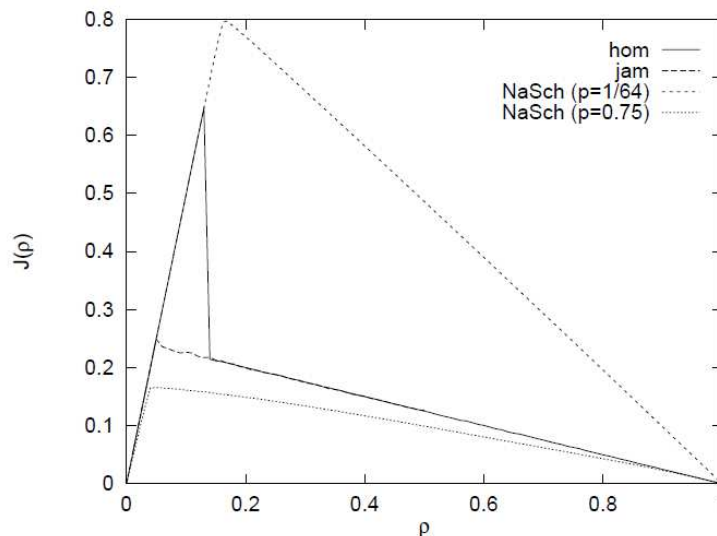
Figure 3.5:   Figure extracted of Ref [11]. Difference between fundamental diagrams of the VDR and NS models.

$j(\rho)$ can take two values in the density interval between ρ_1 and ρ_2 depending on the initial condition. The larger values of the average flux are obtained using a homogeneous

initialization of the system. The lower branch is obtained starting from a completely jammed state. It is instructive to compare the fundamental diagram of the VDR model with those of the corresponding NS models. For small densities $\rho \ll 1$ there are no slow cars in the VDR model since interactions between cars are extremely rare. Here the flux is given by $j(\rho) = \rho(v_{max} - p)$, i.e., identical to the NS model with randomization p. For large densities $1 - \rho \ll 1$ on the other hand, the flux is given by $j(\rho) = (1 - p_0)(1 - \rho)$ which corresponds to the NS model with randomization p_0. For densities close to $\rho = 1$, only cars with velocities $v = 0$ or $v = 1$ exist.

The microscopic structure of the jammed states in the VDR model differs from those found in the NS model. While jammed states in the NS model contain clusters with an exponential size-distribution, one can find phase separation in the VDR model. The reason for this behaviour is the reduction of the outflow from a jam. If the outflow from a jam is maximal, any small jam in the free flow regime dissolves immediately since the outflow from such a jam is larger than the global flow. Therefore phase separation cannot occur in that case. However, if the outflow from a jam is reduced, the density in the free flow regime is smaller than the density of maximum flux and cars can propagate freely in the low density part of the lattice. Due to the reduction of the density in the free flow regime, no spontaneous formation of jams is observed in the stationary state, if fluctuations in the free flow regime are rare. We can see this phase separation at Fig. 3.6.
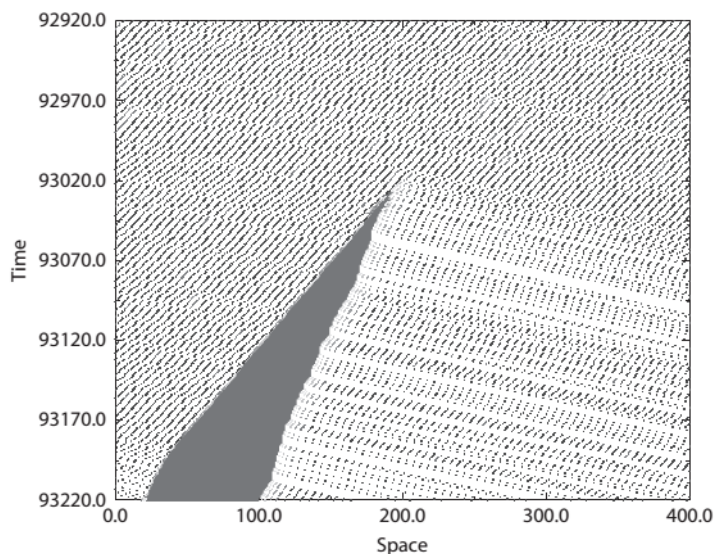
Figure 3.6: Figure extracted of Ref. [11]. Space-time diagram of the VDR model for $\rho = 0.15$; $L = 400$; $p = 0.01$ and $p_0 = 0.5$. The homogeneous initial state is not destroyed immediately, but after approximately 93000 lattice updates. In the outflow regime of the jam the density is reduced compared to the average density.

3.3 Cruise-control model

The cruise-control (cc) model is a simplified version of the NS model [12]. This simplification can be described as a "cruise control limit", since at sufficiently low density all vehicles move deterministically at maximum allowed velocity. As in the NS model the cc model is defined on a one-dimensional lattice of length L, representing a single-lane

freeway. Each site of the lattice can be in one of the $v_{max} + 2$ states: It may be empty, or it may be occupied by one car having an integer velocity between zero and v_{max}. One iteration consists of the following steps, which are each performed simultaneously for all vehicles. A vehicle is stationary when it travels at maximum velocity v_{max} and has free headway: $d \geq v_{max}$. Such a vehicle just maintains its velocity. If a vehicle is not stationary, it is jammed [1]. The following rules are applied to jammed vehicles.

1. **Acceleration**
   With probability 1/2, a vehicle with $d \geq v + 1$ accelerates to $v + 1$, otherwise it keeps the velocity v. A vehicle with $d = v$ just maintains its velocity.

2. **Slowing down and randomization**
   Each vehicle with $d \leq v - 1$ slows down to $v = d$ and can add further deceleration according to:

$$v = \max[v - 1, 0] \quad \text{with probability } 1/2$$
$$v = v \qquad\qquad\quad \text{with probability } 1/2$$

3. **Displacement**
   Each vehicle advances v sites.

The randomization process in this model can produce overreaction as in the NS model, but different from this, introduces a nondeterministic acceleration. The fundamental diagram was obtained numerically [12] as show in Fig. 3.7.

For a spatially infinite system, the following results hold: for $\rho < \rho_c$ jams present in
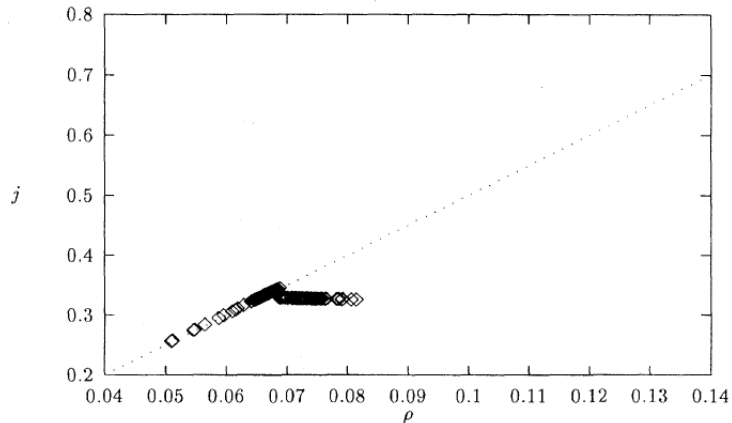
Figure 3.7: Figure extracted of Ref. [12]. Fundamental diagram of the cruise-control model. The dotted line represents deterministic traffic, i.e., when the initial state is prepared such that for each car $n_{gap} > v_{max}$ and $v = v_{max}$. The points are measurement results starting from random initial conditions. Each point corresponds to one run of a closed system of length $L = 30000$ and an average over 2.5×10^6 iterations after discarding a transient period of 5×10^5 iterations.

the initial configuration are eventually sorted out and the stationary deterministic state is jam free with every vehicle moving at maximum velocity. Thus, the flux is a linear function of density with slope $v_{max} = 5$. This behavior is observed up to a maximum

---

[1]In this model the concept of jammed and stationary are different than those used in models with absorbing configurations, stationary means inactive and jammed; active.

flux $j_c(\rho_c)$. For $\rho > \rho_c$ and $\rho < \frac{1}{v_{max}+1}$ the system is bistable. Starting from an initial configuration which has many jams, the jams in this case are never sorted out. The steady state is an inhomogeneous mixture of jam free regions and higher density jammed regions (see Fig. 3.8). Clearly, these jammed regions decrease the average flux in the system. It is possible, nevertheless, to prepare initial configurations that have no jams. Since all motion is deterministic in this state, the steady state will also have no jams and the flux will still be an increasing function of ρ (the dotted line in Fig. 3.7). This is possible up to densities of

$$\rho_{max} = \frac{1}{v_{max}+1},$$

leading to a maximum flux of

$$q_{max} = \frac{v_{max}}{v_{max}+1}.$$

This clearly is much higher than the flux q, for random initial conditions. It is in this sense that this system is bistable. In addition to these features, the authors studied the
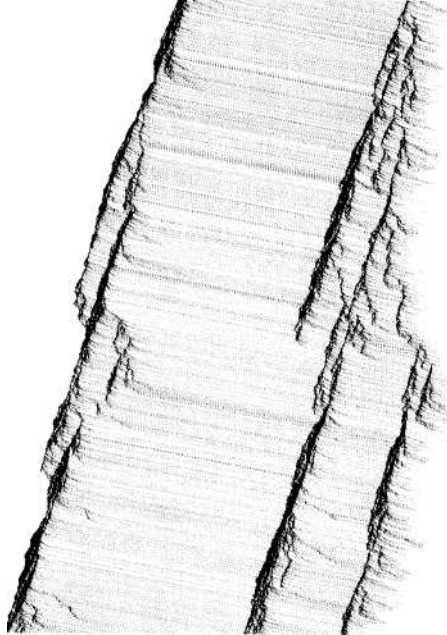
Figure 3.8: Figure extracted of Ref. [12]. Dots represent vehicles which move to the right. The horizontal direction is space and the vertical direction (down) is (increasing) time. We can see that starting from an initial configuration which has many jams, the jams never disappear.

behavior of the free regions when are perturbed. In the deterministic region, one car is randomly perturbed by reducing its velocity to zero. Many different choices for the local perturbation, however, give rise to the same large scale behavior. The perturbed car eventually reaccelerates to maximum velocity. In the meantime, though, a following car may have come too close to the perturbed car and have to slow down. This initiates a chain reaction—the emergent traffic jam. This defines the lifetime, t, of an emergent traffic jam. Using simulation the authors determine the probability distribution of jams as a function of their lifetime, t. Figure 3.9 shows that for $t > 100$, this distribution follows a power law

$$P(t) \sim t^{-\delta},$$

with $\delta = 1.5 \pm 0.01$.
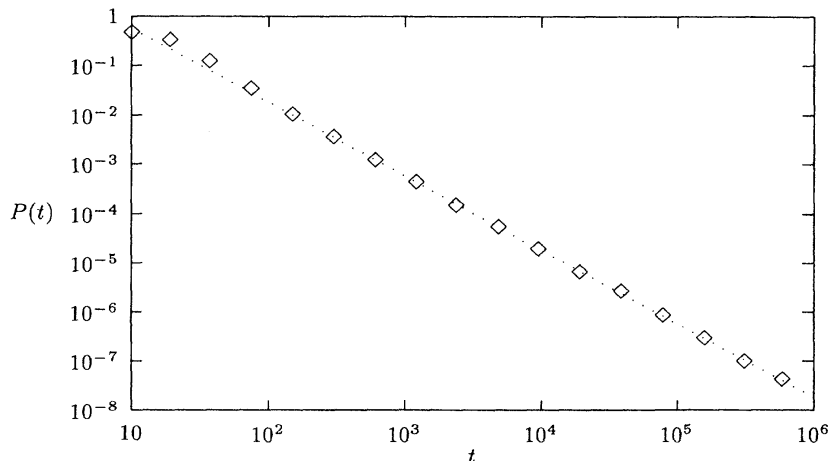
Figure 3.9: Lifetime distribution $P(t)$ for emergent jams in the outflow region; average over more than 65000 clusters (avalanches). The dotted line has slope $\frac{3}{2}$. Numerically imposed cutoff at $t = 10^6$ (figure extracted of Ref. [12]).

3.4   Fukui–Ishibashi Model

Fukui and Ishibashi [13] have introduced a simplified version of the NS model. The main difference to the NS model is the absence of a velocity memory[2]. All vehicles have an intrinsic velocity v_{max}. In each timestep, all drivers try to move at the maximum velocity v_{max}; i.e., they accelerate to it instantaneously. The Fukui–Ishibashi (FI) model is then defined by the following set of rules:

1. **Acceleration**
   The acceleration step assures that FI model does not have velocity memory since the vehicle accelerates to the maximum velocity or to the headway between it and the following vehicle, so
   $$v_n = \min[v_{max}, d_n(t)].$$

2. **Randomization**
   Only the vehicles with $v = v_{max}$ are subjected to the randomization step according to

   $$v_n \to v_{max} - 1 \quad \text{with probability } f,$$
   $$v_n \to v_{max} \qquad \text{with probability } 1 - f.$$

3. **Displacement**

   $$x_n = x_n + v_n.$$

Here, x_n and v_n denote the position and speed, respectively, of the nth vehicle and $d_n = x_{n+1} - x_n - 1$, i.e., the number of empty cells in front of this car (headway). The rules have a simple interpretation; a vehicle that has at least v_{max} empty sites in front will move v_{max} cells with probability $1 - f$ or $v_{max} - 1$ cells with probability f. However, just in the case that the headway is $d < v_{max}$ at time t, then the vehicle moves d sites in the

---

[2]In each iteration of the NS model, the velocity v and headway d have to be accounted for the update process.

38

next step. Here the randomization step is not applied. Therefore, fluctuations occur only at high speeds, which is just the opposite of the cruise-control limit.

For $v_{max} = 1$, the FI model and the NS model are identical since that in the NS model with $v_{max} = 1$, only the vehicles with $v = 1$ are subjected to the randomization step. For general v_{max}, the FI model differs from the NS model in two aspects: the increase of the vehicles speed is not necessarily gradual and the stochastic delay (deceleration step) applies only to high-speed vehicles. Due to these modifications, no overreactions at braking occur and therefore the FI model does not exhibit spontaneous jamming. This type of acceleration (where there is no need to keep track of velocities) allows to introduce a mean-field technique that provides the exact solution. These exact solutions as well as Monte Carlo simulations are shown in Fig 3.10.
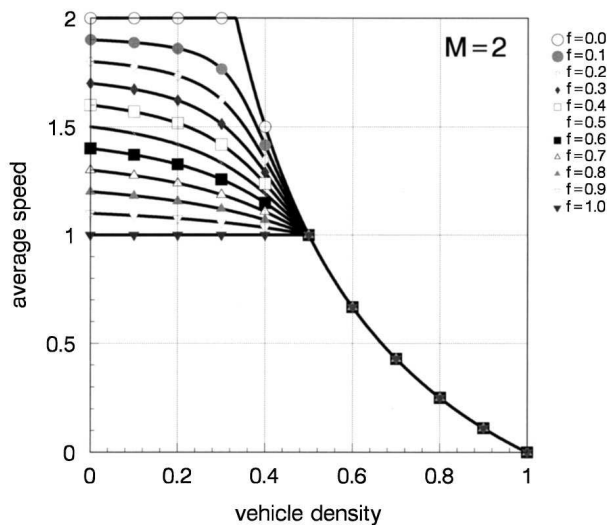
Figure 3.10: Figure extracted of Ref. [14]. The fundamental diagram of the FI model with the maximum car velocity $M = 2$ and for different values of the degree of stochastic delay f. The solid curves are the theoretical results. The points with different symbols represent results obtained by numerical simulations.

3.5 Wang Model

By using the car-oriented meanfield (COMF) was possible to achieve an exact analytical result to the FI model [14]. However, for the NS model with $v_{max} > 1$ and stochastic delay, no exact solution has been found up to now. The acceleration and stochastic delay rules of the NS model lead to complications in the time evolution of the flux, and hence it is very difficult to find exact analytical results. In order to understand how these rules affect the evolution and the corresponding asymptotic state, Wang *et al* [15] study an intermediate model that combines features of both models.

The model is described by the following update rules: Let $C_n(t)$ be the number of empty sites in front of the nth car at time t, $v_n(t)$ be the number of sites that the nth car moves during the time t step, and M the maximum speed. The steps are:

1. **Step 1**

   Let $v'_n(t) = \min(C_n(t), M)$, if $v'_n(t) = C_n(t)$ the nth car is "the car that follows the trail of the car ahead". This means that the nth car may become the neighbor of the car ahead if the car in front stops.

2. **Step 2**

   Stochastic delay is introduced in such a way that all the cars which follow the trail of their car ahead have a probability f to move forward one site less than is allowed by step 1, i.e., we have the following: $v_n(t) = v'_n(t) - 1$, with probability f, if $v'_n(t) = C_n(t)$ and $v'_n(t) > 0$.

3. **Step 3**

   The nth car moves $v_n(t)$ sites ahead.

The number of empty sites in front of the nth car at time $t + 1$ can be written as

$$C_n(t + 1) = C_n(t) + v_{n+1}(t) - v_n(t).$$

For this model, with a maximum car velocity $v_{max} = M$ and a stochastic delay probability f, the velocity of the nth car at time step t as a function of the intercar spacing $C_n(t)$ can be written as

$$v_n(t) = \begin{cases} M & \text{if } c > M, \\ c - 1 & \text{with probability } f & \text{if } 0 < c \leq M, \\ c & \text{with probability } 1 - f & \text{if } 0 < c \leq M, \\ 0 & \text{if } c = 0. \end{cases}$$

As in the FI model, this sort of acceleration allows to simplify the equations used in car-oriented mean field and produces an exact agreement between analytical and numerical (Monte Carlo) results. These results are shown in Fig. 3.11.
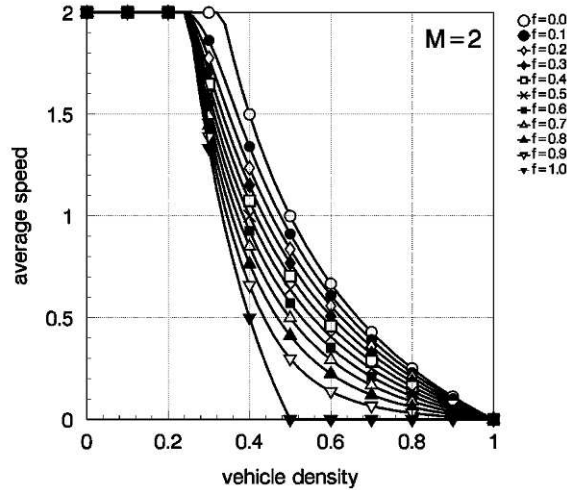
Figure 3.11:   The fundamental diagram with the maximum car velocity $M = 2$ and for different stochastic delay probabilities f. The solid curves are theoretical results. The points with different symbols represent numerical simulations. The curves from the top down along the velocity axis correspond to different values of f ranging from $f = 0$ to 1 in steps of 0.1. (Figure extracted of Ref [15].)

Although not stressed by the authors, this model presents an absorbing phase transition at $\rho_c \leq \frac{1}{M+2}$ independent of f. For densities below ρ_c the stationary state is absorbing since the mean distance between the vehicles is greater than M and according to the update rules the vehicles are not subject to the randomization step. These absorbing states are not unique since they depend on the initial configuration. For density $\rho_c = \frac{1}{M+2}$ the stationary state is unique and described by $v = M$ and $C = M + 1$.

3.6   Multilane traffic

For a realistic description of traffic on highways many authors, as discussed before, improve the NS model by using modified update rules making them more appropriate for real traffic. Despite these efforts a complete description demands the use of multilane lanes in traffic simulation. Beside the use of NS rules we know that the main ingredient required for an appropriate change of a single-lane CA model to multilane situations is lane-changing rules. Lane changing rules for two-lane traffic can be symmetric or asymmetric. For symmetric lane-changing rules, overtaking is allowed in both lanes. However, for asymmetric lane-changing rules, overtaking is forbidden in one lane, e.g., in the right lane (this situation exists in many European countries for example, Germany). Generically, the decision of drivers to change lane is based on two criteria:

1. **Incentive criterion:**
   Drivers determine whether a lane change improves the individual traffic situation, e.g., to move at their desired velocity.

$$v_a > \text{gap} \quad \text{with} \quad v_a = min(v + 1, v_{max}).$$

2. **Safety criterion:**
   The traffic situation in the target lane is checked, especially if the available gap for a lane change is enough for a security transition (without prevent the free flow of the predecessor vehicle located in other lane).

$$\begin{aligned} \text{gap}_{\text{other}} &> \text{gap}, \\ \text{gap}_{\text{back}} &\geq v_{max}. \end{aligned}$$

Here gap is the number of free cells between the car and its predecessor in the actual lane; $\text{gap}_{\text{other}}$ and gap_{back} are the headway in relation to its two neighbor cars, in the other lane, ahead and behind respectively. A lane-change is then only performed if both criteria are satisfied. In general, the update in the two-lane models is divided into two substeps: in one substep, the vehicles may change lanes in parallel following the lane-changing rules and in the other substep, each vehicle may move forward effectively as in the single-lane NS model. Drivers must find some incentive in changing the lane. Two obvious incentives are: the situation in the other lane is more convenient for driving, and the need to overtake the slow vehicle. We show some results about two-lane model using symmetric lane-changing rules, which are more relevant for traffic in towns and on highways, where overtaking in both lanes is allowed.
Fig. 3.12 shows the fundamental diagram of a periodic two-lane system. The simulations reproduce well-known results, e.g., an increase of the maximum flux per lane compared to the flux of a single-lane road. Another unexpected result is the existence of a local minimum of the lane-changing frequency near the density of maximum flux for small braking probabilities p (Fig. 3.13). The behavior of the lane-changing frequency can be explained if one takes into account the number of empty cells necessary for a lane-changing procedure. Two prerequisites have to be fulfilled in order to initiate a lane change. First, the situation on the other lane must be more convenient and second, the safety rules must be fulfilled. Therefore, one needs typically $2v_{max} + 1$ empty cells on the destination lane for a lane-changing maneuver in the free flow regime (Fig. 3.13). Hence, one finds a local maximum of the lane-changing frequency near $\rho_s = \frac{1}{2v_{max}+1}$ if the cars are ordered
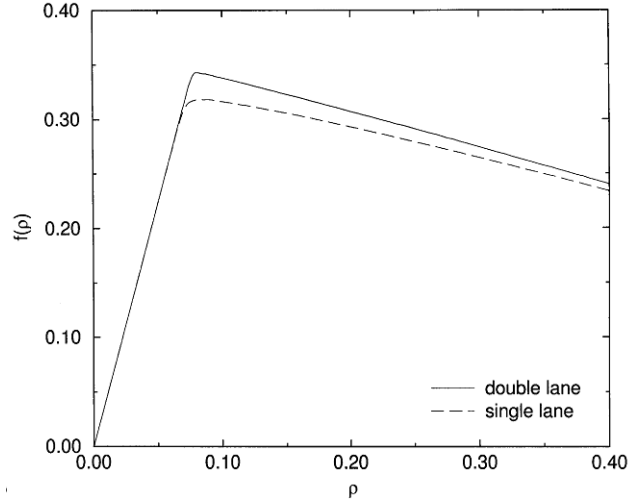
Figure 3.12: Flux per lane of the single-lane model compared with the two-lane model for systems with $v_{max} = 5$ and $p = 0.5$. (Figure extracted of Ref [16]).

homogeneously, which typically happens for small values of p. For larger values of p, e.g., $p = 0.5$, no local maximum is observable. Increasing the density for sufficiently small values of p, one finds a pronounced minimum of the lane-changing frequency. This can be understood in the limit $p \to 0$ where, for $\rho = \frac{1}{v_{max}+1}$, the cars are perfectly ordered with a gap of v_{max} sites between consecutive vehicles. Obviously, in this case both the incentive and the safety criteria are never fulfilled and the lanes are completely decoupled. For small p the ordering mechanism is still present and therefore the number of lane changes is drastically reduced near $\rho = \frac{1}{v_{max}+1}$.
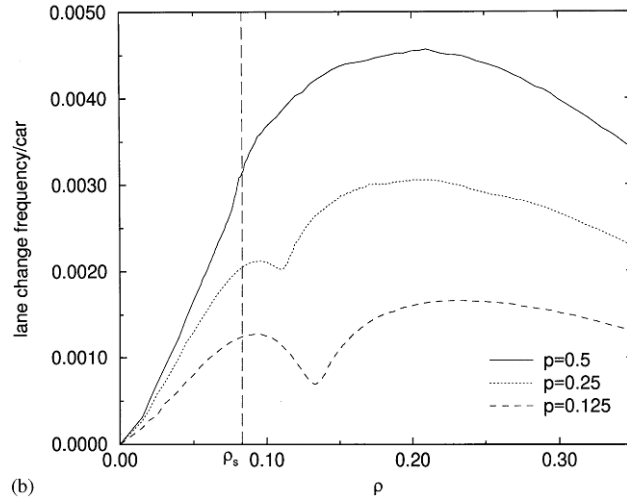
Figure 3.13: Lane-change frequency in the two-lane model for different braking parameters p (Figure extracted of Ref [16]).

The features of two-lane traffic are the same for multiple lanes (taking into account homogeneous systems). We now consider different types of cars which is obviously more relevant for practical purposes. As a first step towards realistic distributions of free flow velocities the authors [16] have chosen two types of cars, e.g., slow cars with $v^s_{max} = 3$ and fast cars with $v^f_{max} = 5$. Simulations were carried out with 5% of slow cars, which are

initially positioned randomly. The fast as well as the slow cars may use both lanes, i.e., both cars are treated equally with respect to the lane-changing behavior. In Fig. 3.14 the effects of the slow cars on the average flux of the two-lane system is compared with the fundamental diagram of a single-lane road with one slow car. Since passing is not allowed for a single-lane system, clearly the slow car dominates the average flux at low densities and platoon formation is observable. Surprisingly the two-lane system shows a quite similar behavior, although passing is allowed and the fraction of slow cars is rather small. Although the multilane traffic models can adopt a lot of different update rules, the
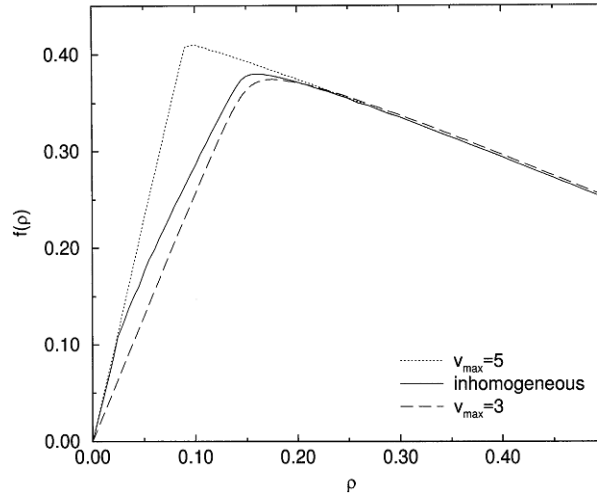
Figure 3.14: Comparison of the flux per lane of the inhomogeneous model with the corresponding homogeneous models for $p = 0.4$.(Figure extracted of Ref [16]).

results in terms of statistical point of view (criticality, phase transition etc.) do not differ when compared with one-line models. For this reason we do not extend this discussion; for a detailed description of multilane models see [17].

Chapter 4

Kinetic traffic theory

4.1   Introduction

In kinetic theory, traffic is treated as a gas of interacting particles where each particle represents a vehicle. The different versions of the kinetic theory of vehicular traffic have been developed by modifying the kinetic theory of gases. In the kinetic theory of gases, $f(\vec{r}, \vec{v}, t)d^3rd^3v$ denotes the number of molecules which, at time t, have positions lying within a volume element d^3r about $\vec{r}$ and velocities lying within the velocity-space element d^3v about v. The Boltzmann equation, which describes the time evolution of the distribution $f(\vec{r}, \vec{v}, t)$, is given by:

$$\left[\frac{\partial f}{\partial t} + \vec{v}.\nabla_r + \vec{a}.\nabla_v\right] f(\vec{r}, \vec{v}, t) = \left(\frac{\partial f}{\partial t}\right)_{coll}, \tag{4.1}$$

where the symbols ∇_r and ∇_v denote gradient operators with respect to $\vec{r}$ and $\vec{v}$, respectively, while $\vec{a}$ is the external acceleration. The term $(\frac{\partial f}{\partial t})_{coll}$ represents the rate of change of f, with time, which is caused by collisions between molecules.

In the earliest version of the kinetic theory of vehicular traffic, Prigogine and Herman[18, 19, 20] modified the kinetic theory of gases embodied in the Boltzmann equation. In their model traffic is treated as a one-dimensional gas of interacting particles (vehicles) described by a distribution function $f(x, v, t)$, such that $f(x, v, t)dxdv$ represents the number of vehicles with positions between x and $x + dx$ and velocities between v and $v + dv$ at time t. The distribution f is normalized so that

$$\int dv f(x, v, t) = c(x, t), \tag{4.2}$$

where $c(x, t)$ is the local density of vehicles. (Unless otherwise specified, all integrals run from $-\infty$ to ∞. Note that $f(x, v, t)$ is zero for $v < 0$.)

The time evolution of f is governed by a Boltzmann-like equation. The principal difference with the original Boltzmann equation is the introduction of a distribution of desired velocities, $f_0(x, v, t)$, in the relaxation term, representing drivers' preferences. Specifically, $f_0(x, v, t)dxdv$ is the number of vehicles between x and $x + dx$ whose drivers have a preferred velocity between v and $v + dv$ at time t. The presence of this function in the statistical description is a novel feature, showing that the "particles"in this system have intentions unlike a molecule, which does not have a desired velocity.

Of principal interest is the stationary velocity distribution, which can be much different from the distribution of desired velocities. We shall see that the stationary velocity distribution changes abruptly at a specific density.

4.2 The Prigogine-Herman-Boltzmann equation

In one-way traffic, vehicles travel in one dimension, and Eq. (4.1) can be simplified to read[19, 20]

$$\frac{\partial f}{\partial t} + v\frac{\partial f}{\partial x} = \left(\frac{\partial f}{\partial t}\right)_{\text{rel}} + \left(\frac{\partial f}{\partial t}\right)_{\text{int}}. \tag{4.3}$$

where $\frac{\partial f}{\partial t}_{\text{rel}}$ accounts for the relaxation of f toward f_0 in the absence of interactions of the vehicles, while $\frac{\partial f}{\partial t}_{\text{int}}$ accounts for the changes of f arising from interactions among the vehicles. Note that the term $\frac{\partial f}{\partial t}_{\text{int}}$ on the right-hand side of Eq. (4.3) may be interpreted as the analog of the term $(\frac{\partial f}{\partial t})_{coll}$ in the Eq. (4.1), whereas the term $\frac{\partial f}{\partial t}_{\text{rel}}$ in Eq. (4.3) may be interpreted as the counterpart of the term $\nabla_v.f(\vec{r},\vec{v},t)$ in the Eq. (4.1).

The idea behind the relaxation term is that drivers adjust their velocity to the desired value, v_0, on a time scale T, called the relaxation time. This assumption is embodied in the expression,

$$\left(\frac{\partial f}{\partial t}\right)_{\text{rel}} = -\frac{f - f_0}{T}. \tag{4.4}$$

In a spatially uniform system, in which $f = f(v,t)$ and interactions between drivers can be ignored, the solution to Eq. (4.3) is

$$f(v,t) = f_0(v) + [f(v,0) - f_0(v)]e^{-t/T}. \tag{4.5}$$

Exponential relaxation describes the approach of many simple systems to a steady state. In the context of the kinetic theory of gases, an analogous simplification involves replacing the collision term with an expression of the form of Eq. (4.4); T becomes the collision time, and f_0 is a local Maxwellian distribution.[21] As will become clear, Prigogine and Herman[18] proposed that T depends on the concentration of vehicles on the road, and the relaxation process subsumes some rather complicated interactions between drivers.

In the absence of interactions between the vehicles, the distribution function evolves to the distribution of desired velocities according to Eq. (4.5). A derivation of the distribution of desired velocities from first principles would require knowledge of human behavior that is beyond our present capabilities. One might try to determine the distribution of desired velocities empirically by studying the velocity distribution at very low concentrations, but we are unaware of studies of this kind. Prigogine and Herman simply investigated several simple model distributions of the desired velocities.[22]

The interaction term in Eq. (4.3) is based on the following assumptions:

1. The vehicles are point-like, that is, they do not occupy volume.

2. Vehicles remain in the same lane except when passing another vehicle.

3. In an encounter between two vehicles, one passes the other with probability P.

4. If one vehicle passes another, neither vehicle changes its velocity. In an encounter without passing, the faster vehicle reduces its velocity to that of the slower one ahead of it.

5. The slowing-down process is instantaneous.

6. Only two-vehicle interactions are considered.

7. The vehicles are statistically independent, that is, the joint two-vehicle distribution is the product of single vehicle distributions: $f(x, v, x', v', t) = f(x, v, t)f(x', v', t)$.

If we use these assumptions, we can write the interaction term as,

$$
\begin{aligned}
\left(\frac{\partial f}{\partial t}\right)_{\text{int}} &= f(x, v, t) \int_v^\infty du (1 - P)(u - v)f(x, u, t) \\
&\quad - f(x, v, t) \int_{-\infty}^v du (1 - P)(v - u)f(x, u, t).
\end{aligned}
\tag{4.6}
$$

The first term on the right-hand-side of Eq. (4.6) corresponds to interactions between vehicles with velocities v and $u > v$; the latter are obliged to adopt the smaller velocity v resulting in an increase in the number of vehicles with velocity v. The second term is related to interactions between vehicles with velocity v and $u < v$. In this case, the interaction results in a decrease in the number of vehicles with velocity v. By combining the two integrals, the interaction term can be rewritten as,

$$
\left(\frac{\partial f}{\partial t}\right)_{\text{int}} = (1 - P)f(x, v, t) \int du (u - v)f(x, u, t).
$$

Because,

$$
\int u f(x, u, t) du = c(x, t)\overline{v}(x, t),
$$

where $\overline{v}(x, t)$ denotes the local mean velocity, and

$$
\int du\, v f(x, u, t) = c(x, t)v,
$$

we have,

$$
\left(\frac{\partial f}{\partial t}\right)_{\text{int}} = (1 - P)c(x, t)[\overline{v}(x, t) - v]f(x, v, t).
\tag{4.7}
$$

If we insert the relaxation term, Eq. (4.4), and interaction term, Eq. (4.7), into Eq. (4.3), we obtain the Prigogine-Herman-Boltzmann equation for traffic:

$$
\frac{\partial f}{\partial t} + v\frac{\partial f}{\partial x} = -\frac{f - f_0}{T} + (1 - P)c(x, t)[\overline{v}(x, t) - v]f. \qquad \text{(Prigogine-Herman-Boltzmann)}
\tag{4.8}
$$

Equation (4.8) is a nonlinear equation because $\overline{v}(x, t)$ is a function (more precisely, a *functional*) of $f(x, v, t)$. A full definition of the model requires that we specify how the passing probability and relaxation time depend on the concentration. Before examining specific choices, we consider some general aspects of the solutions.

4.3   Stationary solutions

As discussed before, the quantity f_0 is a distribution function that characterizes the system in the absence of interactions between the cars. Therefore, f_0 is considered to be

that distribution function which would be achieved by drivers if the interactions between them were negligible. The function f_0 can incorporate into the theory such information as the wishes of the drivers, response of the driver-car system, speed limits, and the characteristics of the road. The term $(1 - P)c(x,t)[\overline{v}(x,t) - v]f$ represents the change in f caused by interactions in which cars, when interacting with cars ahead moving with slower speeds, either pass these cars or assume their slower speeds.

The homogeneous time-independent solution is:

$$f(v) = \frac{f_0(v)}{1 - cT(1 - P)[\overline{v} - v]}. \tag{4.9}$$

where by homogeneous we mean that f_0 is not spatially dependent. The quantity $f(v)$ describes the situation in which there is a steady state between the slowing down of cars caused by interaction processes and the speeding up of cars caused by passing.

4.4   Individual and collective flow

As indicated by Eq. (4.9), we have to distinguish between two cases

- Case A: If we consider the case in which

$$1 - Tc(1 - P)\overline{v} > 0.$$

Then the solution f in Eq. (4.9) is changed to

$$f(v) = \frac{f_0(v)}{1 + Tc(1 - P)(v - \overline{v})}. \tag{4.10}$$

This solution reduces to the ideal or desired speed distribution function in the limit of vanishing concentration. However, it is clear that this solution cannot, in general, be valid for arbitrarily high concentrations because whenever

$$1 - Tc(1 - P)\overline{v} < 0,$$

the distribution function may become negative, which is clearly impossible.

- Case B: In this case we consider:

$$1 - Tc(1 - P)\overline{v} = 0. \tag{4.11}$$

Then Eq. (4.9) reduces to

$$f(v) = \frac{f_0(v)}{Tc(1 - P)v}. \tag{4.12}$$

The important feature to be noted here is that the homogeneous equation corresponding to Eq. (4.12), namely,

$$Tc(1 - P)vf(v) = 0,$$

admits the singular solution:

$$f(v) = \alpha c\delta(v),$$

where α is an arbitrary constant and $\delta(v)$ is the Dirac delta function. Therefore, the general solution of Eq. (4.12) is of the form

$$f(v) = \frac{f_0(v)}{Tc(1-P)v} + \alpha c\delta(v).$$

The solution given in Eq. (4.10) corresponds to what may be called the individual flow pattern and is related in a simple way to the ideal or desired speed distribution function. The second solution corresponds, on the other hand, to what may be called the collective flow pattern. Indeed, as shown by Eq. (4.11), the average speed then depends only on the concentration, the probability of passing P, and the relaxation time T (both P and T are themselves functions of the concentration), and is independent of the desired speed distribution function and, therefore, of the wishes of the drivers. This solution is characterized by the occurrence of a singularity at the origin. However, the critical concentration at which the individual flow becomes collective does depend on the desired speed distribution. In both cases the time-independent solution may be written in the following form:

$$f(v) = \frac{f_0(v)}{1 + Tc(1-P)(v-\overline{v})} + \alpha c\delta(v), \tag{4.13}$$

where α is an undetermined constant that may be identically zero. This solution has to satisfy the following two requirements:

- Normalization. This means that:

$$c = \int_0^\infty \frac{f_0(v)dv}{1 + Tc(1-P)(v-\overline{v})} + \alpha c. \tag{4.14}$$

- Average Speed. Multiplying Eq. (4.13) by v and integrating, we obtain the condition

$$c\overline{v} = \int_0^\infty \frac{f_0(v)dvv}{1 + Tc(1-P)(v-\overline{v})}. \tag{4.15}$$

Eq. (4.15) with the aid of the normalization condition Eq. (4.14) maybe transformed into

$$\alpha(1 - Tc(1-P)\overline{v}) = 0.$$

We see, therefore, that we have two solutions. The first solution corresponds to $\alpha = 0$ (individual flow), whereas the second corresponds to the case

$$Tc(1-P)\overline{v} = 1,$$

with α different from zero (collective flow).

There is a striking analogy in the situation described by these equations with Bose-Einstein condensation [23]. In that case, above a certain concentration (for a given temperature) the population distribution of an ideal Bose gas splits into two parts, a regular part and a singular one. If the concentration is further increased beyond its critical value, the singular part increases relative to the regular part. However, the Bose-Einstein condensation occurs for a quantum system in thermodynamic equilibrium, whereas the situation described here is closer to a nonequilibrium stationary state.

4.5 Numerical Solutions

To simplify the notation let,

$$\gamma \equiv cT(1 - P) \text{ and } \lambda \equiv 1 - \gamma \overline{v}(f), \tag{4.16}$$

remembering the normalization condition (Eq. (4.14)) and replacing $\tilde{f}_0 = \frac{f_0}{c}$, we have:

$$1 = \int_0^\infty \frac{\widetilde{f}_0 dv}{\lambda + \gamma v}, \tag{4.17}$$

for the individual flow. As γ increases, λ decreases, and becomes zero for $\gamma = \gamma_c$ (recall that λ cannot be negative). So we can find γ_c via

$$\int \frac{\tilde{f}_0 dv}{v} = \gamma_c. \tag{4.18}$$

From this point we have a transition between individual flow to collective one and α can be found via

$$1 = \int \frac{\tilde{f}_0 dv}{\gamma v} + \alpha. \tag{4.19}$$

Prigogine and Herman [18] introduced further assumptions regarding the dependence of P and T on the concentration c, which we shall refer to as the Prigogine-Herman model. We expect the passing probability P to decrease with c, because drivers will find it more difficult to overtake a slower vehicle if adjacent lanes are congested. (If vehicles were truly point particles, there would be no such difficulty.) Prigogine and Herman assumed a linear relation between P and c, such that $P = 1$ for $c = 0$, and decreases to zero at some maximum concentration, $c_{\max}$. That is,

$$P = 1 - \eta \text{ with } \eta = \frac{c}{c_{\max}}. \tag{4.20}$$

They further proposed a concentration-dependent relaxation time,

$$T = \frac{\tau(1 - P)}{P}, \tag{4.21}$$

where τ is a constant with dimensions of time. Thus, according to Prigogine and Herman, the greater the value of c, the smaller the value of P, and the longer it takes a driver to attain the desired speed. In their model, T does not represent an intrinsic limitation of drivers (that is, a reaction time) or of their vehicles (inertia), because $T \to 0$ as $c \to 0$. Inserting Eqs. (4.20) and (4.21) in Eq. (4.16), we find,

$$\gamma = \frac{c_{\max} \tau \eta^3}{1 - \eta}. \tag{4.22}$$

For numerical studies we always use the simplified equation (4.17), remembering that γ is given by Eq. (4.22) and λ by Eq. (4.16).

4.5.1 Numerical Method

Consider the numerical solution of Eq. (4.17), yielding the value of λ such that the integral is unity, given the function $\tilde{f}_0(v)$ and γ, which is determined by the concentration via Eq. (4.22). Although the numerical method is simple, some care is required, because in some cases the integral is improper.

Among the many methods for the numerical evaluation of integrals, we choose one that is relatively simple yet accurate by fitting cubic polynomials through successive groups of four points,[24] which is equivalent to the following expression,

$$
\int_{x_1}^{x_n} y(x)dx \simeq h \left[\frac{3}{8}y_1 + \frac{7}{6}y_2 + \frac{23}{24}y_3 + y_4 + y_5 + \cdots \right.
$$
$$
\left. + y_{n-4} + y_{n-3} + \frac{23}{24}y_{n-2} + \frac{7}{6}y_{n-1} + \frac{3}{8}y_n \right],
$$

where $h = (x_n - x_1)/(n-1)$, $y_j \equiv y(x_j)$, and $x_j \equiv x_1 + (j-1)h$, for $j = 1, \dots, n$.

Dealing with an infinite range of integration requires greater care. We might truncate the integral, but the error depends on the choice of the cutoff. A more appealing alternative is to change variables to map the infinite range of integration to a finite one. For an exponential distribution of desired velocities, illustrated in Subsection 4.6 , we are led to Eq. (4.26) for which the substitution $t = e^{-v/v_0}$ results in an integral over the finite interval:

$$
1 = \int_0^1 \frac{dt}{\lambda - \gamma v_0 \ln t}. \tag{4.23}
$$

Once we have a method for evaluating the integral over velocities, we use a root-finding method to solve Eq. (4.26). For equations of the type used in Ref. [18] and the ones of interest here, the secant or Newton-Raphson methods are appropriate [25]. Although both are efficient, we will use the secant method, a recursive method used to find the solution to the equation $f(x) = 0$ via the relation,

$$
x_{n+1} = \frac{x_{n-1}f(x_n) - x_n f(x_{n-1})}{f(x_n) - f(x_{n-1})} ,
$$

starting from a pair of distinct initial values, x_1 and x_2. The idea is to follow the secant line to its x-intercept and use that as an approximation for the root. This idea is similar to the Newton-Raphson method, which follows the tangent line, but the secant method does not require knowledge of the derivative.

The computational procedure for solving Eq. (4.17) is as follows. Let $g(\lambda, n)$ be the value of the integral in Eq. (4.17) over the interval $[v_1, v_2]$, given by a function that employs the method of Eq. (4.23) using n integration points. The latter is chosen according to the desired precision, using a function $\text{int}(\lambda)$, which evaluates the integral using successively larger numbers of points, until the relative difference is smaller than a certain tolerance.

4.6 Some distributions of desired velocities

As example, we present the study of two distributions of desired velocities, the first corresponds to exponential distribution of desired velocities in which was discussed in Ref. [18] and the second corresponds to Gaussian distribution of desired velocities performed in our article attached.

4.6.1 Exponential distribution of desired velocities

As an illustration, we solve the Prigogine-Herman model for an exponential distribution of desired velocities, as discussed in Ref. [18]. Let

$$f_0 = \Theta(v)\frac{\eta c_{\max}}{v_0}e^{-v/v_0},\tag{4.24}$$

for which the mean velocity is v_0. In this case the most probable desired velocity is zero, and because $f_0(v = 0) > 0$, there is no transition. The stationary solution is

$$f = \frac{c_{\max}\eta e^{-v/v_0}}{v_0(\lambda + \gamma v)},\tag{4.25}$$

where λ is determined by the normalization condition,

$$1 = \frac{1}{v_0}\int_0^\infty \frac{e^{-v/v_0}}{\lambda + \gamma v}dv.\tag{4.26}$$

The value of λ for given values of γ and v_0 is obtained numerically as we have described.

Figure 4.1a shows the normalized flux $q/c_{\max}$ as a function of the normalized concentration $\eta = c/c_{\max}$. Note the linear relation between flux and concentration for small η. In this regime the slope of each curve depends on v_0, the average desired velocity. At high concentrations the normalized flux is independent of v_0. The mean velocity is plotted versus η in Fig. 4.1b for several values of v_0. As for the case of the normalized flux, all curves exhibit the same behavior at high concentrations.
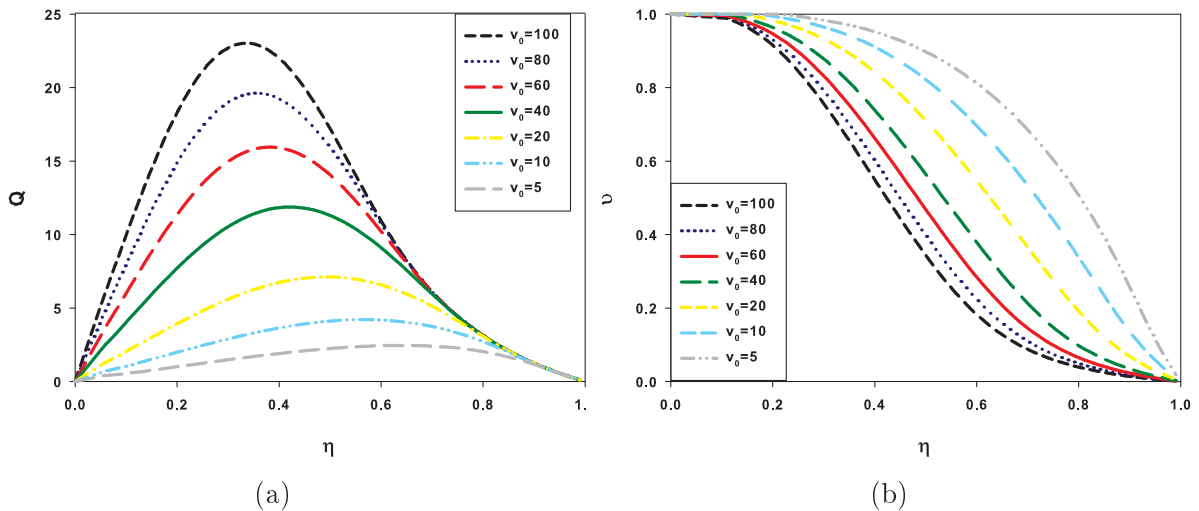
Figure 4.1: (a) The normalized flux $Q \equiv q/c_{\max}$ and (b) normalized mean velocity $v = \bar{v}/v_0$ versus the normalized concentration $\eta = c/c_{\max}$ for $c_{\max}\tau = 0.1$ and mean desired velocity v_0. At low concentrations the mean velocity is close to its desired value, and the normalized flux is proportional to v_0. At larger concentrations the normalized fluxes for different values of v_0 approach a common function.

It is interesting to compare the stationary velocity distribution with the corresponding distribution of desired velocities. Figure 4.2 shows that the stationary velocity distribution is close to the distribution of desired velocities for a relatively low concentration ($\eta = 0.2$). At a higher concentration ($\eta = 0.4$, Fig. 4.3), the two distributions differ, with higher probabilities for low velocities in the stationary velocity distribution than in the distribution of desired velocities.
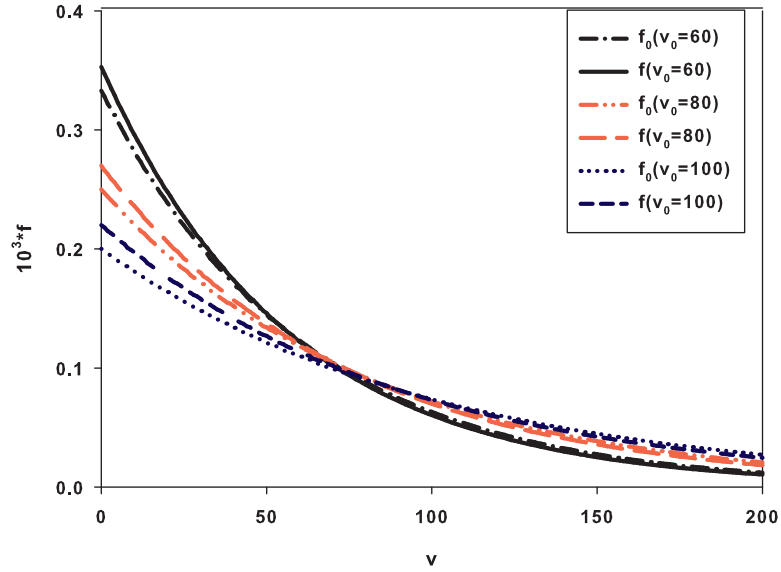
Figure 4.2: (Color online) Distribution of desired velocities (dashed lines) and stationary velocity distribution (continuous lines) for exponential desired velocity distributions with v_0 as indicated; $\eta = 0.2$. In all cases, the stationary distribution exceeds the desired one at low velocities, and vice-versa.
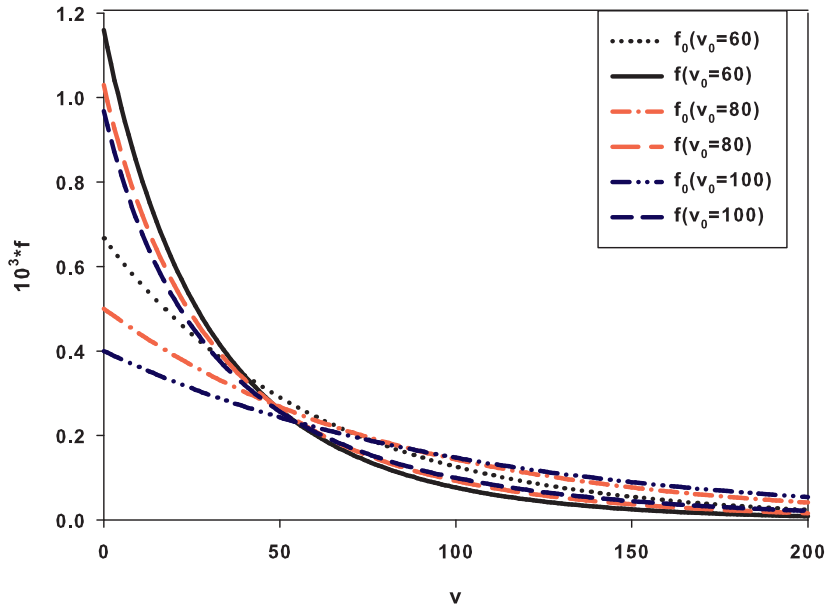
Figure 4.3: (Color online) Distribution of the desired velocity and stationary velocity distribution as in Fig. 4.2 for $\eta = 0.4$. At this concentration the differences between the stationary and desired distributions are more dramatic than in Fig. 3.

4.6.2 Gaussian distribution of desired velocities

We now consider a more realistic example that has received little attention until now – a Gaussian-like distribution of desired velocities,

$$f_0(v) = cA \left[e^{-(v-v_0)^2/v_a^2} - e^{-v_0^2/v_a^2} \right] \Theta(v) \, \Theta(2v_0 - v). \tag{4.27}$$

The parameter v_0 represents the mean desired velocity, and v_a is a measure of the dispersion of the distribution. Because of the step functions, f_0 is zero outside the interval $[0, 2v_0]$. The second term in brackets ensures that f_0 goes to zero continuously at the endpoints of this interval. The normalization factor A is approximately $(v_a\sqrt{\pi})^{-1}$ for $v_0 \gg v_a$.

Because $\int (f_0/v)dv < \infty$, there is a transition between individual and collective flow. According to Eq. (4.18), the critical point is given by

$$\gamma_c = A \int_0^{2v_0} \frac{dv}{v} \left[e^{-(v-v_0)^2/v_a^2} - e^{-v_0^2/v_a^2} \right],$$

which is readily evaluated numerically. We proceed as before and calculate the stationary velocity distribution, $f(v)$, and the stationary mean velocity and flux. Figure 4.4 shows the flux Q as a function of normalized concentration for several values of v_0, and $v_a = 20$. As expected, the slope of $q(\eta)$ jumps from a positive to a negative value at the transition from individual to collective flow. In the latter regime, $q(\eta)$ is characterized by a single function, independent of v_0. The larger the value of v_0, the smaller the critical density η_c.
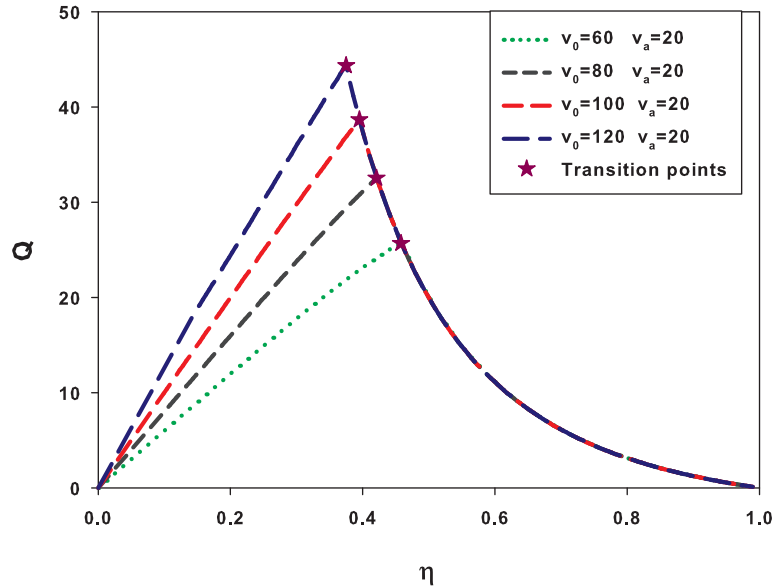
Figure 4.4: (Color online) The flux Q as a function of the normalized concentration η in the Prigogine-Herman model using the distribution of desired velocities of Eq. (4.27), with $v_a = 20$. The transition points are $\eta_c = 0.375$, 0.395, 0.421, and 0.458, for for $v_0 = 120$, 100, 80, and 60, respectively. Above the critical concentration, the flux follows a master curve independent of v_0.

A notable aspect of the transition is the sudden change in the stationary distribution at the critical concentration at which the distribution splits into a regular and a singular part. In Fig. 4.5, which compares the stationary velocity distribution and distribution of desired velocities for several concentrations in the individual flow regime, we see that the two distributions have the same area, as required by normalization. For $\eta = 0.15$ the distributions are indistinguishable; at higher concentrations small differences appear. The critical concentration, $\eta_c = 0.421$, represents the limit for individual flow; for $\eta > \eta_c$ the stationary velocity distribution is the sum of a regular part, given by $f_0/(\gamma v)$, and a singular part, $\alpha c\delta(v)$, with α given by Eq. (4.19). In Fig. 4.6 we compare the regular

part of the stationary velocity distribution with the corresponding distribution of desired velocities for $\eta > \eta_c$. The area of the regular part of the stationary velocity distribution is smaller than that of the distribution of desired velocities. The difference corresponds to the δ-function at the origin.
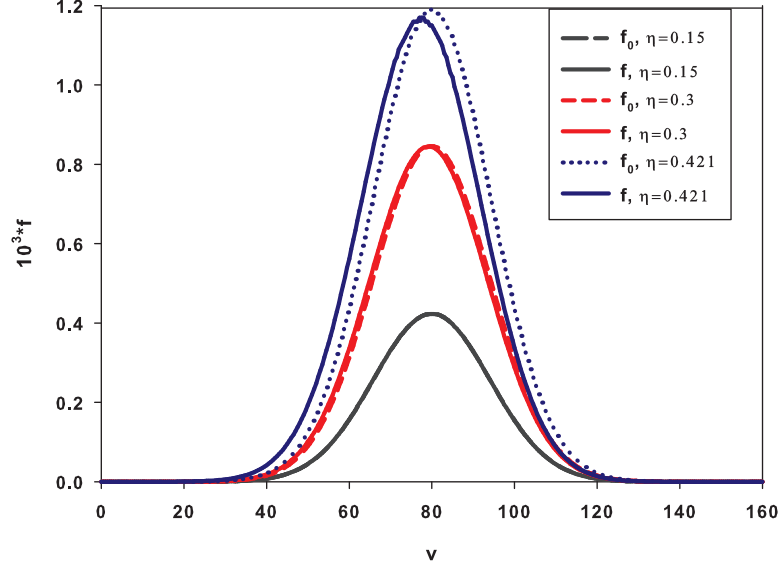
Figure 4.5: The stationary velocity distribution (solid line) and corresponding distribution of desired velocities (dashed line), for concentrations in the individual flow regime. The distribution of desired velocities is given by Eq. (4.27) with $v_0 = 80$ and $v_a = 20$. The difference between the stationary and desired distributions grows with increasing concentration.

4.7   Paveri-Fontana model

In the basic Prigogine-Boltzmann (PB) model, the changes of vehicular speeds are assumed to be due to two main processes: the binary interaction process (namely, the slowing down process undergone by a fast car which encounters a slow one); and the relaxation process (the process due to the change in speed which occurs when a driver accelerates a vehicle towards a desired speed). Employing a set of appropriate assumptions, the original Prigogine-Boltzmann equation was proposed, for the case where drivers do not change their desired speeds according to traffic conditions. In order to account for the adaptive behavior of drivers, that is in order to account for the fact that traffic conditions do actually affect the "programs" (desired speeds) of drivers, an adjustment term was introduced on the right side of the basic Prigogine-Boltzmann equation by Paveri-Fontana. Let $g(x, v, t; \omega)$ be the one-vehicle distribution function for vehicles whose desired speed is ω. Namely, let $g(x, v, t; \omega) dx dv d\omega$ equal the (expected) number of vehicles, at time t, in dx (around x) and dv (around v) with desired speed in $d\omega$ (around ω). Then one finds that:

$$f(x, v, t) = \int_0^\infty g(x, v, t; \omega) d\omega \quad \text{and} \quad f_0(x, \omega, t) = \int_0^\infty g(x, v, t; \omega) dv,$$

where $f(x, v, t)$ and $f_0(x, \omega, t)$ are the previously defined one-vehicle speed distribution function and desired speed distribution function, respectively. Vehicular concentration
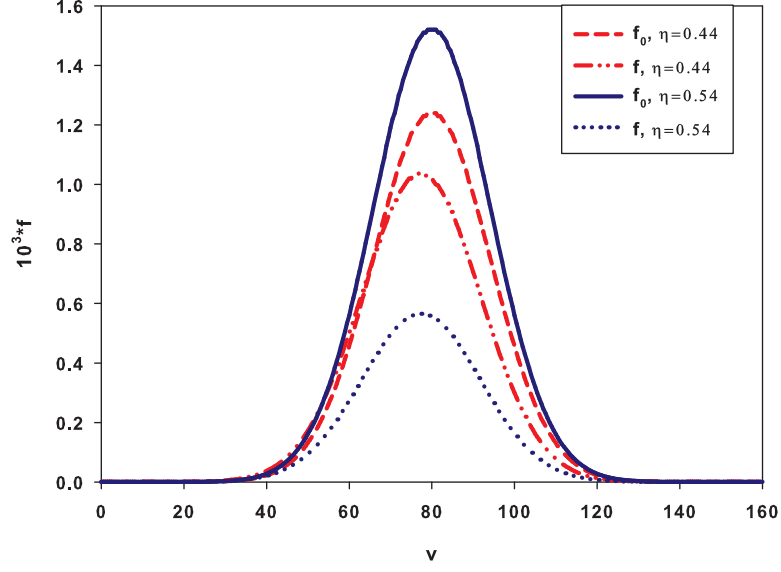
Figure 4.6: Regular part of the stationary velocity distribution (solid line) and the corresponding distribution of desired velocities (dashed line) for densities in the collective flow regime; parameters as in Fig. 4.5. Note the differences in amplitude between the stationary and desired distributions, associated with a population of cars having velocity zero in the stationary distribution.

$c(x,t)$ and flux $q(x,t)$ are defined by:

$$c(x,t) = \int_0^\infty \int_0^\infty g(x,v,t;\omega)d\omega dv \quad \text{and} \quad q(x,t) = \int_0^\infty \int_0^\infty vg(x,v,t;\omega)d\omega dv$$

the assumptions regarding the interaction term are the same as those employed by PB. so

$$\left(\frac{\partial f}{\partial t}\right)_{\text{int}} = f(x,v,t)\int_v^\infty (1-P)(u-v)g(x,u,t;\omega)du$$

$$- g(x,v,t;\omega)\int_{-\infty}^v du(1-P)(v-u)f(x,u,t).$$

The improved Prigogine-Herman equation is:

$$\left[\frac{\partial}{\partial t} + v\frac{\partial}{\partial x}\right]g(x,v,t;\omega) + \frac{\partial}{\partial v}\left[\frac{\omega-v_0}{T}g(x,v,t;\omega)\right] =$$

$$f(x,v,t)\int_v^\infty (1-P)(u-v)g(x,u,t;\omega)du$$

$$-g(x,v,t;\omega)\int_{-\infty}^v du(1-P)(v-u)f(x,u,t),$$

with

$$f(x,v,t) = \int_0^\infty g(x,v,t;\omega)d\omega.$$

The term $\partial/\partial v[[(\omega-v)/T]g(x,v,t;\omega)]$ is related to relaxation. Different from original PB model for each x value, we expect that a vehicle with initial velocity v_0 approaches to its desirable velocity ω according to:

$$v(t) = \omega - (w-v_0)exp^{-t/T}.$$

The acceleration of a vehicle moving with initial speed v_0 and desired speed ω is

$$a = \frac{w - v_0}{T}.$$

To compare the equation proposed here with the original PB equation, note that the main change depends on the introduction of $g(x, v, t; \omega)$. The collision process is described in the same way in both treatments. The description of the time relaxation process is based, in both approaches, on assumption I (existence of a unique time relaxation) and assumption II (no changes in driving programs): assumption III (on the exponential approach to the desired velocity) replaces the assumption of an exponential relaxation. The main shortcoming of the Paveri-Fontana equation is the difficulty encountered in seeking analytical solutions when the collisional process cannot be neglected. In this sense, the PB equation is much easier to manipulate. Nevertheless this contribution has been used extensively in recent approaches in kinetic models. Wagner *et al.* [26] proposed a traffic flow model using the desired velocity proposed by Paveri and Fontana [27]. By taking into account the nonzero length of vehicles, these authors extend the description of Paveri and Fontana to the high-density regime. In Ref. [28] a successive slowing-down process is considered, in which drivers react to traffic conditions in a more cautious manner.

Chapter 5

ANaSch Model

5.1   Introduction

The Nagel-Schreckenberg (NS) model holds a central position in traffic modeling via cellular automata, because it reproduces features commonly found in real traffic, such as the transition between free flow and a jammed state, start-and-stop waves, and shocks (due to driver overreaction) [3]. This simple model represents the effect of fluctuations in driving behavior by incorporating a stochastic element: the spontaneous reduction of velocity with probability p.

Although the NS model has been studied extensively, the nature of the transition between free and jammed flow, in particular, whether it corresponds to a critical point, remains controversial [5, 4, 7, 29]. A proposed definition of the order parameter in the NS model [30], and a subsequent comment [31, 32] are pertinent to this issue. According to the authors of Ref. [31], results for the lifetime distribution, spatial correlations, and relaxation time provide evidence for a "crossover type jamming transition"from free flow to the jammed regime, but not for a well defined phase transition.

In the original NS model, at each time step (specifically, in the reduction substep), a driver with nonzero velocity reduces her speed with probability p. Here we propose a simple yet crucial modification, eliminating changes in speed in this substep when the distance to the car ahead is greater than the current speed. We believe that this rule reflects driver behavior more faithfully than does the original reduction step, in which drivers may decelerate for no apparent reason. While one might argue that distractions such as cell phones cause drivers to decelerate unnecessarily, we can expect that highways will be increasingly populated by driverless vehicles exhibiting more rational behavior. The modified model, which we call the Absorbing Nagel-Schreckenberg (ANS) model, exhibits a line of absorbing-state phase transitions between free and congested flow in the $\rho - p$ plane. (Here ρ denotes the *density*, i.e., the number of vehicles per site.) The modification proposed here allows us to understand the nature of the phase transition in the original model, and to identify a proper order parameter. The ANS model exhibits a surprising reentrant phase diagram. Some time ago, Wang studied a model with the same modified reduction step, and found that free flow is absorbing for all densities $\leq 1/7$, regardless of p [15]. This model differs from ours in that acceleration to the maximum allowed speed occurs in a single update, rather than in increments.

Regarding the nature of the phase transition in the original NS model, the key insight is that, for $p = 0$, it exhibits a transition between an absorbing state (free flow) and an active state (congested flow) at density $\rho = 1/(v_{max}+1)$, where v_{max} denotes the maximum

speed. Free flow is absorbing because each car advances the same distance in each time step, so that the configuration simply executes rigid-body motion (in the co-moving frame it is frozen). We note that for $\rho < 1/(v_{max} + 1)$, many absorbing configurations exist; which one is attained by the dynamics depends on the initial condition. Congested flow, by contrast, is active in the sense that the distances between vehicles change with time. Below the critical density, activity (if present initially) dies out, and an absorbing configuration is reached; for $\rho > 1/(v_{max} + 2)$ there must be activity, due to lack of sufficient space between vehicles. Setting $p > 0$ in the original model is equivalent to including a *source* of spontaneous activity. Since such a source eliminates the absorbing state [33], the original NS model *does not possess a phase transition for $p > 0$*. (It should nonetheless be possible to observe scaling phenomena as $p \to 0$.) A similar conclusion was reached by Souza and Vilar [29], who drew an analogy between the phase transition at $p = 0$ and a quantum phase transition at temperature $T = 0$. In their analogy, $p > 0$ corresponds to $T > 0$, for which, *sensu stricto*, there is again no phase transition.

5.2 Model

The NS model and its absorbing counterpart (ANS) are defined on a ring of L sites, each of which may be empty or occupied by a vehicle with velocity $v = 0, 1, ..., v_{max}$. (Unless otherwise noted, we use $v_{max} = 5$, as is standard in studies of the NS model.) The dynamics, which occurs in discrete time, conserves the number N of vehicles; the associated intensive control parameter is $\rho = N/L$. Denoting the position of the i-th vehicle by x_i, we define the headway $d_i = x_{i+1} - x_i - 1$ as the number of empty sites between vehicles i and $i + 1$. Each time step consists of four substeps, as follows:

- Each vehicle with $v_i < v_{max}$ increases its velocity by one unit: $v_i \to v_i + 1$

- Each vehicle with $v_i > d_i$ reduces its velocity to $v_i = d_i$.

- NS model: each vehicle reduces its velocity by one unit with probability p.
  ANS model: each vehicle with $v_i = d_i$ reduces its velocity by one unit with probability p.

- All vehicles advance their position in accord with their velocity.

In practice, given the velocities v_i and headways d_i, there is no need to keep track of positions: the final substep is simply $d_i \to d_i - v_i + v_{i+1}$ for $i = 1, ..., N - 1$, and $d_N \to d_N - v_N + v_1$.

The modification of the third substep leads to several notable changes in behavior, as reflected in the fundamental diagram shown in Fig. 5.1, which contrasts the flux-density relation in the NS and ANS models. In the ANS model the flux exhibits a discontinuous first derivative at a certain density $\rho_c(p)$ (for any p between zero and one), while in the NS model the flux and other observables are smooth functions of density for $p > 0$. Thus the ANS model exhibits a phase transition for general p, whereas the NS model has a phase transition only for $p = 0$ [30, 31]. The flux q generally takes its maximum value at the transition. (For small p, however, maximum flux occurs at a density above $\rho_c = 1/(v_{max} + 2)$, approaching $\rho = \frac{1}{v_{max}+1}$ for $p = 0$). The low-density, absorbing phase has $v_i = v_{max}$ and $d_i \geq v_{max} + 1$, $\forall i$; in this phase all drivers advance in a deterministic manner, with the flux given by $j = \rho v_{max}$. In the active state, by contrast, a nonzero
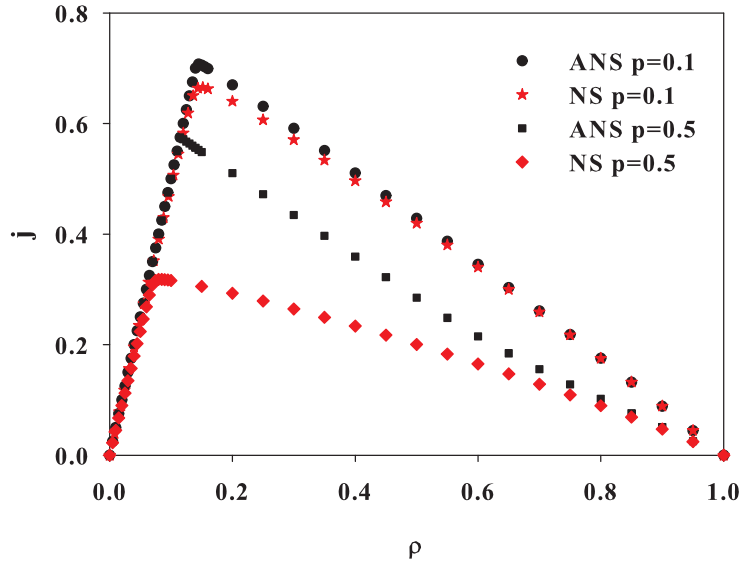
Figure 5.1: (Color online) Flux j versus density in the NS and ANS models for probabilities $p = 0.1$ (upper) and $p = 0.5$ (lower). System size $L = 10^5$; vehicles are distributed randomly at $t = 0$. Error bars are smaller than symbols.

fraction of vehicles have $d_i \leq v_{max}$. For such vehicles, changes in velocity are possible, and the configuration is nonabsorbing. The stationary fluxes in the NS and ANS models differ significantly over a considerable interval of densities, especially for high values of p. Below the critical density ρ_c, this difference is due the existence of an absorbing phase in the ANS model. For densities slightly above ρ_c, most vehicles have velocity $v_i = v_{max}$ and $d_i = v_{max} + 1$, although there is no absorbing state. As the density approaches unity, the differences between the fluxes in the ANS and NS models become smaller.
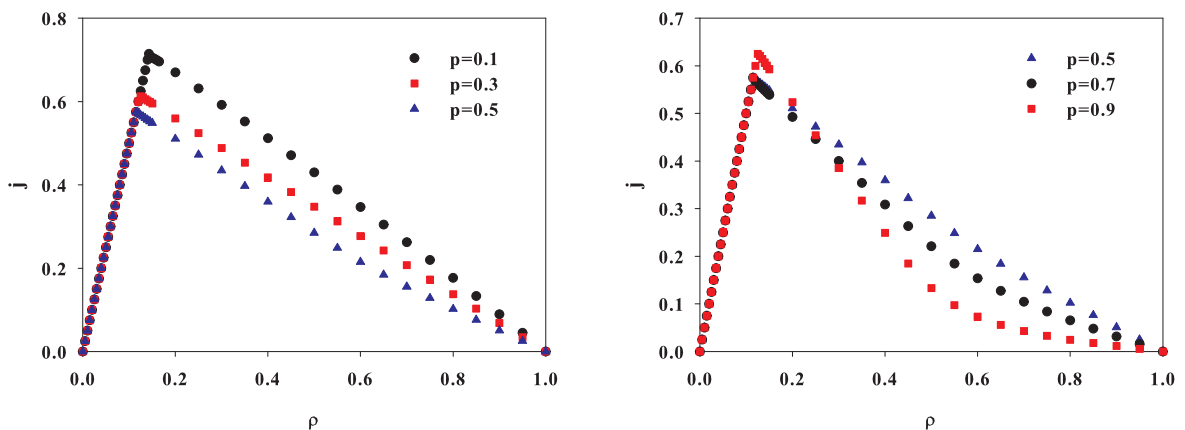
Figure 5.2: (Color online) Steady-state flux versus density in the ANS model for (a) $p = 0.1$, 0.3 and 0.5, and (b) $p = 0.5$, 0.7 and 0.9. Note that the density of maximum flux first decreases, and then increases, with increasing p; the minimum occurs near $p \simeq 0.5$. System size $L = 10^5$; vehicles are distributed randomly at $t = 0$. Error bars are smaller than symbols.

For fixed deceleration probability p, the flux $j = \rho \overline{v}$ first grows, and then decreases as we increase the vehicle density ρ. An intriguing feature is the dependence of the density

at maximum flux on the probability p: Fig. 5.2 shows that the density at maximum flux decreases with increasing p until reaching a minimum near $p = 0.5$, and subsequently increases with increasing p. This reflects the reentrant nature of the phase diagram, as discussed in Sec. 5.3.

5.2.1 Models with Many Absorbing States

The universality of DP (directed pecolation) critical behavior for models with a unique absorbing state is well established, models such as the contact process (CP), Schlögl's first model, and monomer-dimer model of Ziff, Gulari, and Barshad (ZGB) belong to the same universality class. The study of many other models demonstrates the robustness of DP critical behavior in spite of quite dramatic differences in the evolution rules of the various models. Presently there is substantial evidence in favor of the hypothesis that models with a scalar order parameter exhibiting a continuous transition to a unique absorbing state generically belong to the universality class of directed percolation. For models with more than one absorbing state there are no clear ideas about the possible universality classes.

A new kind of critical behaviour at an absorbing-state phase transition was first demonstrated by Grassberger, Krause, and von der Twer in a study of a model involving the processes $X \rightarrow 3X$ and $2X \rightarrow 0$. This model is very similar to a class of models known as branching annihilating walks (BAW). In the BAW a particle jumps, with probability p, to a nearest neighbor, and if this site is occupied both particles are annihilated. With probability $1 - p$ the particle produces n offspring which are placed on the neighboring sites. If an offspring is created on a site which is already occupied, it annihilates with the occupying particle leaving an empty site. For n even these models have non-DP behavior, while for n odd the behavior is compatible with DP. Note that in both the model proposed by Grassberger, Krause, and von der Twer and in BAW with an even number of offspring the number of particles is conserved modulo 2. This conservation law might be responsible for the non-DP behaviour. So due the importance in studying the critical behaviour of systems with many absorbing states, we present a brief discussion about two models that show many absorbing states and have DP behaviour. These models are Dimer reaction model (DR) and pair contact process (PCP).

In a one-dimensional lattice the DR model [34] particles may not occupy neighboring sites. If sites i, $i - 1$, and $i + 1$ are vacant, we say that site i is open; adsorption happens only at open sites. If we think of the sites as corresponding to bonds in the dual lattice, the particles correspond to dimers occupying bonds in the dual lattice[1]. Suppose a particle has just arrived at site i. If sites $i - 3$, $i - 2$, $i + 2$, and $i + 3$ are all vacant, the particle remains. If any of the four sites is occupied, the new particle reacts with one other particle with probability $1 - p$ and remains with probability p. The second neighbors have priority in the reaction: the new particle can react with a third neighbor only if both second-neighbor sites are empty. The reaction rules are illustrated in Fig. 5.3. We note that reactions with third neighbors are essential, for without them there is no active steady state even for $p = 0$. There are many absorbing configurations for the DR: any configuration without a three-site vacancy cluster, i.e., devoid of open sites.

---

[1]The lattice points of the dual lattice are defined by the centers of the unit cells of the lattice. A bond in the dual lattice is placed wherever it does not cross a bond of the lattice.
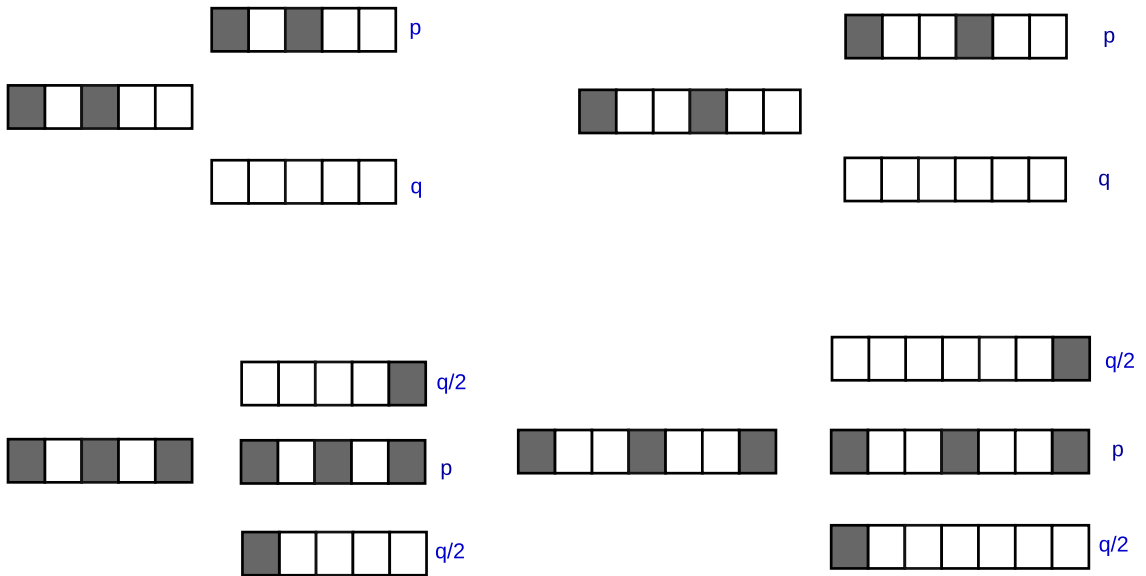
Figure 5.3: Illustrative picture shows dimer reaction rules involving a newly adsorbed particle (at the center of the cluster) and a second or third neighbor.

Of these absorbing states, the one with maximal particle density consists of alternating vacant and occupied sites; in the one with minimal density, occupied sites alternate with pairs of vacant sites. Clearly any sequence *ogogogog*, where *o* means occupied and *g* can be a one- or two-site gap, is absorbing.

In Jensen's pair contact process PCP [35], each site of the one-dimensional lattice Z is either vacant or occupied by a particle. Each nearest-neighbor (NN) pair of particles has a rate p of mutual annihilation, and a rate $1 - p$ of attempted creation. In a creation event involving particles at sites i and $i+1$, a particle may appear (with equal likelihood) at site i $i-1$ or at $i+2$, provided the chosen site is vacant. (Attempts to place a particle at an occupied site fail.) In an annihilation event, a NN pair of particles is removed. The rules are illustrated in Fig. 5.4 (a) and the possible absorbing states are shown in 5.4 (b).

In the ANS model the density $\rho = 1/7$ has an only absorbing configuration composed by a homogeneous distribution (one vehicle followed by six empty cells). For densities $\rho < 1/7$, many states are absorbing since $d_i \geq 6$ and $\sum_{i=1}^{n} d_i = (1-\rho)L/\rho$. We show in fig 5.5 the unique absorbing configuration for $\rho = 1/7$ and possible absorbing configurations for $\rho = 1/8$ and $1/9$. We discuss in the following sections the critical exponents of ANS model and its universality class.

5.2.2 Special cases: $p = 0$ and $p = 1$

For the extreme values $p = 0$ and $p = 1$ the ANS model is deterministic; these two cases deserve comment. For completeness we mention the corresponding results pertaining to the NS model given in [36], which also includes a discussion of mean field theories. For $p = 0$, the NS and ANS models are identical. The system reaches an absorbing state, $v_i = v_{max}$, $\forall i$, for densities $\rho \leq 1/(v_{max} + 1)$. For higher densities we observe nonzero activity in the steady state. We note however that there are special configurations, in which $v_i = d_i$, $\forall i$, with some $v_i < v_{max}$, whose evolution corresponds to a rigid rotation of the pattern. (A simple example is $v_i = d_i = n$, $\forall i$, with $n = 1, 2, 3$ or 4, and density
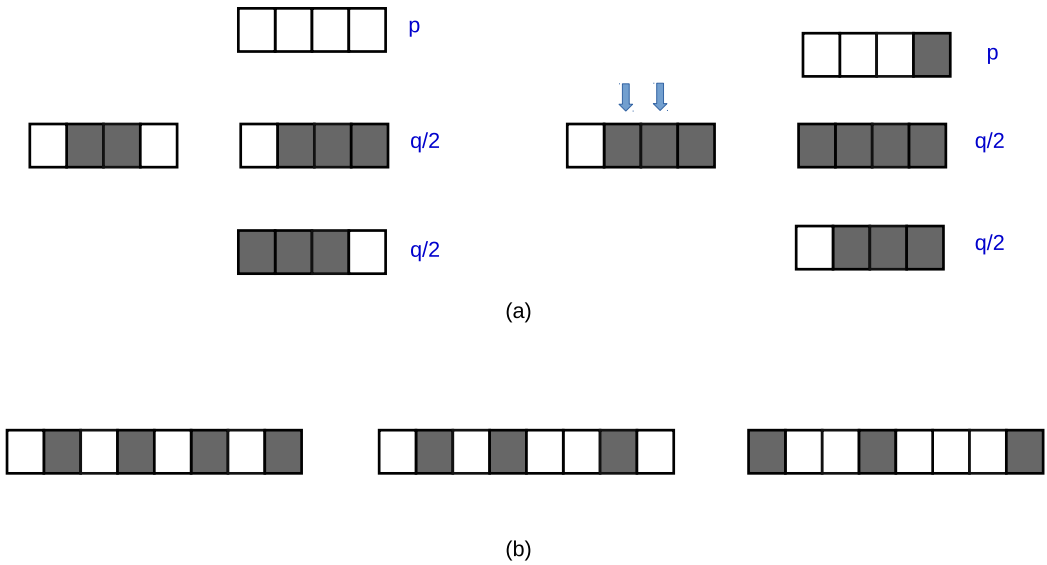
Figure 5.4: Illustrative picture shows the update rules of PCP model (a). Possible absorbing configurations (b).
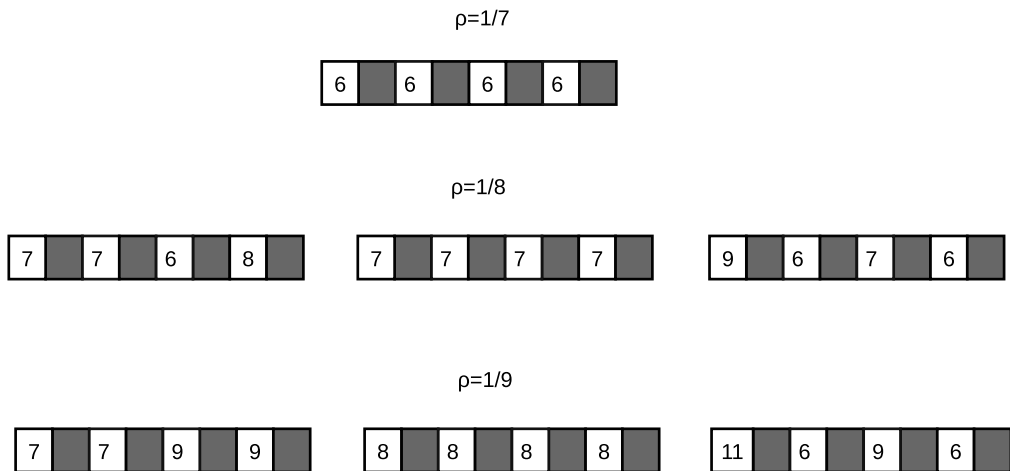
Figure 5.5: Illustrative picture shows the possible ANS absorbing configurations for densities $\rho = 1/7$, $1/8$ and $1/9$. Note that for $\rho = 1/7$ the absorbing configuration is unique.

$\rho = 1/(n+1)$.) Since our interest here is in the model with $0 < p < 1$ we do not comment further on such configurations.

For the NS model with $p = 1$, from one step to the next, each velocity v_i is nonincreasing. (Of course $v_i \to v_i + 1$ at the acceleration substep, but this is immediately undone in the subsequent substeps.) Thus if the evolution leads to a state in which even one vehicle has velocity zero, all vehicles eventually stop. Such an event is inevitable for $\rho > 1/3$, since in this case $d_i \leq 1$ for at least one vehicle, which is obliged to have $v_i = 0$

after one step. For $\rho \leq \frac{1}{3}$, steady states with nonzero flux are possible, depending on the choice of initial condition. Such configurations are *metastable* in the sense that the stationary state depends on the initial distribution. In the ANS model with $p = 1$ the mean velocity in steady state is zero only for $\rho \geq 1/2$. For $\rho \leq 1/(v_{max} + 2)$, we find that the system always reaches an absorbing configuration with $\overline{v} = v_{max}$. In the remaining interval, $1/(v_{max} + 2) < \rho \leq 1/2$, we find $\overline{v} = 1 - 2\rho$.

Figure 5.6: Fundamental Diagram for ANS model with $p = 1$.

5.3 Phase diagram

5.3.1 Initial condition dependence

In studies of traffic, states are called *metastable* if they can be obtained from some, but not all initial conditions [37, 38, 11, 39, 40]; such states are an essential component of real traffic. Since the NS model is not capable of reproducing this feature, models with modified update rules have been investigated by several authors [37, 38, 11]. In the ANS model, by contrast, there is a region in the $\rho - p$ plane in which, depending on the initial condition, the system may evolve to an active state or an absorbing one. Our results are consistent with the usual scenario for absorbing-state phase transitions [33, 41, 42]: activity in a finite system has a finite lifetime; in the active phase, however, the mean lifetime diverges as the system size tends to infinity. Properties of the active phase may be inferred from simulations that probe the *quasistationary regime* of large but finite systems [44].

To verify the existence of metastable states in the ANS model, we study its evolution starting from two very different classes of initial conditions (ICs): homogeneous and jammed. In a homogeneous IC, the headways d_i are initially uniform as possible, given the density $\rho = 1/(1 + \overline{d})$, where $\overline{d}$ denotes the mean headway. In this case the initial velocity is v_{max} for all vehicles. In a jammed IC, N vehicles occupy N contiguous sites, while the remaining $N(\rho^{-1} - 1)$ sites are vacant; in this case $d_i = 0$ for $i = 1, ..., N - 1$,

and only vehicle N has a nonzero initial velocity ($v_N = v_{max}$). Homogeneous ICs are much closer to an absorbing configuration than are jammed ICs. We note that random initial conditions lead to the same steady state as jammed ICs.
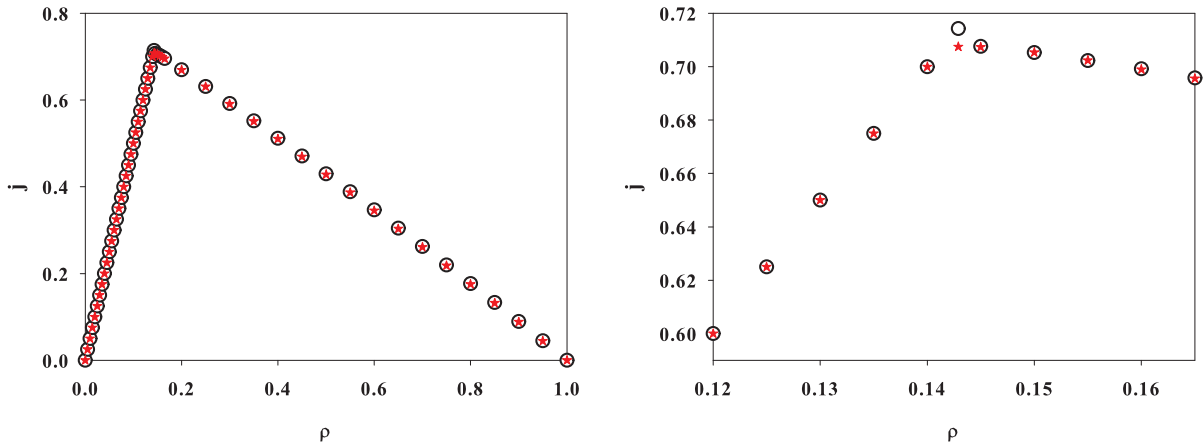
Figure 5.7: (Color online) Steady-state flux versus density for $p = 0.1$ and $L = 10^5$. Homogeneous (stars) and jammed (circles) ICs lead to identical stationary states (panel a) except for a small interval of densities near maximum flux highlighted in panel b. Error bars are smaller than symbols.

Figure 5.7 shows the fundamental diagram obtained using homogeneous and jammed ICs for $p = 0.1$; for this value of p the stationary state is the same, regardless of the IC, except near $\rho = \frac{1}{7}$ where, for the homogeneous ICs, an absorbing configuration is attained, having a greater steady-state flux than obtained using jammed ICs. For higher probabilities p, we find a larger interval of densities in which the stationary behavior depends in the choice of IC. In Fig. 5.8, for $p = 0.5$, this interval corresponds to $0.118 \leq \rho \leq 0.143$; higher fluxes (black points) are obtained using homogeneous ICs, and lower fluxes (red) using jammed ICs. Homogeneous ICs rapidly evolve to an absorbing configuration, while jammed ICs, which feature a large initial activity, do not fall into an absorbing configuration for the duration of the simulation ($t_{max} = 10^7$), for the system size ($L = 10^5$) used here. In Fig. 5.8, the flux obtained using jammed ICs (red stars) exhibits a discontinuous first derivative, signaling a continuous phase transition. The flux for homogeneous ICs (black circles), exhibits a downward jump at $\rho = 1/7$. While the latter might be interpreted as evidence of a discontinuous phase transition, we note that the absorbing state, to which homogenous ICs evolve for smaller densities, ceases to exist for $\rho > 1/7$. Thus $\rho = 1/7$ can be seen as the terminal line of the absorbing phase. As in sandpile models, the absorbing-state phase transition occurs at a smaller density (in the ANS model, that marking the discontinuity in the derivative of j), at which a nonabsorbing (active) phase first appears. For $0 < p < 1$, the properties of the active phase (obtained using either jammed or random ICs) are nonsingular at $\rho = 1/7$.

Systematic investigation of the steady-state flux obtained using homogeneous and jammed ICs leads to the conclusion that the ρ - p plane can be divided into three regions. To begin, we recall that for $\rho > 1/(v_{max} + 2)$ and $p > 0$, the mean velocity $\overline{v}$ must be smaller than v_{max}. Thus the activity is nonzero and the configuration (i.e., the set of values v_i and d_i) changes with time. In this region, homogeneous and jammed ICs always lead to the same steady state.

For $\rho \leq 1/(v_{max} + 2)$, absorbing configurations exist for any value of p. There is nevertheless a region with $\rho < 1/(v_{max} + 2)$ in which activity is long-lived. In this region,
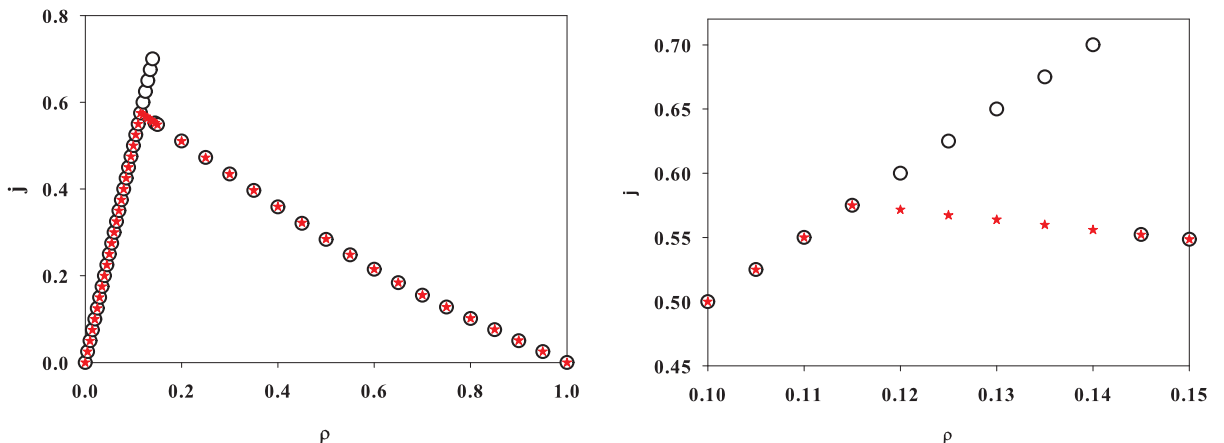
Figure 5.8: (Color online) Steady-state flux versus density as in Fig. 5.7, but for $p = 0.5$.

which we call the *active phase*, the steady state depends on whether the IC has little activity (homogeneous) or much activity (jammed). For smaller densities, all ICs evolve to an absorbing configuration; we call this the *absorbing phase*. The boundary between the active and absorbing phases, determined via the criterion of different steady states for homogeneous and jammed ICs, is shown in Fig. 5.9. We note that in Wang's model [15] there are only two regions: an absorbing phase for $\rho \leq 1/7$ and an active one for $\rho > 1/7$.

Our results are consistent with the following scenario, familiar from the study of phase transitions to an absorbing state [33, 41, 42]: for finite systems, all ICs with $\rho < 1/(v_{max} + 2)$ and $p > 0$ eventually fall into an absorbing configuration. Within the active phase, however, the mean lifetime of activity grows exponentially with system size. The phase boundary represents a line of critical points, on which the lifetime grows as a power law of system size. (Further details on critical behavior are discussed in Sec. 5.4.) A surprising feature of the phase boundary is that it is *reentrant*: for a given density in the range $0.116 < \rho < 1/(v_{max} + 2)$, the absorbing phase is observed for both small and large p values, and the active phase for intermediate values. The reason for this is discussed in Sec. III.C. We denote the upper and lower branches of the phase boundary by $p_+(\rho)$ and $p_-(\rho)$, respectively; they meet at $\rho_{c,<} \simeq 0.116$.

The phase boundary is singular at its small-p limit. As p tends to zero from positive values, the critical density approaches $1/7$, but for $p = 0$ the transition occurs at $\rho = 1/6$. The phase diagram of the ANS model for $0 < p < 1$ is similar to that of a stochastic sandpile [45, 46]. In the sandpile, there are no absorbing configurations for particle density $\rho > z_c - 1$, where z_c denotes the toppling threshold; nevertheless, the absorbing-state phase transition at a density strictly smaller than this value. Similarly, in the ANS model there are no absorbing configurations for $\rho > 1/7$, but the phase transition occurs at some smaller density, depending on the deceleration probability p. Further parallels between the ANS model and stochastic sandpiles are noted below.

The phase boundary shown in Fig. 5.9 represents a preliminary estimate, obtained using the following criterion. Points along the lower critical line $p_-(\rho)$ correspond to the smallest p value such that each of 200 arbitrary ICs remain active during a time of 10^7 steps, in a system of $L = 10^5$ sites. Similarly, $p_+(\rho)$ corresponds to the largest p value such that all 200 realizations remain active. For selected points, a precise determination was performed, as described in Sec. 5.4. We defer a more precise mapping of the overall phase diagram to future work.
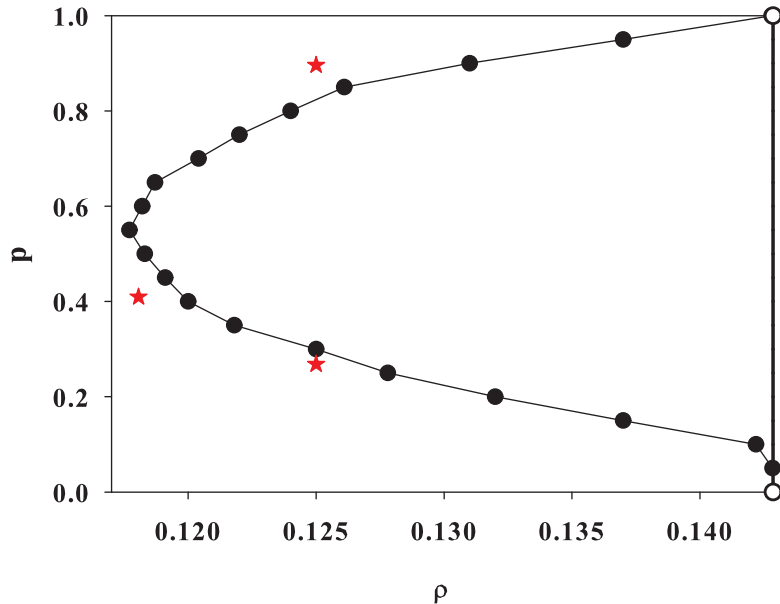
Figure 5.9: (Color online) Boundary between active and absorbing phases in the ρ - p plane. Black points (circles) joined by lines: preliminary estimates from initial-condition dependence as explained in text. Isolated red points (stars): precise estimates obtained via finite-size scaling as described in Sec. IV. The open circle at $\rho = 1/7$, $p = 0$ is not part of the phase boundary: for $p = 0$ the transition occurs at $\rho = 1/6$. The open circle $\rho = 1/7$, $p = 1$ marks the other end of the phase boundary; we note however that at this point, all initial conditions evolve to the absorbing state.

The phase transitions at $p_-(\rho)$ and $p_+(\rho)$ appear to be continuous. Figure 5.10 shows the steady-state activity (defined below) versus p for density $\rho = 1/8$. In the vicinity of the transition, the curves become sharper with increasing system size, as expected at a continuous phase transition to an absorbing state.

5.3.2 Order parameter

Having identified a continuous absorbing-state phase transition in the ANS model, further analysis requires that we define an appropriate order parameter or activity density. Since the absorbing state is characterized by $v_i = v_{max}, \forall i$, one might be inclined to define the activity density simply as $\rho_a = v_{max} - \overline{v}$. The problem with this definition is that not all configurations with $v_i = v_{max}, \forall i$ are absorbing: a vehicle with $d_i = v_{max}$ may reduce its speed to $v_{max} - 1$, yielding activity in the first sense. We define the activity density as:

$$\rho_a = v_{max} - \overline{v} + p\rho_{a,2} \equiv \rho_{a,1} + p\rho_{a,2}, \tag{5.1}$$

where $\rho_{a,2}$ denotes the fraction of vehicles with $v_i = d_i = v_{max}$. According to this definition, the activity density is zero if and only if the configuration is absorbing, that is, if $v_i = v_{max}$, and $d_i > v_{max}$, $\forall i$. Studies of large systems near the critical point reveal that $\rho_{a,1} >> \rho_{a,2}$, so that the latter can be neglected in scaling analyses. It is nonetheless essential to treat configurations with $\rho_{a,2} > 0$ as *active*, even if $\rho_{a,1} = 0$.
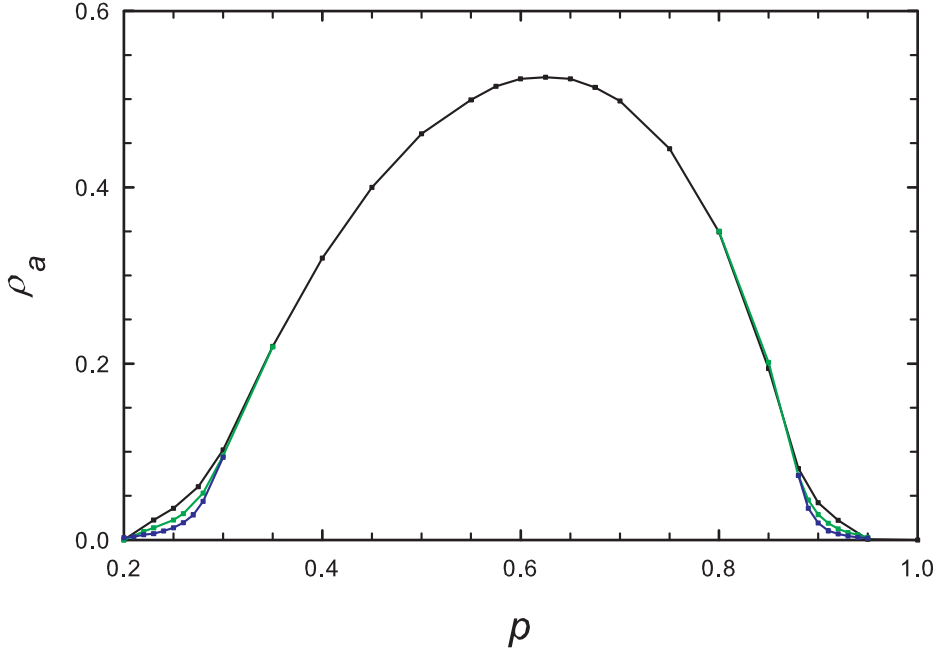
Figure 5.10: (Color online) Steady-state activity ρ_a versus p for vehicle density $\rho = 1/8$. System sizes (upper to lower curves) $N = 1000, 2000$ and 4000. Error bars smaller than symbols.

5.3.3 Reentrance

In this subsection we discuss the reason for reentrance, that is, why, for $\rho_{c,<} < \rho < \rho_c$, the system reaches the absorbing state for *large p* as well as small p. Since deceleration is associated with generation of activity (i.e., of speeds $< v_{max}$), a reduction in activity as p tends to unity seems counterintuitive. The following intuitive argument helps to understand why this happens. For $p \simeq 0$, vehicles rarely decelerate if they have sufficient headway to avoid reaching the position of the car in front. This tends to increase the headway of the car behind, so that (for $\rho < \rho_c$), all headways attain values $\geq v_{max} + 1$, which represents an absorbing configuration. For $p = 1$, a car with speed $v_i = d_i$ always decelerates, which tends to increase its own headway. In either case, $p = 0$ or $p = 1$, as reduced headway (i.e., inter-vehicle intervals with $d_i < v_{max} + 1$) is transferred down the line, vehicles may be obliged to decelerate, until the reduced headway is transferred to an interval with headway d_i large enough that no reduction in velocity is required. [Intervals with $d_i > v_{max} + 1$, which we call *troughs*, always exist for $\rho < \rho_c = 1/(v_{max} + 2)$]. When all reduced headways are annihilated at troughs, the system attains an absorbing configuration.

Call events in which a vehicle having $v_i = d_i$ decelerates *D events*, and those in which such a vehicle does not decelerate *N events*. For $\rho < \rho_c$, if only D events (or only N events) are allowed, the system attains an absorbing configuration via annihilation of reduced headways with troughs. Thus some alternation between D and N events is required to maintain activity, and the active phase corresponds to intermediate values of p.

These observations are illustrated in Fig. 5.11, for a system of twenty vehicles with $v_{max} = 2$ and density $\rho = 2/9 < \rho_c = 0.25$. Initially, all vehicles have $v_i = v_{max}$. The headways d_i initially alternate between three and four (the latter are troughs), except for $d_{19} = 0$ and $d_{20} = 7$. In the left panel, for $p = 0$, the system reaches an absorbing

configuration after four time steps. Similarly, in the right panel, for $p = 1$, an absorbing configuration is reached after 7 steps. For $p = 0.6$ (middle panel), the evolution is stochastic. Most realizations reach an absorbing configuration rapidly, but some remain active longer, as in the example shown here. From the distribution of D and N events, it appears that activity persists when vehicles first suffer an N event, reducing their own headway, and subsequently (one or two steps later) suffer a D event, reducing the headway of the preceding vehicle. Such an alternation of N and D events allows a region with reduced headways to generate more activity before reaching a trough [43].
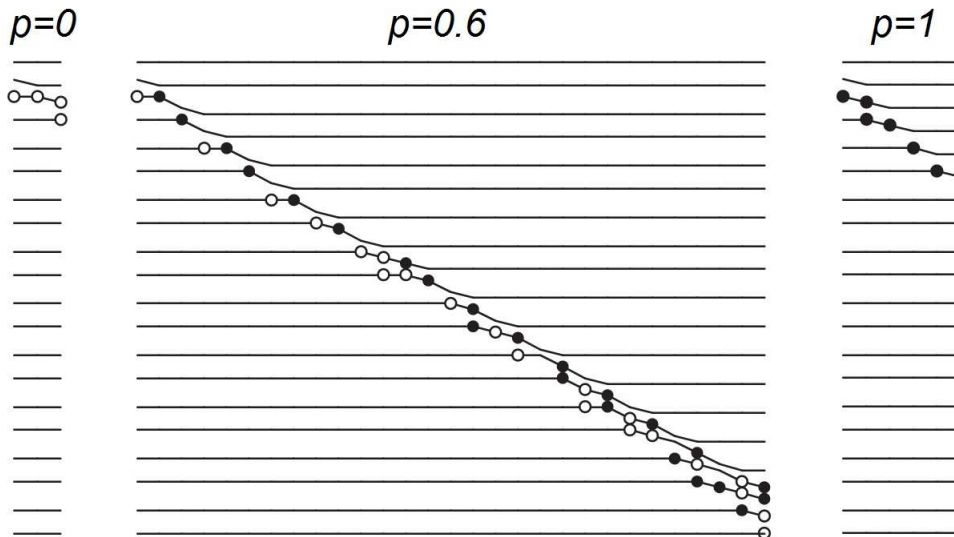
Figure 5.11: Vehicle positions relative to the first (lowest) vehicle versus time t (horizontal) for $t \geq 2$, in a system with $N = 20$, $v_{max} = 2$ and vehicle density $\rho = 2/9 < \rho_c = 0.25$. Initially, all vehicles have $v_i = v_{max}$. The headways d_i initially alternate between three and four, except for $d_{19} = 0$ and $d_{20} = 7$. Filled (open) circles denote D (N) events, i.e., events in which a vehicle with speed $v(i) = d(i)$ decelerates (does not decelerate). In an absorbing configuration all velocities are equal, yielding a set of horizontal lines with spacings $\geq v_{max} + 1$. Left panel: $p = 0$, system inactive for $t > 4$; right panel: $p = 1$, system inactive for $t > 7$; center panel: example of a realization with $p = 0.6$ in which activity persists until $t = 56$ (evolution for $t > 30$ not shown).

5.4   Critical behavior

5.4.1   Quasistationary simulation

Before studying the critical behavior of the ANS model we discuss briefly quasistationary simulations. Initially we have to define the quasistationary distribution. We start considering a continuous-time Markov process X_t taking values $n = 0, 1, 2, ..., S$, with the state $n = 0$ absorbing. We use $p_n(t)$ to denote the probability that $X_t = n$, given some initial state X_0. The survival probability $P_s(t) = \Sigma_{n \geq 1} p_n(t)$ is the probability that the process has not become trapped in the absorbing state up to time t. We suppose that as $t \to \infty$, $p_n(t)$ normalized by survival probability $P_s(t)$, attain a time-independent form. The quasistationary distribution $\overline{p_n}$ is then defined via

$$\overline{p_n} = \lim_{t \to \infty} \frac{p_n(t)}{P_s(t)}, \tag{5.2}$$

with $\overline{p_0} = 0$. The QS distribution is normalized. So

$$\sum_{n \geqslant 1} \overline{p_n} = 1. \tag{5.3}$$

In a conventional simulation the system starts from a random configuration and after a transient time one starts to measure quantities, e.g., order parameter, until the system attains the absorbing state. We restart the simulation many times choosing different random initial configurations. The problem in using this procedure is time of simulation. For many stochastic process with an absorbing state the quasistationary distributions provide a wealth of information about their behavior. In applying finite-size scaling theory to ANS model, and similar models that have an absorbing state, a slight complication arises, namely that for a finite system the only true stationary state is the absorbing state. To solve this problem the authors [44] suggest a simulation scheme for sampling the QS distribution. In a Monte Carlo simulation one generates a set of realizations of a stochastic process. In what follows they call a simulation of the original process X_t possessing an absorbing state a conventional simulation. The goal is to define a related process X_t^*, whose stationary probability distribution is the quasistationary distribution of X_t. To learn about the active state from simulations of finite systems we study the quasistationary state, which describes the statistical properties of surviving trials following an initial transient. When X_t enters the absorbing state, however, X_t^* instead jumps to a nonabsorbing one, and then resumes its usual evolution (with the same transition probabilities as X_t), until such time as another visit to the absorbing state is imminent.

Initial configurations are prepared by placing vehicles as uniformly as possible. A vehicle j is chosen at random and its distance from the vehicle ahead is reduced by $d_j \to d_j - 1$, so $d_{j-1} = d_{j-1} + 1$. This procedure is performed $2N$ times. As the system evolves, a list of states is created based on the system's evolution. Initially these first states do not represent a good choice for quasistationary states. With the intention of eliminating the vestiges of the initial configuration, during the relaxation period the probability of collecting them is p_{r1}. When the system attains the relaxation period, the probability p_{r1} is reduces to p_{r2} and the list of collected states is sampled with less frequency. The number of states in this list is fixed (in our simulations we use 1000 states) but as the system does not attain the absorbing state these states are renewed constantly. In our simulation we used $p_{r1} = 20/N$ and $p_{r2} = p_{r1}/10 = 2/N$.

5.4.2 Critical Exponents

According to finite-size scaling theory (FSS), in the vicinity of the critical point, intensive properties depend strongly on the system size. In the ANS model, FSS implies that the order parameter ρ_a depends on the system size and distance from the critical point as

$$\rho_a(\Delta, L) \propto L^{-\beta/v_\perp} f(\Delta L^{1/v_\perp}), \tag{5.4}$$

where $\Delta = \rho - \rho_c$[2]. When $\Delta = 0$ equation (5.4) yields

$$\rho_a(\rho, L) \propto L^{-\beta/v_\perp}, \tag{5.5}$$

for $\Delta < 0$ (subcritical regime) ρ_a falls off as L^{-1}, while for $\Delta > 0$ (supercritical regime), ρ_a approaches a nonzero value as $L \to \infty$. The scaling function

$$f(x) \propto x^\beta \quad \text{for} \quad x \to \infty, \tag{5.6}$$

---

[2]in the ANS model, there is a critical line in the $\rho - p$ plane, and Δ is the distance from this line.

allows that ρ_a, when $L \to \infty$, has a power law behaviour

$$\rho_a \propto \Delta^\beta. \tag{5.7}$$

In the vicinity of critical point, the correlation length ξ and correlation time τ diverge according to

$$\xi \propto \Delta^{-v_\perp} \quad \text{and} \quad \tau \propto \Delta^{-v_\parallel}. \tag{5.8}$$

So we expect that

$$\tau(\Delta, L) \propto L^z g(\Delta L^{1/v_\perp}), \tag{5.9}$$

where τ is the mean lifetime of a system and $z = v_\parallel / v_\perp$ is the dynamic exponent. To find the exponents β, $v_\perp$ we need to use another size scaling function. Finite-size scaling implies that for $\rho \simeq \rho_c$ the moment ratio $m = \langle \rho_a^2 \rangle / \rho_a^2$ obeys the relation:

$$m(\Delta, L) \propto f_m(\Delta L^{1/v_\perp}), \tag{5.10}$$

where f_m is a scaling function. This implies that

$$\left| \frac{\partial m}{\partial \rho} \right|_{\rho_c} \propto L^{1/v_\perp}, \tag{5.11}$$

moreover, the finite-size expression (5.4) implies that

$$\left| \frac{\partial \ln \rho}{\partial \rho} \right|_{\rho_c} \propto L^{1/v_\perp}. \tag{5.12}$$

Eventually according to finite-size expression (5.9) we expect that

$$\left| \frac{\partial \ln \tau}{\partial \rho} \right|_{\rho_c} \propto L^{1/v_\perp}. \tag{5.13}$$

5.4.3 Critical Exponents in the ANS model

We turn now to characterizing the phase transition along the lines $p_-(\rho)$ and $p_+(\rho)$. Since the transition is continuous, this requires that we determine the associated critical exponents, in order to identify the universality class of the ANS model. The analysis turns out to be complicated by strong finite-size effects: different from simple systems exhibiting an absorbing-state phase transition, such as the contact process, for which studies of systems with $L \leq 1000$ yield good estimates for critical exponents [33], here we require systems of up to 10^5 sites to obtain reliable results. We are nevertheless able to report precise results at several points along the phase boundary.

We use quasistationary (QS) simulations to probe the behavior at long times conditioned on survival of activity [44]. Since the deceleration probability p is continuous while the density ρ can only be varied in discrete steps, we keep the latter fixed and vary the former in each series of studies. As in other studies of QS behavior at absorbing-state phase transitions, we focus on the finite-size scaling (FSS) of the activity density, ρ_a, the lifetime, τ, and the moment ratio $m = \langle \rho_a^2 \rangle / \rho_a^2$, as functions of system size, N [33, 44]. At a critical point, these variables are expected to exhibit scale-free (power-law) dependence on N, that is, $\rho_a \sim N^{-\beta/\nu_\perp}$ and $\tau \sim N^z$, where β is the order-parameter exponent and

$\nu_\perp$ the exponent that governs the divergence of the correlation length as one approaches the critical point. In the active phase, ρ_a approaches a nonzero constant value, while τ grows exponentially as $N \to \infty$. In the absorbing phase, $\rho_a \sim 1/N$ while τ grows more slowly than a power law as $N \to \infty$. At the critical point, the moment ratio is expected to converge to a nontrivial limiting value, $m = m_\infty + \mathcal{O}(N^{-\lambda})$, with $\lambda > 0$. In the active (inactive) phase, m curves sharply downward (upward) when plotted versus $1/N$. These are the criteria we employ to determine the critical point, $p_c(\rho)$. The distance from the critical point can be estimated from the curvature of log-log plots of ρ_a and τ versus N.

As noted in Sec. III.B, the order parameter is the sum of two contributions: $\rho_a = \rho_{a,1} + p\rho_{a,2}$. In simulations, we therefore determine $\rho_{a,1}$ and $\rho_{a,2}$ separately. In the vicinity of the critical point we find $\rho_{a,1} \sim N^{-0.5}$ and $\rho_{a,2} \sim N^{-0.9}$, showing that the fraction $\rho_{a,2}$ of vehicles with $v_i = d_i = v_{max}$ decays more rapidly than $\rho_{a,1} = v_{max} - \overline{v}$, so that it makes a negligible contribution to the activity density for large N. We therefore adopt $\rho_{a,1}$ as the order parameter for purposes of scaling analysis. Configurations $\rho_{a,1} = 0$ and $\rho_{a,2} > 0$ are nevertheless considered to be active; only configurations with $v_i = v_{max}$ and $d_i > v_{max}$, $\forall i$, are treated as absorbing.

We study rings of 1000, 2000, 5000, 10 000, 20 000, 50 000 and 100 000 sites, calculating averages over a set of 20 to 160 realizations. Even for the largest systems studied, the activity density reaches a stationary value within 10^6 time steps. We perform averages over the subsequent 10^8 steps. As detailed in [44], the QS simulation method probes the quasistationary probability distribution by restarting the evolution in a randomly chosen active configuration whenever the absorbing state is reached. A list of N_c such configurations, sampled from the evolution, is maintained; this list is renewed by exchanging one of the saved configurations with the current one at rate p_r. Here we use $N_c = 1000$, and $p_r = 20/N$. During the relaxation phase, we use a value of p_r that is ten times greater, to eliminate the vestiges of the initial configuration from the list. The lifetime τ is taken as the mean time between attempts to visit an absorbing configuration, in the QS regime.

Initial configurations are prepared by placing vehicles as uniformly as possible (for example, for density $\rho = 1/8$, we set $d_i = 7$, $\forall i$), and then exchanging distances randomly. In such an exchange a site j is chosen at random and the changes $d_j \to d_j - 1$ and $d_{j+1} \to d_{j+1} + 1$ are performed, respecting the periodic boundary condition, $d_{N+1} \equiv d_1$. The random exchange is repeated N_e times (in practice we use $N_e = 2N$), avoiding, naturally, negative values of d_j. Since headways $d_j < v_m$ are generated in this process, at the first iteration of the dynamics, velocities $v_j < v_{max}$ arise, leading to a relatively large, statistically uniform initial activity density.

We performed detailed studies for densities $\rho = 1/8$, on both the upper and lower critical lines, and for density $17/144 = 0.11805\overline{5}$, on the lower line. Figures 5.12, 5.13 and 5.14 show, respectively, the dependence of the order parameter, lifetime and moment ratio m on system size for density $1/8$ and p values in the vicinity of the lower critical line. In the insets of Figs. 5.12 and 5.13 the values of ρ_a and τ are divided by the overall trend to yield $\rho_a^* \equiv N^{0.5}\rho_a$ and $\tau^* = \tau/N$. These plots make evident subtle curvatures hidden in the main graphs, leading to the conclusion that $p_c(\rho = 1/8)$ is very near 0.2683.

A more systematic analysis involves the curvatures of these quantities: we fit quadratic polynomials,

$$\ln \rho_a = \text{const.} + a \ln N + b(\ln N)^2, \tag{5.14}$$

and similarly for $\ln \tau$, to the data for the four largest system sizes. The coefficient of the quadratic term, which should be zero at the critical point, is plotted versus p in
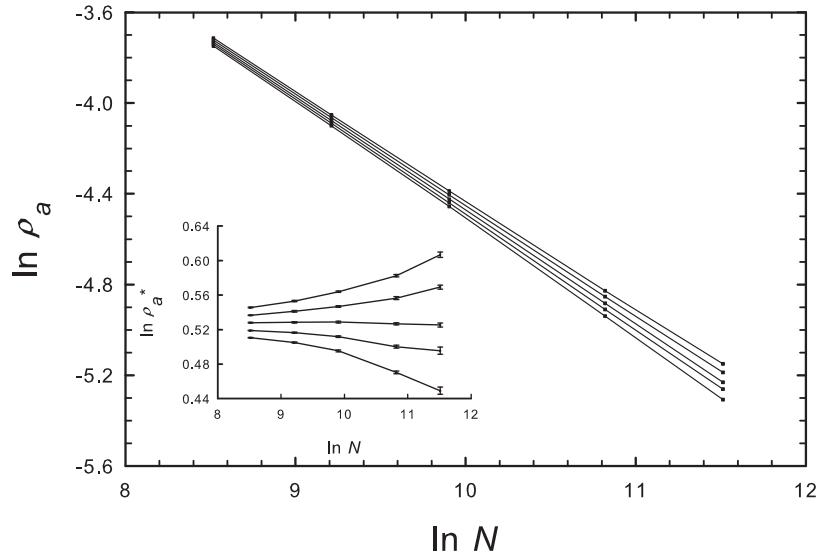
Figure 5.12: Activity density versus number of vehicles for density $1/8$ and (lower to upper) $p = 0.2679$, 0.2681, 0.2683, 0.2685 and 0.2687. Error bars are smaller than symbols. Inset: scaled activity density $\rho_a^* = N^{0.5}\rho_a$ versus number of vehicles.
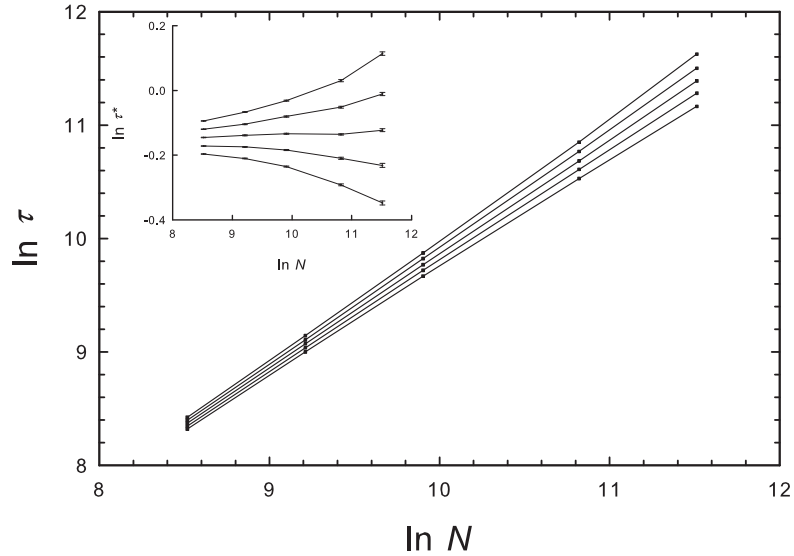
Figure 5.13: Lifetime versus number of vehicles for density $1/8$ and (lower to upper) $p = 0.2679, 0.2681$, $0.2683, 0.2685$ and 0.2687. Error bars are smaller than symbols. Inset: scaled lifetime $\tau^* = N^{-1.0}\tau$ versus number of vehicles.

Fig. 5.15. Linear interpolation to $b = 0$ yields the estimates $p_c = 0.26830(3)$ (data for activity density) and $p_c = 0.26829(2)$ (data for lifetime); we adopt $p_c = 0.26829(3)$ as our final estimate. (Figures in parentheses denote statistical uncertainties.) The data for m, although more scattered, are consistent with this estimate: from Fig. 5.14 it is evident that p_c lies between 0.2681 and 0.2683.

To estimate the critical exponents $\beta/\nu_\perp$ and z we perform linear fits to the data for $\ln \rho_a$ and $\ln \tau$ versus $\ln N$ (again restricted to the four largest N values), and consider the
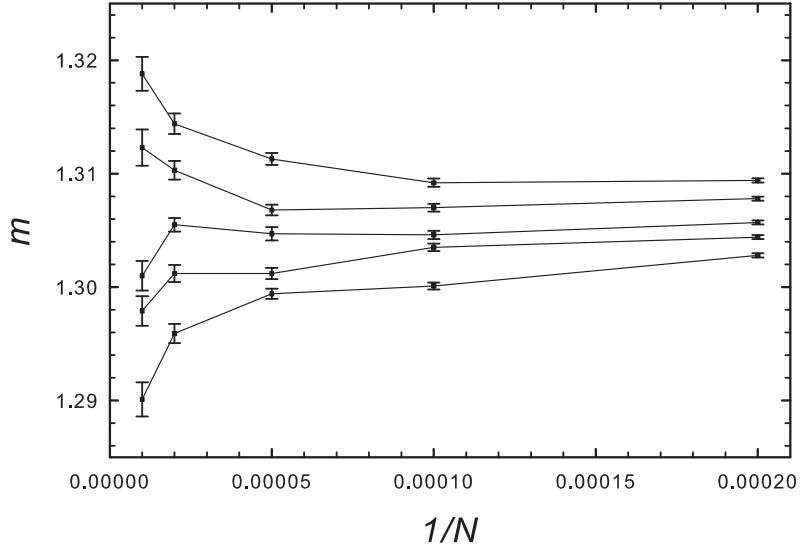
Figure 5.14: Moment ratio m versus reciprocal system size for density 1/8 and (upper to lower) $p = 0.2679, 0.2681, 0.2683, 0.2685$ and 0.2687.

slopes as functions of p. Interpolation to p_c yields the estimates: $\beta/\nu_\perp = 0.500(3)$ and $z = 1.006(8)$. A similar analysis yields $m_c = 1.306(6)$. The principal source of uncertainty in these estimates is the uncertainty in p_c.
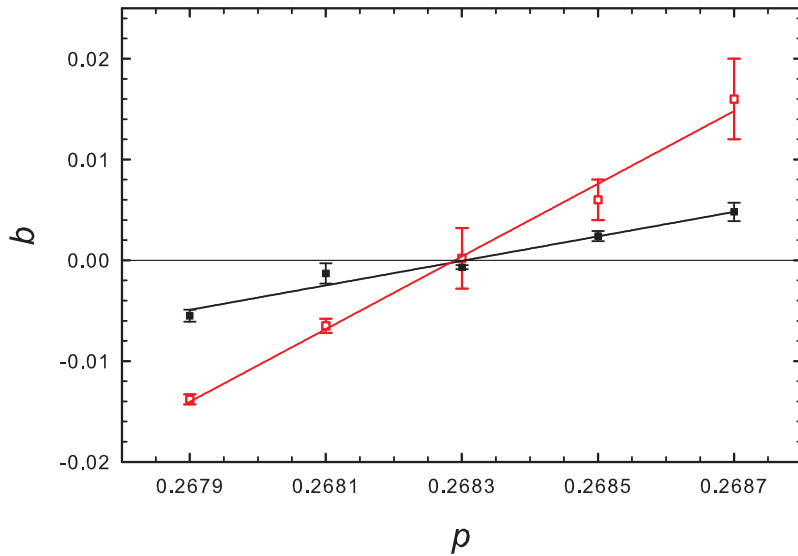
Figure 5.15: (Color online) Curvature of $\ln \rho_a$ (filled symbols) and $\ln \tau$ (open symbols) as functions of $\ln N$, as measured by the coefficient b of the quadratic term in least-squares quadratic fits to the data in Figs. 5.12 and 5.13. Straight lines are least-squares linear fits to b versus deceleration probability p, for vehicle density $\rho = 1/8$. Intercepts with the line $b = 0$ furnish estimates of p_c.

Using the data for ρ_a, τ and m we also estimate the critical exponent $\nu_\perp$. Finite-size scaling implies that the derivatives $|dm/dp|$, $d \ln \tau/dp$ and $d \ln \rho_a/dp$, evaluated at the critical point, all grow $\propto L^{1/\nu_\perp}$. We estimate the derivatives via least-squares linear fits to the data on an interval that includes p_c. (The intervals are small enough that

the graphs show no significant curvature.) Power-law dependence of the derivatives on system size is verified in Fig. 5.16. Linear fits to the data for the four largest sizes, for $\ln \rho_p$, $\ln \tau$, and m yield $1/\nu_\perp = 0.494(15)$, $0.495(15)$, and $0.516(29)$, respectively, leading to the estimate $\nu_\perp = 2.00(5)$. Repeating the above analysis for simulations at vehicle density $\rho = 17/144$, we find $p_-(17/144) = 0.4096(1)$, $\beta/\nu_\perp = 0.503(6)$, $z = 1.011(15)$, $m = 1.302(2)$, and $\nu_\perp = 2.02(2)$.
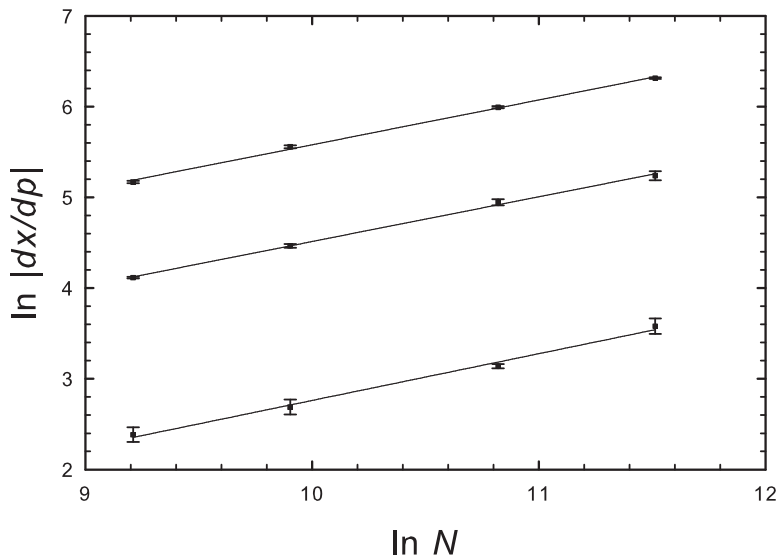
Figure 5.16: Derivatives of (lower to upper) m, $\ln \rho_a$ and $\ln \tau$ with respect to p in the vicinity of p_c, versus N for vehicle density $\rho = 1/8$. Lines are least-squares linear fits to the data.

Thus, for the two points studied on the lower critical line, the results are consistent with a simple set of exponent values, namely, $z = 1$, $\nu_\perp = 2$, and $\beta = 1$. The same set of critical exponents appears in a system of activated random walkers (ARW) on a ring, when the walkers hop in one direction only [47]. The critical moment ratio for ARW is $m_c = 1.298(4)$, quite near present estimates.

We suggest that these values characterize a universality class of absorbing-state phase transitions in systems with a conserved density (of walkers in ARW, and of vehicles in the present instance), and anisotropic movement. The ARW with *symmetric* hopping is known to belong to the universality class of conserved directed percolation [48], which also includes conserved stochastic sandpiles [45, 46].

A study on the upper critical line for vehicle density $\rho = 1/8$ yields results that are similar but slightly different. Repeating the procedure described above, we find $p_+(1/8) = 0.89590(5)$, $\beta/\nu_\perp = 0.487(8)$, $z = 1.021(15)$, $\nu_\perp = 1.98(6)$, and $m_c = 1.315(5)$. The exponent values are sufficiently near those obtained on the lower critical line that one might attribute the differences to finite-size effects. We defer to future work more detailed analyses, to determine whether scaling properties along the upper and lower critical lines differ in any respect.

Chapter 6

Summary and Open Questions

6.1 Summary

We review some traffic models studied in the literature. Start from the early models (hydrodynamic) to the three phases theory (Kerner), we summarize the key aspects of each model. We review the kinetic theory of traffic proposed by Prigogine and Herman in which the Boltzmann equation is adapted to vehicular traffic.The kinetic equation and its solution is discussed, and a novel distribution of desired velocities that is more suitable for describing real traffic conditions is analyzed. We also study the stationary velocity distribution at the transition between individual and collective flow patterns. At this transition the distribution splits into a smoothly varying regular part, in which vehicles have nonzero velocities, and a singular one, corresponding to stopped vehicles. Computational methods for obtaining the stationary velocity distribution, and the full space-time evolution of the vehicular distribution, are explained.

After the kinetic models, we study the cellular automaton (CA) models in which space, time and velocity are discretized. The most known study via CA is the NS model. Despite of your simplicity, this model is capable of reproducing features commonly found in real traffic, such as the transition between free flow and a jammed state, start-and-stop waves, and shocks (due to driver overreaction). This simple model represents the effect of variations in driving behavior by incorporating a simple stochastic element: the spontaneous reduction of velocity with probability p. Although the NS model has been studied extensively, the nature of the transition between free and jammed flow, in particular, whether it corresponds to a critical point, remains unsolved.

We consider a version of the Nagel-Schreckenberg model in which probabilistic deceleration is possible only for vehicles whose velocity is equal to the headway, $v_i = d_i$. In the resulting ANS model, a free-flow configuration, $v_i = v_{max}$ and $d_i > v_{max}$, $\forall i$, is *absorbing* for any value of the deceleration probability p. The phase transition in the original NS model at deceleration probability $p = 0$ is identified with the absorbing-state transition in the ANS model: the two models are identical for $p = 0$. In the original model, a nonzero deceleration probability corresponds to a spontaneous source of activity which eliminates the absorbing state, and along with it, the phase transition.

The ANS model, by contrast, exhibits a line of absorbing-state phase transitions in the ρ-p plane; the phase diagram is reentrant. We present preliminary estimates for the phase boundary and several critical exponents. The latter appear to be associated with a universality class of absorbing-state phase transitions in systems with a conserved density and asymmetric hopping, such as activated random walkers (ARWs) with particle transfer

only in one direction [47]. In this context it is worth noting that in traffic models, as well as in sandpiles and ARW, activity is associated with a local excess of density: in sandpiles, activity requires sites with an above-threshold number of particles; in ARW, it requires an active particle jumping to a site occupied by an inactive one; and in the ANS model, it requires headways d smaller than $v_{max} + 1$. One may hope that the connection with stochastic sandpiles will lead to a better understanding of traffic models, and perhaps of observed traffic patterns.

6.2 Open questions in the ANS model

6.2.1 Critical exponents

From the diagram shown in Fig. 5.9 we know that for each density there are two probabilities p_+ and p_- due the reentrance, i.e., the absorbing phase is reentrant. Surprisingly, when we determine the critical exponents for $p_+(1/8)$ and $p_-(1/8)$, there is a slight difference between them. We don't know if these differences reflect the asymptotic behavior of the model, or should be attributed to finite-size effects. Furthermore, we need to find the critical probabilities for other densities to estimate with precision the phase boundary. In future studies we shall investigate the possible differences in the critical exponents according to the density.

6.2.2 Mean-Field Theory

A key challenge in our work is to find an appropriate description of ANS model via mean-field theory. Although the ANS model belongs to the same universality class as the asymmetric ARW model [47], the approach used in the ARW model cannot be used here. The main reason is the difference between the update procedure: the ARW model uses the sequential update rules while the ANS model uses parallel updating. Although we try to develop an approach based on the current mean field technique used in the NS model [8], the first results show us that this approach seems don't recognize the absorbing states. We think that one of the reasons is the assumption that in the stationary states, the probability distributions become spatially independent. This assumption is true when the system does not attain the absorbing state. We can use this approach only for estimating with better precision the fundamental diagram with $v_{max} = 1$ and $v_{max} = 2$.

6.2.3 Other CA models with ANS rules

We can implement the randomization step of the ANS model in other models already studied in the literature. For instance we can investigate the possible absorbing states in an ANS version of a two-line model. We can introduce vehicles with different maximum speeds and study the possible configurations of absorbing states. Furthermore we know, from the other models as sandpile, contact process, activated random walkers etc, that the simple inclusion of a different update rule can, in some cases, modify the critical exponents and therefore the universality class.

Chapter 7

Appendix

7.1 Matriz T^t

Although we can obtain the matrix T^t writing down the initial state in the basis of eigenvectors, the work in doing it increases according to the value of v_{max}. For this reason we prefer to adopt the following strategy: T_{ij}^t means the probability of a vehicle starts at the state $|j-1\rangle$ and evolves to $|i-1\rangle$ at the time t. The analysis for each initial state is shown below. P^{mn} means the probability of the system starts with velocity m and evolves to velocity n at the time t.

$$v(0) = 0$$

$$
\begin{aligned}
P^{00}(t) &= p^t \\
P^{01}(t) &= \binom{t}{1} q p^{t-1} \\
P^{02}(t) &= \binom{t}{2} q^2 p^{t-2} \\
P^{03}(t) &= \binom{t}{3} q^3 p^{t-3} \\
P^{04}(t) &= \binom{t}{4} q^4 p^{t-4} + \binom{t-1}{5} q^5 p^{t-5} \ldots \binom{t-1}{t-1} q^{t-1} p \\
P^{05}(t) &= \binom{t-1}{4} q^5 p^{t-5} \ldots \binom{t-1}{t-2} q^{t-1} p + \binom{t-1}{t-1} q^t
\end{aligned}
$$

$$v(0) = 1$$

77

$$
\begin{aligned}
P^{11}(t) &= p^t \\[4pt]
P^{12}(t) &= \binom{t}{1} q p^{t-1} \\[4pt]
P^{13}(t) &= \binom{t}{2} q^2 p^{t-2} \\[4pt]
P^{14}(t) &= \binom{t}{3} q^3 p^{t-3} + \binom{t-1}{4} q^4 p^{t-4} \cdots \binom{t-1}{t-1} q^{t-1} p \\[4pt]
P^{15}(t) &= \binom{t-1}{3} q^4 p^{t-4} \cdots \binom{t-1}{t-2} q^{t-1} p + \binom{t-1}{t-1} q^t
\end{aligned}
$$

$$
v(0) = 2
$$

$$
\begin{aligned}
P^{22}(t) &= p^t \\[4pt]
P^{23}(t) &= \binom{t}{1} q p^{t-1} \\[4pt]
P^{24}(t) &= \binom{t}{2} q^2 p^{t-2} + \binom{t-1}{3} q^3 p^{t-3} \cdots \binom{t-1}{t-1} q^{t-1} p \\[4pt]
P^{25}(t) &= \binom{t-1}{2} q^3 p^{t-3} \cdots \binom{t-1}{t-2} q^{t-1} p + \binom{t-1}{t-1} q^t
\end{aligned}
$$

$$
v(0) = 3
$$

$$
\begin{aligned}
P^{33}(t) &= p^t \\[4pt]
P^{34}(t) &= \binom{t}{1} q^1 p^{t-1} + \binom{t-1}{2} q^2 p^{t-2} \cdots \binom{t-1}{t-1} q^{t-1} p \\[4pt]
P^{35}(t) &= \binom{t-1}{1} q^2 p^{t-2} \cdots \binom{t-1}{t-2} q^{t-1} p + \binom{t-1}{t-1} q^t
\end{aligned}
$$

The states corresponding to the velocities $v_{max} = 4$ and $v_{max} = 5$ are absorbing, i.e., since the configuration starts or evolves to these states, the final state will be always $|4\rangle$ (with probability p) and $|5\rangle$ (with probability q). So the matrix T^t is:

$$
T^t = \begin{pmatrix}
p^t & 0 & 0 & 0 & 0 & 0 \\
\binom{t}{1} q p^{t-1} & p^t & 0 & 0 & 0 & 0 \\
\binom{t}{2} q^2 p^{t-2} & \binom{t}{1} q p^{t-1} & p^t & 0 & 0 & 0 \\
\binom{t}{3} q^3 p^{t-3} & \binom{t}{2} q^2 p^{t-2} & \binom{t}{1} q p^{t-1} & p^t & 0 & 0 \\
p^{04}(t) & p^{14}(t) & p^{24}(t) & p^{34}(t) & p & q \\
p^{05}(t) & p^{15}(t) & p^{25}(t) & p^{35}(t) & p & q
\end{pmatrix}.
$$

where

$$P^{j4}(t) \;=\; \binom{t}{4-j} q^{4-j} p^{t+j-4} + \sum_{i=5-j}^{t-1} \binom{t-1}{i} q^i p^{t-i}$$

$$P^{j5}(t) \;=\; \sum_{i=4-j}^{t-1} \binom{t-1}{i} q^{i+1} p^{t-i-1}$$

evaluating the limit

$$lim_{t \longrightarrow \infty} \left(\frac{P^{j4}(t)}{P^{j5}(t)} \right) = \frac{\binom{t}{4-j} q^{4-j} p^{t+j-4} + \binom{t-1}{5-j} q^{5-j} p^{t+j-5} + \sum_{i=4-j}^{t-1} \binom{t-1}{i} q^i p^{t-i}}{\sum_{i=4-j}^{t-1} \binom{t-1}{i} q^{i+1} p^{t-i-1}}$$

for $t \to \infty$, the two first terms of the numerator tend to zero, so

$$lim_{t \to \infty} \left(\frac{p^{j4}(t)}{p^{j5}(t)} \right) = \frac{\sum_{i=4-j}^{t-1} \binom{t-1}{i} q^i p^{t-i}}{\sum_{i=4-j}^{t-1} \binom{t-1}{i} q^{i+1} p^{t-i-1}} = \frac{p}{q}.$$

using $\sum_{i=1}^{6} T_{ij}^t = 1$ e $lim_{t \to \infty} \sum_{i=1}^{4} T_{ij}^t = 0$, we have that

$$P(t \to \infty) = \begin{pmatrix} 0 \\ 0 \\ 0 \\ 0 \\ p \\ 1-p \end{pmatrix}.$$

7.2   Mean Field Theory

Solution for c_0

Using $\sum_{\beta=1}^{v_{max}} c_\beta = c - c_0$, we can find c_0 as a function of c, p e d;

$$c_0(1 - c - pd + c + pdc) = c^2(1 + pd)$$

$$c_0(1 - pd(1 - c)) = c^2(1 + pd)$$

$$c_0(1 - pd^2) = c^2(1 + pd),$$

leading to

$$\boxed{c_0 = \frac{c^2(1 + pd)}{1 - pd^2}}.$$

Solution for c_1

Using $\sum_{\beta=2}^{v_{max}} c_\beta = c - c_0 - c_1$, we can find c_1

$$c_1 = d\left[qc_0 + (qc + pd)c_1 + (q + pd)c(c - c_0 - c_1)\right]$$

$$c_1(1 - qcd - pd^2 + qcd + pd^2c) = d\left[c_0(q - qc - pdc) + (q + pd)c^2\right]$$

$$c_1(1 - pd^2(1 - c)) = d\left[\frac{c^2(1 + pd)(q - qc - pdc)}{1 - pd^2} + (q + pd)c^2\right]$$

$$c_1(1 - pd^3) = \frac{c^2d}{(1 - pd^2)}\left[q + q(1 - c) + pdq(1 - c) - pd^2q + pd(1 - c) - p^2d^2c - p^2d^3\right]$$

$$c_1(1 - pd^3) = \frac{c^2d}{(1 - pd^2)}\left[q(1 + d) + pd^2[1 - p(c + d)]\right]$$

$$c_1(1 - pd^3) = \frac{c^2d}{(1 - pd^2)}\left[q(1 + d + pd^2)\right],$$

leading to

$$\boxed{c_1 = qc^2d\frac{1 + d + pd^2}{(1 - pd^3)(1 - pd^2)}.}$$

Solution for $1 < \alpha < v_{max} - 1$

To finding a recursion relation for the other coefficients c_α, we use the identity

$$c_\alpha - dc_{\alpha-1} = d^\alpha\left[q(c_{\alpha-1} - c_{\alpha-2}) + (qc + pd)(c_\alpha - c_{\alpha-1}) + (q + pd)c\left[\sum_{\beta=\alpha+1}^{v_{max}} c_\alpha - \sum_{\beta=\alpha}^{v_{max}} c_\alpha\right]\right]$$

$$c_\alpha - dc_{\alpha-1} = d^\alpha\left[c_{\alpha-1}(q - qc - pd) - qc_{\alpha-2} + (qc + pd - qc - pdc)c_\alpha\right]$$

$$c_\alpha - dc_{\alpha-1} = d^\alpha\left[c_{\alpha-1}(q - qc - pd) - qc_{\alpha-2} + pd^2c_\alpha\right]$$

$$c_\alpha(1 - pd^{\alpha+2}) = d^\alpha\left[c_{\alpha-1}(qd - pd)\right] + dc_{\alpha-1} - qd^\alpha c_{\alpha-2}$$

$$c_\alpha(1 - pd^{\alpha+2}) = dc_{\alpha-1}\left[(q - p)d^\alpha + 1\right] - qd^\alpha c_{\alpha-2},$$

leading to

$$\boxed{c_\alpha = \frac{1 + (q - p)d^\alpha}{1 - pd^{\alpha+2}}dc_{\alpha-1} - \frac{qd^\alpha}{1 - pd^{\alpha+2}}c_{\alpha-2}.}$$

Solution for $c_{v_{max}}$

$c_{v_{max}-1}$ and $c_{v_{max}}$ can be found via

$$c_{v_{max}-1} = d^{v_{max}-1}\left[qc_{v_{max}-2} + \left(qc + pd\right)\left(c_{v_{max}-1} + c_{v_{max}}\right)\right]$$

$$c_{v_{max}} = qd^{v_{max}}\left[c_{v_{max}-1} + c_{v_{max}}\right]$$

we start, for simplicity, with $c_{v_{max}}$:

$$c_{v_{max}} = qd^{v_{max}}\left[c_{v_{max}-1} + c_{v_{max}}\right]$$

$$c_{v_{max}}\left(1 - qd^{v_{max}}\right) = qd^{v_{max}}c_{v_{max}-1} \qquad c_{v_{max}} = \frac{qd^{v_{max}}}{1 - qd^{v_{max}}}c_{v_{max}-1},$$

leading to

$$\boxed{c_{v_{max}} = \frac{qd^{v_{max}}}{1 - qd^{v_{max}}}c_{v_{max}-1}}.$$

Solution for $c_{v_{max}-1}$

$c_{v_{max}-1}$ can be found developing the expressions:

$$c_{v_{max}-1} = d^{v_{max}-1}\left[qc_{v_{max}-2} + \left(qc + pd\right)\left(c_{v_{max}-1} + c_{v_{max}}\right)\right]$$

$$c_{v_{max}-1}\left[1 - d^{v_{max}-1}(qc + pd)\left(1 + \frac{qd^{v_{max}}}{1 - qd^{v_{max}}}\right)\right] = qd^{v_{max}-1}c_{v_{max}-2}$$

$$c_{v_{max}-1}\left[1 - d^{v_{max}-1}(qc + pd)\left(\frac{1 - qd^{v_{max}} + qd^{v_{max}}}{1 - qd^{v_{max}}}\right)\right] = qd^{v_{max}-1}c_{v_{max}-2}$$

$$c_{v_{max}-1}\left[\frac{1 - qd^{v_{max}} - d^{v_{max}-1}(qc + pd)}{1 - qd^{v_{max}}}\right] = qd^{v_{max}-1}c_{v_{max}-2}$$

$$c_{v_{max}-1}\left[\frac{1 - d^{v_{max}-1}(qd + qc + pd)}{1 - qd^{v_{max}}}\right] = qd^{v_{max}-1}c_{v_{max}-2},$$

leading to

$$\boxed{c_{v_{max}-1} = \frac{1 - qd^{v_{max}}}{1 - d^{v_{max}-1}(q + pd)}qd^{v_{max}-1}c_{v_{max}-2}}.$$

Bibliography

[1] B. S. Kerner, *The Physics of Traffic*, (Springer, Berlin, 2004).

[2] M. Bando, K. Hasebe, A. Nakayama, A. Shibata, and Y. Sugiyama, "Dynamical model of traffic congestion and numerical simulation," Phys. Rev. E **51**, 1035–1042 (1995).

[3] K. Nagel and M. Schreckenberg, "A cellular automaton model for freeway traffic," J. Phys. I (France) **2**, 2221–2229 (1992).

[4] B. Eisenblätter, L. Santen, A. Schadschneider, and M. Schreckenberg, "Jamming transition in a cellular automaton model for traffic flow," Phys. Rev. E **57**, 1309 (1998).

[5] G. Csányi and J. Kertész, "Scaling behaviour in discrete traffic models," J. Phys. A **28**, L427 (1995).

[6] L.C.Q. Vilar, A.M.C. de Souza, "Cellular automata models for general traffic conditions on a line," Physica A **211**, 84-92 (1994)

[7] M. Gerwinski and J. Krug, "Analytic approach to the critical density in cellular automata for traffic flow," Phys. Rev. E **60**, 188 (1999).

[8] M. Schreckenberg, A. Schadschneider, K. Nagel and N. Ito, "Discrete stochastic models for trafficc flow," Phys. Rev. E **51**, 2939 (1995).

[9] A. Schadschneider and M. Schreckenberg, "Garden of Eden states in traffic models," J. Phys. A: Math. Gen. **31**, L225–L231 (1998).

[10] Y. Xue, L. Dong, L. Li, and S. Dai, "Effects of changing orders in the update rules on traffic flow," Phys. Rev. E **71**, 026123 (2005).

[11] R. Barlovic, L. Santen, A. Schadschneider and M. Schreckenberg, "Metastable states in cellular automata for traffic flow," Eur. Phys. J. B **5**, 793 (1998).

[12] K. Nagel and M. Paczuski, "Emergent traffic jams," Phys. Rev. E **51** 2909 (1995).

[13] Y. Ishibashi and M. Fukui, "One-Dimensional Fukui-Ishibashi Traffic Flow Model," J. Phys. Soc. Jpn. **63**, 2882 (1994).

[14] B. Wang, L. Wang, P. M. Hui, and B. Hu, "Analytical results for the steady state of traffic flow models with stochastic delay," Phys. Rev. E **58**, 2876 (1998).

[15] L. Wang, B. Wang and B. Hu, "Cellular automaton traffic flow model between the Fukui-Ishibashi and Nagel-Schreckenber models," Phys. Rev. E **63**, 56117 (2001).

[16] W. Knospe, L. Santen, A. Schadschneider and M. Schreckenberg, "Disorder effects in cellular automata for two-lane traffic," Physica A **265** 614 (1999).

[17] K. Nagel, D. E. Wolf, P. Wagner, and P. Simon, "Two-lane traffic rules for cellular automata: A systematic approach," Phys. Rev. E **58**, 1425 (1998).

[18] I. Prigogine and R. C. Herman, *Kinetic Theory of Vehicular Traffic* (Elsevier, New York, 1971).

[19] I. Prigogine and F. C. Andrews, "A Boltzmann-like approach for traffic flow," Oper. Res. **8**, 789–797 (1960).

[20] I. Prigogine, R. C. Herman, and R. L. Anderson, "On the statistical distribution function theory of traffic flow," Oper. Res. **10**, 180–196 (1962).

[21] R. L. Liboff, *Kinetic Theory: Classical, Quantum, and Relativistic Descriptions* (Springer-Verlag, New York, 2003).

[22] See Ref. [18], pp. 42–51 for further details.

[23] M. Plischke and B. Bergersen, *Equilibrium Statistical Physics* (World Scientific, Singapore, 1994).

[24] W. H. Press, S. A. Teukolsky, W. T. Velterling and B. P. Flannery, *Numerical Recipies in Fortran* (Cambridge University Press, New York, 1993). See p. 128.

[25] See Ref. 21, p. 347 and 355.

[26] C. Wagner, C. Hoffmann, R. Sollacher, J. Wagenhuber and B. Schurmann, "Second-order continuum traffic flow model," Phys. Rev. E **54**, 5073–5085 (1996).

[27] S. L. Paveri-Fontana, "On Boltzmann-like treatments for traffic flow: A critical review of the basic model and an alternative proposal for dilute traffic analysis," Trans. Res. **9**, 225–235 (1975).

[28] C. Wagner, "Successive deceleration in Boltzmann-like traffic equations," Phys. Rev. E **55**, 6969–6978 (1997).

[29] A. M. C. Souza and L. C. Q. Vilar, "Traffic-flow cellular automaton: Order parameter and its conjugated field," Phys. Rev. E **80**, 021105 (2009).

[30] L. Roters, S. Lübeck and K. D. Usadel, "Critical behaviour of a traffic flow model," Phys. Rev. E **59**, 2672 (1999).

[31] D. Chowdhury, J. Kertész, K. Nagel, L. Santen and A. Schadschneider, "Comment on 'Critical behaviour of a traffic flow model'," Phys. Rev. E **61**, 3270 (2000).

[32] L. Roters, S. Lübeck and K. D. Usadel, "Reply to Comment on Critical behaviour of a traffic flow model," Phys. Rev. E **61**, 3272 (2000).

[33] J. Marro and R. Dickman, *Nonequilibrium Phase Transitions in Lattice Models* (Cambridge University Press, Cambridge, 1999).

[34] I. Jensen, R. Dickman, "Nonenquilibrium phase transition in systems with infinitely many absorbing states," Phys. Rev. E **48**, 1710 (1993).

[35] I. Jensen, "Critical Behaviour of the Pair Contact Process," Phys. Rev. Lett. **70**, 1465 (1993). 34

[36] A. Schadschneider "The Nagel-Schreckenberg model revisited," Eur. Phys. J. B **10**, 573 (1999).

[37] M. Takayasu and H. Takayasu, "1/f noise in a traffic model," Fractals 1 **4** 860 (1993).

[38] S. C. Benjamin, N. F. Johnson, "Cellular automata models of traffic flow along a highway containing a junction," J. Phys. A **29** 3119 (1996).

[39] S. Krauss, P. Wagner and C. Gawron, "Metastable states in a microscopic model of traffic flow," Phys. Rev. E **55**, 5597 (1997).

[40] X. Li, Q. Wu and R. Jiang, "Cellular automaton model considering the velocity effect of a car on the sucessive car," Phys. Rev. E **64**, 066128 (2001).

[41] G. Ódor, *Universality In Nonequilibrium Lattice Systems: Theoretical Foundations* (World Scientific, Singapore, 2007).

[42] M. Henkel, H. Hinrichsen and S. Lubeck, *Non-Equilibrium Phase Transitions Volume I: Absorbing Phase Transitions* (Springer-Verlag, The Netherlands, 2008).

[43] J. M. Carlson, J. T. Chayes, E. R. Grannan, and G. H. Swindle, "Self-organized criticality in sandpiles: Nature of the critical phenomenon," Phys. Rev. A **42**, 2467(R) (1990).

[44] M. M. de Oliveira and R. Dickman, "How to simulate the quasistationary state," Phys. Rev. E **71**, 016129 (2005).

[45] M. A. Muñoz, R. Dickman, R. Pastor-Satorras, A. Vespignani, and S. Zapperi, "Sandpiles and absorbing-state phase transitions: recent results and open problems," in *Modeling Complex Systems*, Proceedings of the 6th Granada Seminar on Computational Physics, J. Marro and P. L. Garrido, eds., AIP Conference Proceedings v. 574 (2001).

[46] G. Pruessner, *Self-Organised Criticality*, (Cambridge University Press, Cambridge, 2012). 44

[47] R. Dickman, L. T. Rolla and V. Sidoravicius, "Activated Random Walkers: Facts, Conjectures and Challenges," J. Stat. Phys. **138**, 126 (2010).

[48] J. C. Mansur Filho and R. Dickman, "Conserved directed percolation: exact quasistationary distribution of small systems and Monte Carlo simulations," J. Stat. Mech. **2011**, P05029 (2011). 46

Published Articles

COMPUTATIONAL PHYSICS

Kinetic theory of vehicular traffic

M. L. L. Iannini[a)] and Ronald Dickman[b)]
Departamento de Física, ICEx, Universidade Federal de Minas Gerais, Caixa Postal 702, Belo Horizonte, MG 30161-970, Brazil

We review the kinetic theory of traffic proposed by Prigogine and Herman in which the Boltzmann equation is adapted to vehicular traffic. The kinetic equation and its solution are discussed, and a novel distribution of desired velocities that is more suitable for describing real traffic conditions is analyzed. We also study the stationary velocity distribution at the transition between individual and collective flow patterns. At this transition, the distribution splits into a smoothly varying regular part, in which vehicles have nonzero velocities, and a singular one, corresponding to stopped vehicles. Computational methods for obtaining the stationary velocity distribution and the full space-time evolution of the vehicular distribution are explained. © *2016 American Association of Physics Teachers.*
[http://dx.doi.org/10.1119/1.4935895]

I. INTRODUCTION

The application of numerical and theoretical methods developed in physics to areas traditionally viewed as belonging to the social sciences has recently accelerated, with studies of economic interactions,[1,2] linguistics,[3] and social networks[4] becoming standard fare in physics. Although this trend might seem novel, it began, albeit slowly, some time ago. A case in point is the use of ideas from the kinetic theory of gases to describe vehicular traffic, pioneered by Prigogine and Herman,[5–7] among others, more than sixty years ago.

Just as the statistical mechanics of molecular systems depends on a model of the molecules and their interactions, the study of traffic requires that we model the behavior of drivers. Once we have a suitable model, a system of many interacting molecules (or drivers) can be studied at various levels of detail: direct study (usually numerical) of a microscopic model, kinetic theory, or a macroscopic (thermodynamic or hydrodynamic) approach. An important class of microscopic models of traffic are stochastic lattice systems in which space, time, and vehicle velocities are all discretized. A key example is the stochastic cellular automaton introduced by Nagel and Schreckenberg.[8]

Kinetic theory is an intermediate level of description, which follows the evolution of a probability distribution for single vehicles. It offers advantages and disadvantages compared to microscopic models. Among the advantages are that there is no need to discretize space, time, or velocity, and it requires substantially less effort to analyze than a stochastic cellular automaton, which typically must be run repeatedly to obtain reliable results. In some cases, analytical solutions are possible, affording a certain insight. Thus kinetic theory affords a rapid and approximate survey of parameter space, facilitating the identification of general trends. The principal shortcoming of kinetic theory is the absence of fluctuations, and events (such as traffic jams) that result from rare configurations of drivers. Therefore, it is interesting to perform both simulations of detailed models and kinetic theories and to compare their results.

The initial efforts in modeling vehicular traffic via kinetic theory were made in an era of very limited computational resources, so that large-scale simulations of stochastic cellular automata were not an option. Nevertheless, it was possible to draw interesting conclusions from kinetic theory. The most remarkable conclusion is the conflict between the desire of individual drivers to realize their own goals and the interactions between vehicles that frustrate this desire. These interactions lead to a clear distinction between individual and collective flow regimes. At a certain concentration, the flow patterns become independent of the desires of individual drivers, and instead represent collective behavior.

In the earliest version of the kinetic theory of vehicular traffic, Prigogine and Herman[5–7] modified the kinetic theory of gases embodied in the Boltzmann equation. In their model, traffic is treated as a one-dimensional gas of interacting particles (vehicles) described by a distribution function $f(x, v, t)$, defined such that $f(x, v, t)\, dx\, dv$ represents the number of vehicles with positions between x and $x + dx$ and velocities between v and $v + dv$ at time t. The distribution f is normalized so that

$$\int dv f(x, v, t) = c(x, t), \tag{1}$$

where $c(x, t)$ is the local density of vehicles. (Unless otherwise specified, all integrals run from $-\infty$ to ∞. Note that $f(x, v, t)$ is zero for $v < 0$.)

The time evolution of f is governed by a Boltzmann-like equation. The principal difference with the original Boltzmann equation is the introduction of a distribution of desired velocities, $f_0(x, v, t)$, in the relaxation term, representing drivers' preferences. Specifically, $f_0(x, v, t)\, dx\, dv$ is the number of vehicles between x and $x + dx$, whose drivers have a preferred velocity between v and $v + dv$ at time t. The presence of this function in the statistical description is a novel feature, showing that the "particles" in this system have intentions unlike a molecule, which does not have a desired velocity.

Of principal interest is the stationary velocity distribution, which can be much different from the distribution of desired velocities. We shall see that the stationary velocity distribution changes abruptly at a specific density.

In Sec. II, we outline the modifications in the Boltzmann equation introduced by Prigogine and Herman and emphasize the features relevant to vehicular traffic. For simplicity, we study in Sec. III only the stationary solutions. Despite this simplicity, some notable features appear. This study is followed in Sec. IV by a discussion of the additional assumptions regarding driver behavior incorporated in the Prigogine–Herman model. In Sec. V, we devise a numerical solution method for the stationary velocity distribution, and apply it to two examples. Then in Sec. VI we turn to numerical integration of the full space- and time-dependent equation, propose a simple algorithm, and discuss two illustrative examples. Section VII summarizes our results, and is followed in Sec. IX by suggestions for further study.

II. THE PRIGOGINE–HERMAN–BOLTZMANN EQUATION

In the kinetic theory of gases, the evolution of the distribution function $f(\mathbf{x}, \mathbf{v}, t)$ is governed by the Boltzmann equation[9]

$$\frac{\partial f}{\partial t} + \mathbf{v} \cdot \mathbf{V}_r f + \mathbf{a} \cdot \mathbf{V}_v f = \left(\frac{\partial f}{\partial t}\right)_{\text{coll}}. \tag{2}$$

Here, $f(\mathbf{x}, \mathbf{v}, t)\, d^3x\, d^3v$ is the number of molecules at time t with positions in the volume d^3x centered on point $\mathbf{x}$, and velocities in the volume element d^3v centered on velocity $\mathbf{v}$. The terms $\mathbf{v} \cdot \mathbf{V}_r f$ and $\mathbf{a} \cdot \mathbf{V}_v f$ describe the redistribution of molecules due to changes in position and velocity, the latter resulting from an external force $\mathbf{F}_{\text{ext}}$, leading to an acceleration $\mathbf{a} = \mathbf{F}_{\text{ext}}/m$, where m is the molecular mass. (Note that $\mathbf{V}_v$ denotes a gradient in velocity space.) These streaming terms derive from the motion of independent particles, and are equivalent to a continuity equation describing conservation of the total number of molecules in the six-dimensional space of position and velocity. The right-hand-side of Eq. (2) describes the effect of interactions between particles and represents the change in the number of molecules with velocity $\mathbf{v}$ due to collisions with other molecules at position $\mathbf{x}$.

In one-way traffic, vehicles travel in one dimension, and Eq. (2) can be simplified to read[5,6]

$$\frac{\partial f}{\partial t} + v \frac{\partial f}{\partial x} = \left(\frac{\partial f}{\partial t}\right)_{\text{rel}} + \left(\frac{\partial f}{\partial t}\right)_{\text{int}}. \tag{3}$$

The first term on the right-hand-side of Eq. (3) represents a relaxation process, and the second represents the interactions

between vehicles. The idea behind the relaxation term is that drivers adjust their velocity to the desired value v_0 on a time scale T, called the relaxation time. This assumption is embodied in the expression

$$\left(\frac{\partial f}{\partial t}\right)_{\text{rel}} = -\frac{f - f_0}{T}. \tag{4}$$

In a spatially uniform system, in which $f = f(v, t)$ and interactions between drivers can be ignored, the solution to Eq. (3) is

$$f(v, t) = f_0(v) + [f(v, 0) - f_0(v)]e^{-t/T}. \tag{5}$$

Exponential relaxation describes the approach of many simple systems to a steady state. In the context of the kinetic theory of gases, an analogous simplification involves replacing the collision term with an expression of the form of Eq. (4); T becomes the collision time, and f_0 is a local Maxwellian distribution.[9] As will become clear, Prigogine and Herman[7] proposed that T depends on the concentration of vehicles on the road, and the relaxation process subsumes some rather complicated interactions between drivers.

In the absence of interactions between the vehicles, the distribution function evolves to the distribution of desired velocities according to Eq. (5). A derivation of the distribution of desired velocities from first principles would require knowledge of human behavior that is beyond our present capabilities. One might try to determine the distribution of desired velocities empirically by studying the velocity distribution at very low concentrations, but we are unaware of studies of this kind. Prigogine and Herman simply investigated several simple model distributions of the desired velocities.[10]

The interaction term in Eq. (3) is based on the following assumptions:

(1) The vehicles are point-like, that is, they do not occupy volume.
(2) Vehicles remain in the same lane except when passing another vehicle.
(3) In an encounter between two vehicles, one passes the other with probability P.
(4) If one vehicle passes another, neither vehicle changes its velocity. In an encounter without passing, the faster vehicle reduces its velocity to that of the slower one ahead of it.
(5) The slowing-down process is instantaneous.
(6) Only two-vehicle interactions are considered.
(7) The vehicles are statistically independent; that is, the joint two-vehicle distribution is the product of single vehicle distributions: $f(x, v, x', v', t) = f(x, v, t)f(x', v', t)$.

If we use these assumptions, we can write the interaction term as

$$\left(\frac{\partial f}{\partial t}\right)_{\text{int}} = f(x, v, t) \int_v^\infty du\, (1 - P)(u - v)f(x, u, t)$$
$$- f(x, v, t) \int_{-\infty}^v du\, (1 - P)(v - u)f(x, u, t). \tag{6}$$

The first term on the right-hand-side of Eq. (6) corresponds to interactions between vehicles with velocities v and $u > v$;

the latter are obliged to adopt the smaller velocity v resulting in an increase in the number of vehicles with velocity v. The second term is related to interactions between vehicles with velocity v and $u < v$. In this case, the interaction results in a decrease in the number of vehicles with velocity v. By combining the two integrals, the interaction term can be rewritten as

$$\left(\frac{\partial f}{\partial t}\right)_{\text{int}} = (1 - P)f(x, v, t) \int du \, (u - v)f(x, u, t). \qquad (7)$$

Because

$$\int uf(x, u, t) \, du = c(x, t)\bar{v}(x, t), \qquad (8)$$

where $\bar{v}(x, t)$ denotes the local mean velocity, and

$$\int du \, vf(x, u, t) = c(x, t)v, \qquad (9)$$

we have

$$\left(\frac{\partial f}{\partial t}\right)_{\text{int}} = (1 - P)c(x, t)[\bar{v}(x, t) - v]f(x, v, t). \qquad (10)$$

If we insert the relaxation term, Eq. (4), and interaction term, Eq. (10), into Eq. (3), we obtain the Prigogine–Herman–Boltzmann equation for traffic

$$\frac{\partial f}{\partial t} + v\frac{\partial f}{\partial x} = -\frac{f - f_0}{T} + (1 - P)c(x, t)[\bar{v}(x, t) - v]f. \qquad (11)$$

The above equation is a nonlinear equation because $\bar{v}(x, t)$ is a function (more precisely, a *functional*) of $f(x, v, t)$. A full definition of the model requires that we specify how the passing probability and relaxation time depend on the concentration. Before examining specific choices, we consider some general aspects of the solutions.

III. STATIONARY SOLUTIONS

We consider uniform, stationary solutions in which $f = f(v)$, c, and $\bar{v}$ are time-independent. This case represents the simplest situation that we might expect to hold at long times, far from any entrances and exits on a long, straight highway. Due to the interactions between vehicles, the stationary solution $f(v)$ is not usually equal to the distribution of desired velocities, $f_0(v)$. A spatially uniform, time-independent solution $f(v)$ of Eq. (11) must satisfy

$$f(v) = \frac{f_0(v)}{1 - cT(1 - P)[\bar{v} - v]}. \qquad (12)$$

The above equation is also nonlinear, because $\bar{v}$ depends on $f(v)$, and it has two kinds of solution corresponding to individual and collective flow patterns.

A. Individual and collective flow

To simplify the notation, let

$$\gamma \equiv cT(1 - P) \quad \text{and} \quad \lambda \equiv 1 - \gamma\bar{v}(f), \qquad (13)$$

so that Eq. (12) becomes

$$f = \frac{f_0}{\lambda(f) + \gamma v}. \qquad (14)$$

In Eqs. (13) and (14), the parameter λ is specifically written as a function of f to stress that the nonlinearity induced by the term $\bar{v}$ is included in λ; from here on, we simply write λ.

Equation (14) implies that if $\lambda < 0$, we can find values of v such that $\lambda + \gamma v < 0$ for fixed γ. These values are physically unacceptable because $f(v)$ cannot be negative; only the values $\lambda > 0$ and $\lambda = 0$ have physical meaning. For $\lambda = 0$, Eq. (14) reduces to

$$\gamma vf(v) = f_0(v). \qquad (15)$$

An important feature is that the homogeneous equation $\gamma vf = 0$ admits the singular solution $f = \alpha c \, \delta(v)$, where α is an arbitrary constant and $\delta(v)$ is the Dirac delta function. Thus, for $\lambda = 0$ the general solution is

$$f = \frac{f_0}{\gamma v} + \alpha c \, \delta(v). \qquad (16)$$

For $\lambda > 0$, we have Eq. (14). In either case the solution must be consistent with the conditions established by Eqs. (1) and (8)

$$c = \int \frac{f_0 \, dv}{\lambda + \gamma v} + \alpha c \qquad (17)$$

and

$$c\bar{v} = \int \frac{vf_0 \, dv}{\lambda + \gamma v}. \qquad (18)$$

Suppose that $\lambda > 0$. The stationary velocity distribution is given by Eq. (14) in which f_0 is a function and γ is a constant determined by the concentration, relaxation time, and the passing probability. The only unknown is the parameter λ. We write $f_0(v) = c\tilde{f}_0(v)$, and obtain from Eq. (17) (with $\alpha = 0$) that

$$\int \frac{\tilde{f}_0 \, dv}{\lambda + \gamma v} = 1 \qquad (19)$$

as the condition determining λ. Once Eq. (19) is solved, the mean velocity is given by $\bar{v} = (1 - \lambda)/\gamma$, and the flux (the number of vehicles passing a given point per unit time) is $q = c\bar{v}$. We see that, given the distribution of desired velocities f_0, the flux and mean velocity depend on c, T, and P only though the combination γ. In most cases, the integral in Eq. (19) needs to be evaluated numerically.

Because $\tilde{f}_0 = 0$ for $v < 0$, we see that the integral in Eq. (19) is a decreasing function of γ for fixed λ. As γ increases, λ must therefore decrease. If $\int (f_0/v) \, dv = \infty$, then Eq. (19) can always be satisfied for some $\lambda > 0$, no matter how large γ becomes. Divergence of the integral implies that $f_0 > 0$ for $v = 0$; that is, there are drivers whose preferred velocity is zero. (Such drivers should stay off the road!) Thus, for a plausible distribution of desired velocities, we expect $\int (f_0/v) \, dv < \infty$. In this case, we can define a critical value γ_c from the condition

$$\int \frac{\tilde{f}_0 \, dv}{v} = \gamma_c. \tag{20}$$

As γ increases, λ decreases and becomes zero for $\gamma = \gamma_c$. Recall that λ cannot be negative. For $\gamma > \gamma_c$, λ remains zero, allowing the inclusion of the term $\propto \delta(v)$ in f. The normalization condition now reads

$$1 = \int \frac{\tilde{f}_0 \, dv}{\gamma v} + \alpha, \tag{21}$$

showing that α, which governs the fraction of vehicles at rest, increases continuously from zero as γ is increased beyond its critical value: $\alpha = (\gamma - \gamma_c)/\gamma$ for $\gamma > \gamma_c$. In this regime, $\bar{v} = 1/\gamma$ regardless of the form of the distribution of desired velocities.

The appearance of a nonzero fraction of stopped vehicles at $\gamma = \gamma_c$ can be seen as a phase transition, formally analogous to that of Bose–Einstein condensation in an ideal Bose gas.[11] In Bose–Einstein condensation, the density ρ_0 of bosons in the state of zero momentum increases as $\rho_0 = \rho - \rho_c$ for densities above the critical density, which depends on the particle mass and the temperature. Because the kinetic theory of traffic deals with classical objects, this analogy is purely formal.

One objective in the kinetic theory of traffic is to find the stationary velocity distribution $f(v)$, given the concentration c and a traffic model (or empirical data) consisting of the distribution of desired velocities f_0 and the functions $P(c)$ and $T(c)$. Then, given c the value of γ is fixed, and all that remains is to determine λ via Eq. (19). A numerical solution method is discussed in Sec. V.

An alternative approach is to rewrite Eq. (19) in the form

$$\gamma = \int \frac{\tilde{f}_0 \, dv}{\lambda^* + v}, \tag{22}$$

where $\lambda^* = \lambda/\gamma$. Equation (22) defines a function $\gamma(\lambda^*)$, given the form of f_0.

A simple yet illuminating application of this analysis is for the case[12] $\tilde{f}_0 = \delta(v - u)$, that is, all drivers have the same desired velocity u. (Perhaps all drivers wish to go as fast as possible, and all vehicles have a maximum speed of u.) By using Eq. (22), we find that $\lambda = \max[0, 1 - \gamma u]$ and $\gamma_c = 1/u$. For $\gamma > \gamma_c$, the fraction of stopped vehicles is $\alpha = 1 - 1/(\gamma u)$. The mean velocity is given by

$$\bar{v} = \begin{cases} u & (\gamma < 1/u) \\ 1/\gamma & (\gamma > 1/u). \end{cases} \tag{23}$$

Thus, all drivers can move at their desired speed if γ is not too large. When γ exceeds γ_c, due to increased density, reduced passing probability, and/or longer relaxation time, a certain fraction of the vehicles are at rest.

Although these conclusions are consistent with our general analysis, there is something strange about this result. If all vehicles move at the same velocity u, there is no need for passing, and each vehicle would simply maintain its velocity. Why would any vehicle have to stop in this situation? The answer is that, for $\gamma > \gamma_c$, the distribution $f(v) = f_0(v) = c \, \delta(v - u)$ continues to be a stationary solution of Eq. (11), but is *unstable*. To see this, suppose that at a certain moment, a fraction a_0 of the vehicles are stopped. If a_0

decreases (increases) with time, then the solution $f_0(v)$ is stable (unstable). To implement the stability analysis, we perturb the reference solution by letting

$$f(v,t) = c[a_0 \, \delta(v) + (1 - a_0) \, \delta(v - u)], \tag{24}$$

with $0 < a_0 < 1$. If we substitute Eq. (24) in Eq. (11) and perform the integral over u, we obtain

$$c\dot{a}_0[\delta(v) - \delta(v-u)] = -\frac{a_0 c}{T}[\delta(v) - \delta(v-u)] + c^2(1-P)$$
$$\times [a_0 \, \delta(v) + (1 - a_0) \, \delta(v-u)]$$
$$\times [-v a_0 + (1 - a_0)(u - v)], \tag{25}$$

where the dot denotes a time derivative. We equate coefficients of $\delta(v)$ and find

$$\dot{a}_0 = a_0 \left[c(1 - P)(1 - a_0)u - \frac{1}{T} \right]. \tag{26}$$

If we now let $\tilde{t} = t/T$ and $\tilde{\gamma} = \gamma u = \gamma/\gamma_c$, Eq. (26) becomes

$$\frac{da_0}{d\tilde{t}} = (\tilde{\gamma} - 1)a_0 - \tilde{\gamma} a_0^2, \tag{27}$$

which is the logistic or Pearl-Verhulst equation.[13] It is straightforward to show that the solution is

$$a_0(t) = \frac{a_0(0)e^{\epsilon \tilde{t}}}{1 + \kappa a_0(0)[e^{\epsilon \tilde{t}} - 1]}, \tag{28}$$

where $\epsilon = \tilde{\gamma} - 1 = (\gamma - \gamma_c)/\gamma_c$ and $\kappa = \gamma/(\gamma - \gamma_c)$. This result shows that for $0 < a_0(0) < 1$, as $t \to \infty$, $a_0(t) \to 0$ if $\gamma \le \gamma_c$, and $a_0(t) \to \alpha = (\gamma - \gamma_c)/\gamma$ if $\gamma > \gamma_c$. Thus, the solution with all vehicles moving at the same velocity u is stable if and only if $\gamma < \gamma_c = 1/u$.

Another example that has an analytic solution is a distribution of desired velocities uniform on the interval $[v_0 - v_a, v_0 + v_a]$

$$\tilde{f}_0 = \frac{\Theta[v - (v_0 - v_a)]\Theta[v_0 + v_a - v]}{2v_a}, \tag{29}$$

where $\Theta(y)$ is the step function, equal to zero for $y < 0$ and to unity for $y > 0$. (We assume $v_0 > v_a$ so that all drivers prefer some nonzero speed.) In this case, the transition occurs at

$$\gamma = \gamma_c = \frac{1}{2v_a} \ln \left(\frac{v_0 + v_a}{v_0 - v_a} \right), \tag{30}$$

and we have

$$\lambda = \max[\gamma\{v_a \coth(\gamma v_a) - v_0\}, 0], \tag{31}$$

leading to

$$\bar{v} = \begin{cases} \dfrac{1}{\gamma} + v_0 - v_a \coth(\gamma v_a) & (\gamma < \gamma_c) \\[2mm] \dfrac{1}{\gamma} & (\gamma > \gamma_c). \end{cases} \tag{32}$$
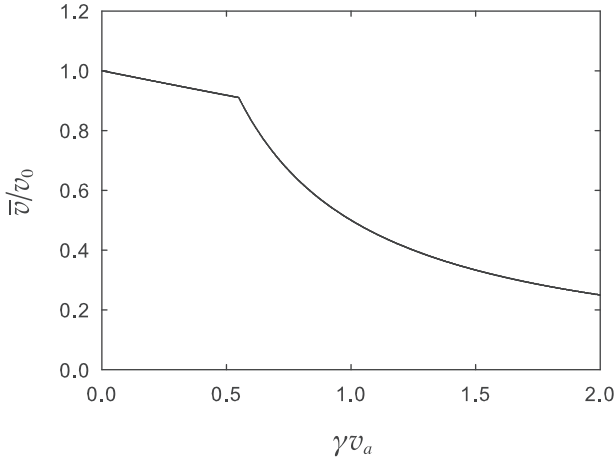
Fig. 1. The (dimensionless) mean speed versus γv_a for a uniform distribution of desired velocities, Eq. (29), with $v_a = v_0/2$. Note the discontinuous derivative signaling a transition from individual to collective behavior.

In Fig. 1, the dimensionless mean speed $\bar{v}/v_0$ is plotted versus γv_a for $v_a = v_0/2$.

IV. THE PRIGOGINE–HERMAN MODEL

Prigogine and Herman[7] introduced further assumptions regarding the dependence of P and T on the concentration c, which we shall refer to as the Prigogine–Herman model.

We expect the passing probability P to decrease with c, because drivers will find it more difficult to overtake a slower vehicle if adjacent lanes are congested. (Of course if vehicles were truly point particles there would be no such difficulty.) Prigogine and Herman assumed a linear relation between P and c, such that $P = 1$ for $c = 0$ and decreases to zero at some maximum concentration $c_{\max}$

$$P = 1 - \eta \quad \text{with} \quad \eta = \frac{c}{c_{\max}}. \tag{33}$$

They further proposed a concentration-dependent relaxation time

$$T = \frac{\tau(1 - P)}{P}, \tag{34}$$

where τ is a constant with dimensions of time. Thus, according to Prigogine and Herman, the greater the value of c the smaller the value of P and the longer it takes a driver to attain the desired speed. In their model, T does not represent an intrinsic limitation of drivers (that is, a reaction time) or of their vehicles (inertia), because $T \to 0$ as $c \to 0$. By inserting Eqs. (33) and (34) into Eq. (13), we find

$$\gamma = \frac{c_{\max}\tau\eta^3}{1 - \eta}. \tag{35}$$

Note that $c > c_{\max}$ is unphysical because it implies a negative passing probability. However, there is no intrinsic mechanism (such as a repulsive interaction between vehicles) for maintaining the concentration below its maximum value in Eq. (11). Hence, in spatially nonuniform situations, the concentration can evolve to exceed $c_{\max}$ in certain regions, even

if, initially, $c(x) < c_{\max}$ in the entire system. We consider examples using the Prigogine–Herman model in Sec. V, once a suitable numerical method is developed.

V. NUMERICAL METHOD

Consider the numerical solution of Eq. (19), yielding the value of λ such that the integral is unity, given the function $\tilde{f}_0(v)$ and γ, which is determined by the concentration via Eq. (35). Although the numerical method is simple, some care is required because in some cases the integral is improper.

Among the many methods for the numerical evaluation of integrals, we choose one that is relatively simple yet accurate by fitting cubic polynomials through successive groups of four points,[14] which is equivalent to the expression

$$\int_{x_1}^{x_n} y(x)dx \simeq h\left[\frac{3}{8}y_1 + \frac{7}{6}y_2 + \frac{23}{24}y_3 + y_4 + y_5 + \cdots \right.$$
$$\left. + y_{n-4} + y_{n-3} + \frac{23}{24}y_{n-2} + \frac{7}{6}y_{n-1} + \frac{3}{8}y_n\right], \tag{36}$$

where $h = (x_n - x_1)/(n - 1)$, $y_j \equiv y(x_j)$, and $x_j \equiv x_1 + (j - 1)h$, for $j = 1, \ldots, n$.

Dealing with an infinite range of integration requires greater care. We might truncate the integral, but the error depends on the choice of the cutoff. A more appealing alternative is to change variables to map the infinite range of integration to a finite one. For an exponential distribution of desired velocities, illustrated in Subsection V A, we are led to Eq. (41), for which the substitution $t = e^{-v/v_0}$ results in an integral over a finite interval

$$1 = \int_0^1 \frac{dt}{\lambda - \gamma v_0 \ln t}. \tag{37}$$

Once we have a method for evaluating the integral over velocities, we use a root-finding method to solve Eq. (41). For equations of the type used in Ref. 7 and the ones of interest here, the secant or Newton–Raphson methods are appropriate.[15] Although both are efficient, we will use the secant method, a recursive method used to find the solution to the equation $f(x) = 0$ via the relation

$$x_{n+1} = \frac{x_{n-1}f(x_n) - x_n f(x_{n-1})}{f(x_n) - f(x_{n-1})}, \tag{38}$$

starting from a pair of distinct initial values x_1 and x_2. The idea is to follow the secant line to its x-intercept and use that as an approximation for the root. This idea is similar to the Newton–Raphson method, which follows the tangent line, but the secant method does not require knowledge of the derivative.

The computational procedure for solving Eq. (19) is as follows. Let $g(\lambda, n)$ be the value of the integral in Eq. (19) over the interval $[v_1, v_2]$, given by a function that employs the method of Eq. (36) using n integration points. The latter is chosen according to the desired precision, using a function $\text{int}(\lambda)$, which evaluates the integral using successively larger numbers of points until the relative difference is smaller than a certain tolerance. Pseudocode for this procedure is given by

```
begin
define number of intervals n, increment
s, and precision e
a₁ = g(λ, n)
n = n + s
a₂ = g(λ, n)
do while |a₂-a₁|/a₂ > e
    a₁ = a₂
    n = n + s
    a₂ = g(λ, n)
end do
int = a₂
end
```

Because of the efficiency of the method described in Eq. (36), the function $\text{int}(\lambda)$ quickly converges to the correct value. We then search for the value of λ yielding $\text{int}(\lambda) = 1$ using the secant method. To begin we need a pair of distinct initial values, λ_1 and λ_2, with $0 < \lambda_i \leq 1$. We then evaluate $\text{int}(\lambda_1)$ and $\text{int}(\lambda_2)$, and apply the secant method to obtain a refined estimate for λ, which brings $\text{int}(\lambda)$ nearer to the desired value of unity. The process is iterated until the relative change in λ is smaller than a specified tolerance e. Because $\text{int}(\lambda)$ is strictly decreasing on the interval $[0, 1]$, the secant method works efficiently to locate λ. Pseudocode for this procedure is given by

```
begin
define λ₁ and λ₂
do while |λ₂ − λ₁|/λ₂ > e
    a = λ₂
    r₁ = int(λ₁) − 1
    r₂ = int(λ₂) − 1
    λ₂ = [λ₁r₂ − λ₂r₁]/[r₂ − r₁]
    λ₁ = a
end do
λ = λ₂
end
```

A. Exponential distribution of desired velocities

As an illustration, we solve the Prigogine–Herman model for an exponential distribution of desired velocities, as discussed in Ref. 7. Let

$$f_0 = \Theta(v) \frac{\eta c_{\max}}{v_0} e^{-v/v_0}, \tag{39}$$

for which the mean velocity is v_0. In this case, the most probable desired velocity is zero, and because $f_0(v = 0) > 0$, there is no transition. The stationary solution is

$$f = \frac{c_{\max} \eta e^{-v/v_0}}{v_0(\lambda + \gamma v)}, \tag{40}$$

where λ is determined by the normalization condition

$$1 = \frac{1}{v_0} \int_0^\infty \frac{e^{-v/v_0}}{\lambda + \gamma v} dv. \tag{41}$$

The value of λ for given values of γ and v_0 is obtained numerically as we have described.

The top panel in Fig. 2 shows the normalized flux $Q = q/c_{\max}$ as a function of the normalized concentration

$\eta = c/c_{\max}$. Note the linear relation between flux and concentration for small η. In this regime, the slope of each curve depends on v_0, the average desired velocity. At high concentrations, the normalized flux is independent of v_0. The (normalized) mean velocity is plotted versus η in the bottom panel of Fig. 2 for several values of v_0. As for the case of the normalized flux, all curves exhibit the same behavior at high concentrations.

It is interesting to compare the stationary velocity distribution with the corresponding distribution of desired velocities. Figure 3 shows that the stationary velocity distribution is close to the distribution of desired velocities for a relatively low concentration ($\eta = 0.2$). At a higher concentration ($\eta = 0.4$, Fig. 4), the two distributions differ, with higher probabilities for low velocities in the stationary velocity distribution than in the distribution of desired velocities.

B. Gaussian distribution of desired velocities

We now consider a more realistic example that has received little attention until now—a Gaussian-like distribution of desired velocities
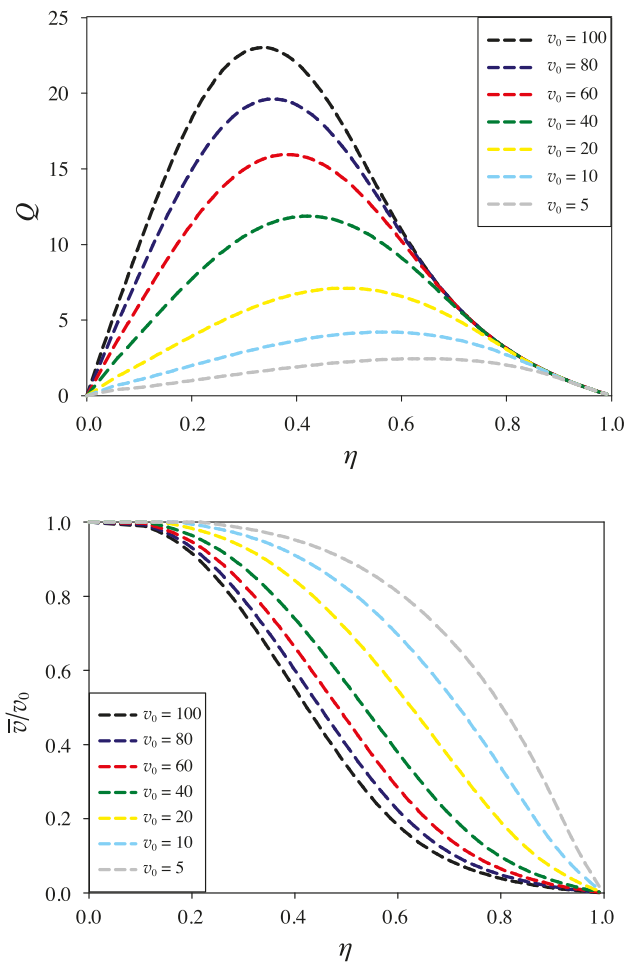
Fig. 2. The normalized flux $Q \equiv q/c_{\max}$ (top) and the normalized mean velocity $\bar{v}/v_0$ (bottom) versus the normalized concentration $\eta = c/c_{\max}$ for $c_{\max}\tau = 0.1$ and mean desired velocity v_0. At low concentrations, the mean velocity is close to its desired value, and the normalized flux is proportional to v_0. At larger concentrations, the normalized fluxes for different values of v_0 approach a common function.
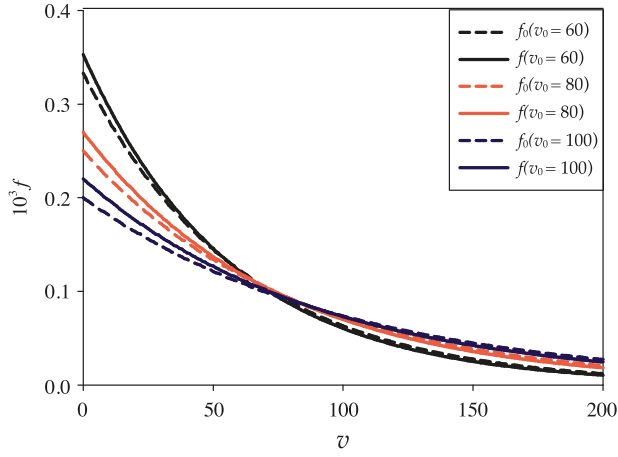
Fig. 3. (Color online) Distribution of desired velocities (dashed) and stationary velocity distribution (solid) for exponential desired velocity distributions with v_0 as indicated; $\eta = 0.2$. In all cases, the stationary distribution exceeds the desired one at low velocities, and vice-versa.

$$f_0(v) = cA[e^{-(v-v_0)^2/v_a^2} - e^{-v_0^2/v_a^2}]\Theta(v)\,\Theta(2v_0 - v). \quad (42)$$

The parameter v_0 represents the mean desired velocity, and v_a is a measure of the dispersion of the distribution. Because of the step functions, f_0 is zero outside the interval $[0, 2v_0]$. The second term in the square brackets ensures that f_0 goes to zero continuously at the endpoints of this interval. The normalization factor A is approximately $(v_a\sqrt{\pi})^{-1}$ for $v_0 \gg v_a$.

Because $\int(f_0/v)\,dv < \infty$, there is a transition between individual and collective flow. According to Eq. (20), the critical point is given by

$$\gamma_c = A \int_0^{2v_0} \frac{dv}{v} \left[e^{-(v-v_0)^2/v_a^2} - e^{-v_0^2/v_a^2}\right], \quad (43)$$

which is readily evaluated numerically. We proceed as before and calculate the stationary velocity distribution $f(v)$ and the stationary mean velocity and flux. Figure 5 shows the flux Q as a function of normalized concentration for several values of v_0, with $v_a = 20$. As expected, the slope of $q(\eta)$

Fig. 5. (Color online) The flux Q as a function of the normalized concentration η in the Prigogine–Herman model using the distribution of desired velocities of Eq. (42), with $v_a = 20$. The transition points are $\eta_c = 0.375$, 0.395, 0.421, and 0.458, for $v_0 = 120$, 100, 80, and 60, respectively. Above the critical concentration, the flux follows a master curve independent of v_0.

jumps from a positive to a negative value at the transition from individual to collective flow. In the latter regime, $q(\eta)$ is characterized by a single function, independent of v_0. The larger the value of v_0, the smaller the critical density η_c.

A notable aspect of the transition is the sudden change in the stationary distribution at the critical concentration at which the distribution splits into a regular and a singular part. In Fig. 6, which compares the stationary velocity distribution and distribution of desired velocities for several concentrations in the individual flow regime, we see that the two distributions have the same area, as required by normalization. For $\eta = 0.15$ the distributions are indistinguishable; at higher concentrations, small differences appear. The critical concentration, $\eta_c = 0.421$, represents the limit for individual flow; for $\eta > \eta_c$ the stationary velocity distribution is the sum of a regular part, given by $f_0/(\gamma v)$, and a singular part, $\alpha c\,\delta(v)$, with α given by Eq. (21). In Fig. 7, we compare the regular part of the stationary velocity distribution with the corresponding distribution of desired velocities for $\eta > \eta_c$.
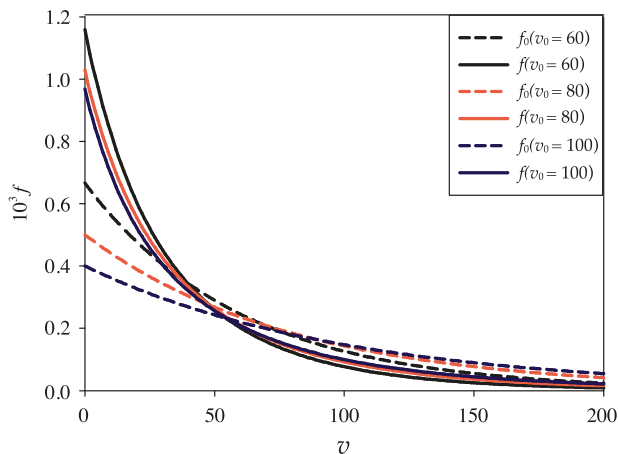

Fig. 4. (Color online) Distribution of the desired velocity and stationary velocity distribution as in Fig. 3 for $\eta = 0.4$. At this concentration, the differences between the stationary and desired distributions are more dramatic than in Fig. 3.
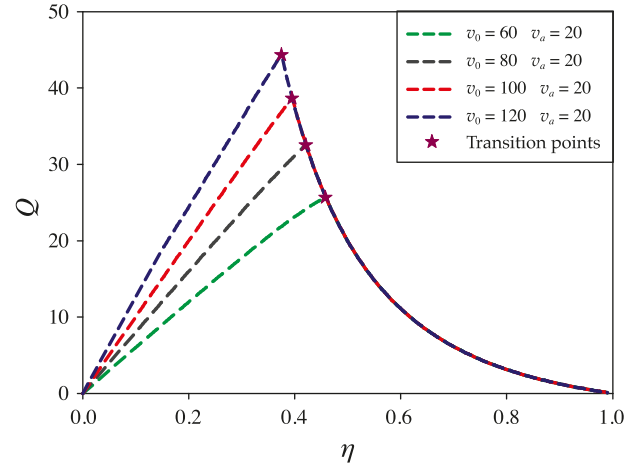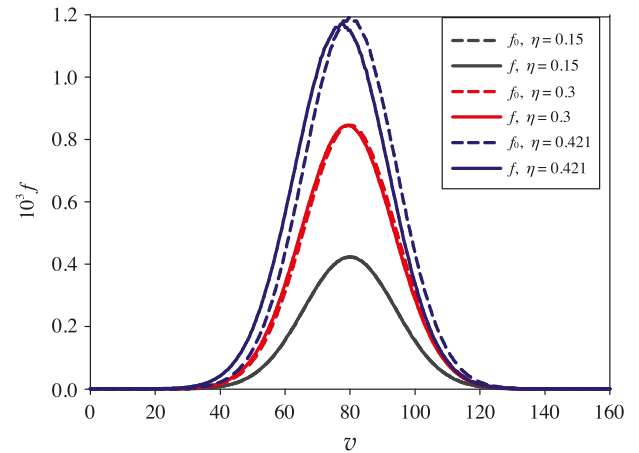

Fig. 6. The stationary velocity distribution (solid) and corresponding distribution of desired velocities (dashed), for concentrations in the individual flow regime. The distribution of desired velocities is given by Eq. (42) with $v_0 = 80$ and $v_a = 20$. The difference between the stationary and desired distributions grows with increasing concentration.
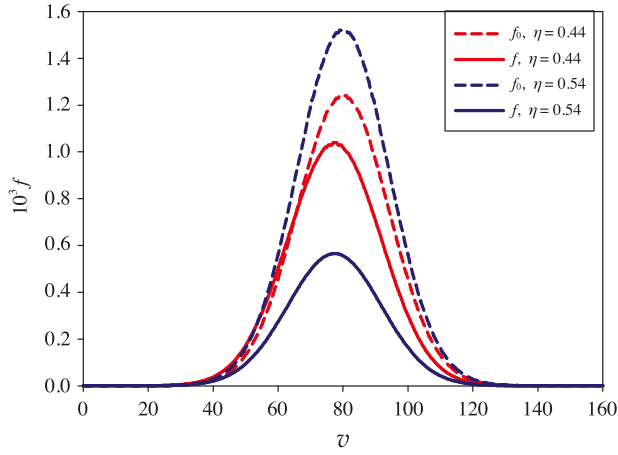
Fig. 7. Regular part of the stationary velocity distribution (solid) and the corresponding distribution of desired velocities (dashed) for densities in the collective flow regime; parameters as in Fig. 6. Note the differences in amplitude between the stationary and desired distributions, associated with a population of cars having velocity zero in the stationary distribution.

The area of the regular part of the stationary velocity distribution is smaller than that of the distribution of desired velocities. The difference corresponds to the δ-function at the origin.

VI. NUMERICAL INTEGRATION OF THE PRIGOGINE–HERMAN–BOLTZMANN EQUATION

The Prigogine–Herman–Boltzmann equation, Eq. (11), lends itself to numerical integration via straightforward discretization of the position, time, and velocity, permitting us to explore the space and time dependence of the density and velocity profiles. For simplicity, we adopt an explicit integration scheme. Let the length of the system be L, with periodic boundaries. We represent the distribution function $f(x, v, t)$ at a set of points

$$x_n = nL/N, \quad n = 0, \ldots, N \tag{44}$$

and velocities

$$v_m = mv_{\max}/M, \quad m = 0, \ldots, M, \tag{45}$$

where $v_{\max}$ is the maximum allowed velocity, larger than any velocity of interest in the problem under study. Similarly, time is discretized in steps $t_j = j\Delta t$, where Δt is a time increment chosen on the basis of efficiency, accuracy, and stability considerations. (A larger time increment reduces computation time but leads to increased discretization errors and possible numerical instabilities.)

Let $f(n, m, j)$ denote the value of f at position x_n, for velocity v_m and time t_j. The integration code uses Eq. (11) to construct the set of values $f(n, m, j + 1)$ based on the $f(n, m, j)$, via $f(n, m, j + 1) = f(n, m, j) + \dot{f}(n, m, j)\Delta t$, where the dot denotes a time derivative. The essential element of the integration algorithm is estimating the time derivatives of f.

From Eq. (11), we see there are three contributions to $\partial f/\partial t$, the first of which is $-v(\partial f/\partial x)$. In the discretized representation, we estimate the spatial derivative as

$$f_x(n, m, j) \simeq [f(n, m, j) - f(n - 1, m, j)]\left(\frac{N}{L}\right). \tag{46}$$

The spatial derivative f_x at position x_n is estimated using the value of f at this point and the one just to the left. Because vehicles move only to the right, there is little sense in including the value of f at point x_{n+1}, as might be done in a more symmetric integration scheme. Note that stability requires that $(Nv_{\max}/L)\Delta t < 1$; in practice we use $\Delta t \leq 0.01L/(Nv_{\max})$.

The second contribution to $\partial f/\partial t$ is the term $-[f(v) - cf_0(v)]/T$. (Here, the desired velocity distribution $f_0(v)$ is multiplied by the local concentration $c(x)$ because, in numerical implementations, it is convenient to normalize $f_0(v)$ so that its integral over velocities is unity.) This contribution is readily evaluated once we have the local concentration $c(n, j) = \sum_m f(n, m, j)$ and an expression for the relaxation time T. In the Prigogine–Herman model, the latter is given by Eq. (34), or simply $T = \tau c(n, j)/[1 - c(n, j)]$, where we set $c_{\max} = 1$. Because the term under consideration involves a factor of $1/T$, we cannot allow $c = 0$ anywhere.

The third contribution takes the discretized form $[c(n, j)]^2[\bar{v}(n, j) - v_m]f(n, m, j)$, where we have used Eq. (33) and introduced $\bar{v}(n, j) = \sum_m v_m f(n, m, j)/c(n, j)$. The following pseudocode details the integration algorithm (se use periodic boundary conditions).

```
begin
define system size L, maximum velocity
v_max, maximum time tmax,
    number of positions N, number of
    velocities M, time step Δt, relaxa-
    tion parameter tau, and normalized
    desired distribution of velocities
    f_0(m)
initialize f(n,m)
t = 0
for t ≤ tmax
    for n = 0, N
        nm = n-1
        if (n=0) nm = N
        c(n) = Σ_m f(n,m)
        v̄(n) = [Σ_m v_m * f(n, m)]/c(n)
        relax = [1-c(n)] / [c(n) * tau]
        for m = 0, M
            fx = [f(n,m) - f(nm,m)] * (N/L)
            df1 = -v_m * fx
            df2 = -relax * [f(n,m) - c(n) * f_0(m)]
            df3 = [c(n)]^2 * [v̄(n) - v_m] * f(n, m, j)
            df(n,m) = df1 + df2 + df3
        end
    end
    for n = 0, N
        for m = 0, M
            f(n,m) = f(n,m) + Δt * df(n,m)
        end
    end
    t = t + Δt
end
```

As examples, we apply the integration code to two cases.[16] In the first, the initial distribution of vehicles is inhomogeneous: the initial concentration is low ($c = 0.01$) except for a small region ($2 < x \leq 3$) that has $c = 0.8$. In the low-concentration region, the initial velocity distribution is taken as the desired one, which is essentially Gaussian, $f_0(j) = Ae^{-10(v_j - 1.6)^2}$, for $j = 2, \ldots, M$ (and zero for j outside

this set), giving a mean desired velocity of 1.5717. In the concentrated region, the initial velocity is 0.08 for all vehicles. (Distance and velocity are dimensionless in this example; the system size $L = 20$.) Integration of Eq. (11) allows us to follow how the concentration and mean velocity become uniform, as shown in Fig. 8.

In the second example, we seek the stationary concentration and mean-velocity profiles in a system with a *nonuniform* desired velocity distribution. Outside the region $8.5 < x \leq 10.5$, $f_0(j)$ is as in the previous example, but within this region we take $f_0(j) = Ae^{-12(v_j - 0.8)^2}$ for $j = 2, \ldots, M$. The reduction in mean desired speed by about half reflects a change in driving conditions, such as a speed trap or narrowing of the road. The inhomogeneous desired velocity distribution causes a pile-up of vehicles (as well as a reduction in speed) within the "slow" region and well beyond it, as shown in Fig. 9. In actual road traffic, we expect the concentration to take a higher than average value to the left of the slow region as well, as drivers slow down in anticipation of the congestion ahead. This feature of real traffic is absent in the Prigogine–Herman–Boltzmann model: drivers interact only with vehicles at the same position and cannot adjust to road conditions ahead of them.

VII. DISCUSSION

We have seen that the Prigogine–Herman–Boltzmann equation describes some basic features of vehicular traffic, and that the Prigogine–Herman model,[5–7] which introduces additional hypotheses regarding driving behavior, leads to interesting predictions such as a transition between individual and collective flows. Nevertheless, this approach has shortcomings. Several problems with the Prigogine–Herman model are discussed in Ref. 17. Letting the relaxation time T depend on the concentration introduces an effective interaction
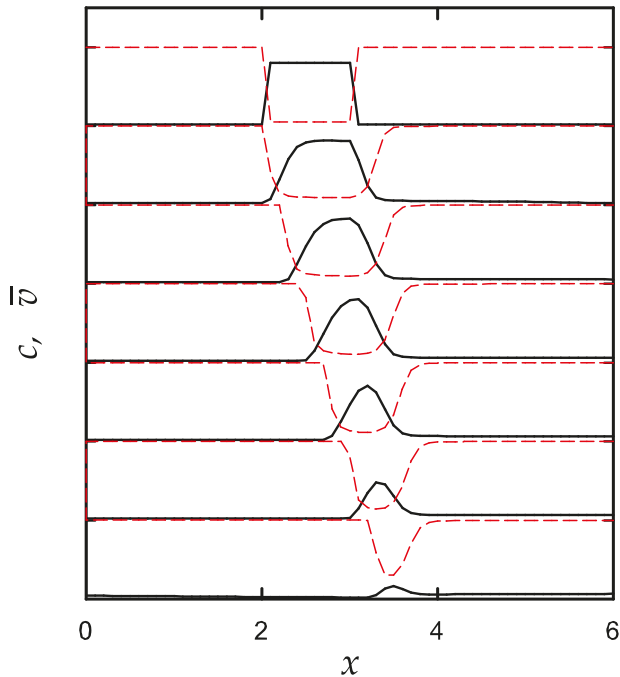

Fig. 8. Concentration (solid) and mean velocity (dashed) profiles obtained from the Prigogine–Herman–Boltzmann equation via numerical integration, for times (upper to lower) 0, 2, 4,…, 12. The mean velocity has been normalized to the desired value of 1.5717. The concentration and mean velocity gradually become uniform.
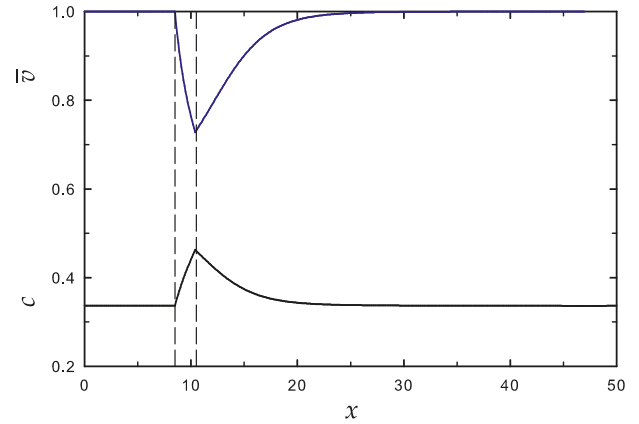

Fig. 9. Concentration (lower curve) and mean velocity (upper curve) profiles in the steady state, obtained from the Prigogine–Herman–Boltzmann equation via numerical integration. The mean velocity has been normalized to its desired value (outside the slow region) of 1.5717. The mean desired velocity in the region between the vertical dashed lines is only half its value outside. Note how the reduction in desired velocity leads to a higher concentration in the slow region and well beyond it.

between vehicles, in addition to the integral term, which represents binary interactions. As a result, the clear separation between individual particle motion (streaming terms) and collisions in the original Boltzmann equation becomes somewhat muddled in the Prigogine–Herman model.

Several modifications of the Prigogine–Herman–Boltzmann equation[17–19] and of the Prigogine–Herman model have been proposed to study traffic more realistically and to extend the model to higher concentrations. The Prigogine–Herman model was modified by Paveri-Fontana[17] to include the joint distribution of position x, velocity v, and desired velocity u. In their description, $g(x, v, u; t) \, dx \, dv \, du$ represents the number of vehicles at time t, with position between x and $x + dx$, having velocity between v and $v + dv$, and desired velocity between u and $u + du$. In this way, the model can include the strong correlation between drivers' speed v and their desired speed u. For example, in the absence of interactions, we expect $g(x, v, u, t) \rightarrow f_0(x, u, t)\delta(v - u)$ as $t \rightarrow \infty$.

Wagner *et al.*[18] proposed a traffic flow model using the desired velocity proposed by Paveri-Fontana.[17] By taking into account the nonzero length of vehicles, these authors extend the description of Paveri-Fontana to the high-density regime. In Ref. 19, a successive slowing-down process is considered, in which drivers react to traffic conditions in a more cautious manner.

Despite various criticisms,[17–19] the Prigogine–Herman model remains important. One can find applications of the model in other contexts, for instance, to network traffic.[20] Nelson and Sopasakis[12] use the model to show that, under some assumptions regarding the relaxation time and passing probability, the stationary solution is not unique above a certain density; the existence of multiple solutions reflects the tendency toward substantial scatter in observational data of traffic flow at high concentrations.

Our impression is that although a passing probability that decreases with vehicle concentration is reasonable, a concentration-dependent relaxation time is not. The relaxation time should rather reflect intrinsic limitations of the drivers (finite reaction times) and their vehicles (inertia), which render instantaneous changes in speed impossible. A linear dependence of passing probability on concentration may also be

unrealistic. To move to the passing lane, drivers must find a gap large enough to safely accommodate their vehicle. Results from the theory of liquids suggest that this probability decays exponentially, not linearly with concentration. We further suggest that drivers adjust their desired speeds according to road conditions, tending to reduce their desired speed as the concentration increases, so as to avoid collisions. If such alterations can be introduced within the Prigogine–Herman–Boltzmann framework without undue complications, it may be possible to enhance understanding of traffic dynamics while providing more reliable predictions.

VIII. COMPARISON WITH OTHER APPROACHES

The first deterministic continuous model of traffic was a dynamical model[21] based on the equations of motion of each vehicle, which are solved numerically. Monte Carlo simulations of the Nagel–Schreckenberg cellular automaton show a transition from free flow to jammed traffic with increasing vehicle density.[8] Both of these microscopic models have a relatively high level of detail as they describe individual drivers' behavior and pairwise interactions. An important advantage of microscopic models is their ability to describe events triggered by fluctuations. Kinetic theories do not include fluctuations and can be interpreted as mean-field theories of traffic. Thus, they share many of the advantages and disadvantages of mean-field theories of phase transitions.

Despite the successes of the Nagel–Schreckenberg automaton and other microscopic models, it is fair to say that they rest on models of driving behavior that are no more realistic than those used in kinetic theories. Notwithstanding the unrealistic assumptions regarding individual drivers, microscopic models do capture collective behavior in the large-system limit. Kinetic theory also captures some aspects of this behavior. More recently, new macroscopic approaches to traffic have been developed, including a lattice Boltzmann model for traffic flow[22] and the application of the Chapman–Enskog and Grad methods to traffic theory.[23]

IX. SUGGESTIONS FOR FURTHER STUDY

The following projects involve possible improvements of the Prigogine and Herman model. Some have been applied by Wagner[18,19] to Fontana's model.[17] It is interesting to study the modifications in the stationary speed distribution due to changes in the collision term of the Prigogine–Herman–Boltzmann equation.

The first modification is to incorporate the fact that vehicles are not point-like objects but have a spatial extension ℓ, and require an additional safety distance $\tau_r v$, where τ_r is the drivers' reaction time. These changes result in a reduced effective road length, reminiscent of the accessible volume in van der Waals theory. In particular, two modifications are introduced in the interaction term:

(1) The effective volume is reduced. Suppose a road of length L contains n vehicles; the concentration $c = n/L$. The effective length is $L - n\ell - \tau_r \sum_{i=1}^{n} v_i$ if we include the vehicle length and the safety distance $d_s = \tau_r v$. Due to the reduced effective length, the interaction frequency is enhanced by

$$\nu(c, \bar{v}) = \frac{1}{1 - c(\ell + \tau \bar{v})}, \tag{47}$$

where $\bar{v}$ is the mean velocity. Because ν and P are functions of c, we can define a modified interaction probability $\sigma = \nu(c, \bar{v})[1 - P(c)]$.

(2) In the Prigogine–Herman model, vehicles with fixed speed v interact with vehicles with speed u at the same position x. In the modified model, a vehicle with velocity u at position x interacts with vehicles with velocity v at position $x + \ell + \tau u$, and vehicles with velocity v at x interact with those with velocity u at $x + \ell + \tau v$, so that we have

$$\left(\frac{\partial f}{\partial t}\right)_{\text{int}} = \int_v^\infty du\, \sigma(u - v) f(x + \ell + u\tau, v, t) f(x, u, t)$$
$$- \int_{-\infty}^v du\, \sigma(v - u) f(x, v, t) f(x + \ell + v\tau, u, t). \tag{48}$$

The project consists in introducing these modifications in the Prigogine–Herman–Boltzmann equation and, using the same distribution of desired velocities, comparing the stationary velocity distribution with that found using the original Prigogine and Herman model. An interesting modification is to include different kinds of vehicles, with different lengths and safety distances. For each kind of vehicle, we must assign a specific distribution function; vehicles of different kinds interact with each other in the collision term. The stationary distributions and the concentration marking the transition from individual to collective flow now depend on the fractions of vehicles belonging to each class.

ACKNOWLEDGMENTS

a)Electronic mail: lobao@div.cefetmg.br

b)Electronic mail: dickman@fisica.ufmg.br

[1] M. Patriarca and A. Chakraborti, "Kinetic exchange models: From molecular physics to social science," Am. J. Phys. **81**, 618–623 (2013).

[2] V. M. Yakovenko and J. Barkley Rosser, Jr., "Colloquium: Statistical mechanics of money, wealth, and income," Rev. Mod. Phys. **81**, 1703–1726 (2009).

[3] R. Reisenauer, K. Smith, and R. A. Blythe, "Stochastic dynamics of lexicon learning in an uncertain and nonuniform world," Phys. Rev. Lett. **110**, 258701-1–4 (2013).

[4] C. Castellano, S. Fortunato, and V. Loreto, "Statistical physics of social dynamics," Rev. Mod. Phys. **81**, 591–646 (2009).

[5] I. Prigogine and F. C. Andrews, "A Boltzmann-like approach for traffic flow," Oper. Res. **8**, 789–797 (1960).

[6] I. Prigogine, R. C. Herman, and R. L. Anderson, "On the statistical distribution function theory of traffic flow," Oper. Res. **10**, 180–196 (1962).

[7] I. Prigogine and R. C. Herman, *Kinetic Theory of Vehicular Traffic* (Elsevier, New York, 1971).

[8] K. Nagel and M. Schreckenberg, "A cellular automaton model for freeway traffic," J. Phys. I (France) **2**, 2221–2229 (1992).

[9] R. L. Liboff, *Kinetic Theory: Classical, Quantum, and Relativistic Descriptions* (Springer-Verlag, New York, 2003).

[10] See Ref. 7, pp. 42–51 for further details.

[11] M. Plischke and B. Bergersen, *Equilibrium Statistical Physics* (World Scientific, Singapore, 1994).

[12] P. Nelson and Sopasakis, "The Prigogine-Herman kinetic model predicts widely scattered traffic flow data at high concentrations," Trans. Res. B **32**, 589–604 (1998).

[13] M. Kot, *Elements of Mathematical Ecology* (Cambridge U.P., Cambridge, 2001).

[14] W. H. Press, S. A. Teukolsky, W. T. Velterling, and B. P. Flannery, *Numerical Recipes in Fortran* (Cambridge U.P., New York, 1993). See p. 128.

[15] See Ref. 14, pp. 347, 355.

[16]In these studies we use $v_{max} = 2.0$, $N = 10L$, $M = 50$, $\tau = 5.0$, and $\Delta t = 0.008L/(Nv_{max})$.

[17]S. L. Paveri-Fontana, "On Boltzmann-like treatments for traffic flow: A critical review of the basic model and an alternative proposal for dilute traffic analysis," Trans. Res. **9**, 225–235 (1975).

[18]C. Wagner, C. Hoffmann, R. Sollacher, J. Wagenhuber, and B. Schurmann, "Second-order continuum traffic flow model," Phys. Rev. E **54**, 5073–5085 (1996).

[19]C. Wagner, "Successive deceleration in Boltzmann-like traffic equations," Phys. Rev. E **55**, 6969–6978 (1997).

[20]I. Antoniou, V. V. Ivanov, and Yu. L. Kalinovsky, "Kinetic model of network traffic," Physica A **308**, 533–544 (2002).

[21]M. Bando, K. Hasebe, A. Nakayama, A. Shibata, and Y. Sugiyama, "Dynamical model of traffic congestion and numerical simulation," Phys. Rev. E **51**, 1035–1042 (1995).

[22]J. Meng, Y. Qian, X. Li, and S. Dai, "Lattice Boltzmann model for traffic flow," Phys. Rev. E **77**, 36108-1–9 (2008).

[23]W. Marques, Jr. and A. R. Méndes, "On the kinetic theory of vehicular traffic flow: Chapman-Enskog expansion versus Grad's moment method," Physica A **392**, 3430–3440 (2013).

Optical Disk

If you want one piece of apparatus for the study of geometrical optics in the introductory laboratory, you need to have an optical disk. The white or silver disk, about 30 cm in diameter, is surrounded by a rotating shade. A rectangular hole in the shade holds a thin metal plate with a series of horizontal slots in it. A parallel beam of light from an incandescent light source placed outside the apparatus shines on the slits, producing a series of parallel, flat beams of light. Alternately, a single slit can be used to produce a single beam of light, or the set of cylindrical diverging lenses in the foreground can be used to produce diverging rays. In all situations the light source is oriented so that one edge of the beams hits the front surface of the disk, thus letting the rays be seen clearly even in semi-darkness, and allowing quantitative observations to be made on the reflection and refraction of the light rays. The picture shows a semicircular refraction tank mounted in the middle of the disk. Thick and thin diverging and converging lenses can be clamped onto the disk, and a glass disk can be used to investigate the formation of a rainbow. This example, made by Cenco, is in the Greenslade Collection. (Notes and picture by Thomas B. Greenslade, Jr., Kenyon College)

Traffic model with an absorbing-state phase transition

M. L. L. Iannini[*] and Ronald Dickman[†]

Departamento de Física and National Institute of Science and Technology for Complex Systems, ICEx,
Universidade Federal de Minas Gerais, C. P. 702, 30123-970 Belo Horizonte, Minas Gerais, Brazil

We consider a modified Nagel-Schreckenberg (NS) model in which drivers do not decelerate if their speed is smaller than the headway (number of empty sites to the car ahead). (In the original NS model, such a reduction in speed occurs with probability p, independent of the headway, as long as the current speed is greater than zero.) In the modified model the free-flow state (with all vehicles traveling at the maximum speed, $v_{\max}$) is *absorbing* for densities ρ smaller than a critical value $\rho_c = 1/(v_{\max} + 2)$. The phase diagram in the ρ-p plane is reentrant: for densities in the range $\rho_{c,<} < \rho < \rho_c$, both small and large values of p favor free flow, while for intermediate values, a nonzero fraction of vehicles have speeds $< v_{\max}$. In addition to representing a more realistic description of driving behavior, this change leads to a better understanding of the phase transition in the original model. Our results suggest an unexpected connection between traffic models and stochastic sandpiles.

I. INTRODUCTION

The Nagel-Schreckenberg (NS) model holds a central position in traffic modeling via cellular automata, because it reproduces features commonly found in real traffic, such as the transition between free flow and a jammed state, start-and-stop waves, and shocks (due to driver overreaction) [1]. This simple model represents the effect of fluctuations in driving behavior by incorporating a stochastic element: the spontaneous reduction of velocity with probability p.

Although the NS model has been studied extensively, the nature of the transition between free and jammed flow, in particular, whether it corresponds to a critical point, remains controversial [2–5]. A proposed definition of the order parameter in the NS model [6], and a subsequent comment [7,8] are pertinent to this issue. According to the authors of Ref. [7], results for the lifetime distribution, spatial correlations, and relaxation time provide evidence for a "crossover type jamming transition" from free flow to the jammed regime, but not for a well-defined phase transition. Modifications in the update rules of the NS model have been found to result in a phase transition [9,10]. Krauss *et al.* [11] proposed a generalized version of the NS model and showed numerically that free- and congested-flow phases may coexist. While the NS model does not exhibit metastable states, which are important in observed traffic flow, including a slow-to-start rule, such that acceleration of stopped or slow vehicles is delayed compared to that of moving or faster cars, can lead to metastability [12–14]. Takayasu and Takayasu [12] were the first to suggest a cellular automaton (CA) model with a slow-to-start rule. Benjamin, Johnson, and Hui introduced a different slow-to-start rule in Ref. [13], while Barlovic *et al.* suggested a velocity-dependent randomization model [14]. Other models with metastable states are discussed in Refs. [15,16]. A review of CA traffic models is presented in Ref. [17].

In the original NS model, at each time step (specifically, in the reduction substep), a driver with nonzero velocity reduces her speed with probability p. Here we propose a simple yet crucial modification, eliminating changes in speed in this substep when the distance to the car ahead is greater than the current speed. We believe that this rule reflects driver behavior more faithfully than does the original reduction step, in which drivers may decelerate for no apparent reason. While one might argue that distractions such as cell phones cause drivers to decelerate unnecessarily, we can expect that highways will be increasingly populated by driverless vehicles exhibiting more rational behavior. The modified model, which we call the absorbing Nagel-Schreckenberg (ANS) model, exhibits a line of absorbing-state phase transitions between free and congested flow in the ρ-p plane. (Here ρ denotes the *density*, i.e., the number of vehicles per site.) The modification proposed here allows us to understand the nature of the phase transition in the original model, and to identify a proper order parameter. The ANS model exhibits a surprising reentrant phase diagram. Some time ago, Wang studied a model with the same modified reduction step, and found that free flow is absorbing for all densities $\leqslant 1/7$, regardless of p [10]. This model differs from ours in that acceleration to the maximum allowed speed occurs in a single update, rather than in increments.

Regarding the nature of the phase transition in the original NS model, the key insight is that, for $p = 0$, it exhibits a transition between an absorbing state (free flow) and an active state (congested flow) at density $\rho = 1/(v_{\max} + 1)$, where $v_{\max}$ denotes the maximum speed. Free flow is absorbing because each car advances the same distance in each time step, so that the configuration simply executes rigid-body motion (in the co-moving frame it is frozen). We note that for $\rho < 1/(v_{\max} + 1)$, many absorbing configurations exist; which one is attained by the dynamics depends on the initial condition. Congested flow, by contrast, is active in the sense that the distances between vehicles change with time. Below the critical density, activity (if present initially) dies out, and an absorbing configuration is reached; for $\rho > 1/(v_{\max} + 2)$ there must be activity, due to lack of sufficient space between vehicles. Setting $p > 0$ in the original model is equivalent

―――――――
[*]lobao@div.cefetmg.br
[†]dickman@fisica.ufmg.br

to including a *source* of spontaneous activity. Since such a source eliminates the absorbing state [19], the original NS model *does not possess a phase transition for* $p > 0$. (It should nonetheless be possible to observe scaling phenomena as $p \to 0$.) A similar conclusion was reached by Souza and Vilar [5], who drew an analogy between the phase transition at $p = 0$ and a quantum phase transition at temperature $T = 0$. In their analogy, $p > 0$ corresponds to $T > 0$, for which, *sensu stricto*, there is again no phase transition.

The remainder of this paper is organized as follows. In the next section we define the ANS model, pointing out how it differs from the original NS model. In Sec. III we explain qualitatively the nature of the phase diagram, and report simulation results for the phase boundary. Section IV presents results on critical behavior, followed in Sec. V by a summary and discussion of our findings.

II. MODEL

The NS model and its absorbing counterpart (ANS) are defined on a ring of L sites, each of which may be empty or occupied by a vehicle with velocity $v = 0, 1, \ldots, v_{max}$. (Unless otherwise noted, we use $v_{max} = 5$, as is standard in studies of the NS model.) The dynamics, which occurs in discrete time, conserves the number N of vehicles; the associated intensive control parameter is $\rho = N/L$. Denoting the position of the ith vehicle by x_i, we define the headway $d_i = x_{i+1} - x_i - 1$ as the number of empty sites between vehicles i and $i + 1$. Each time step consists of four substeps, as follows:

(i) Each vehicle with $v_i < v_{max}$ increases its velocity by one unit: $v_i \to v_i + 1$

(ii) Each vehicle with $v_i > d_i$ reduces its velocity to $v_i = d_i$.

(iii) NS model: each vehicle reduces its velocity by one unit with probability p.

(iv) ANS model: each vehicle with $v_i = d_i$ reduces its velocity by one unit with probability p.

(v) All vehicles advance their position in accord with their velocity.

In practice, given the velocities v_i and headways d_i, there is no need to keep track of positions: the final substep is simply $d_i \to d_i - v_i + v_{i+1}$ for $i = 1, \ldots, N-1$, and $d_N \to d_N - v_N + v_1$.

The modification of the third substep leads to several notable changes in behavior, as reflected in the fundamental diagram shown in Fig. 1, which contrasts the flux-density relation in the NS and ANS models. In the ANS model the flux exhibits a discontinuous first derivative at a certain density $\rho_c(p)$ (for any p between zero and one), while in the NS model the flux and other observables are smooth functions of density for $p > 0$. Thus the ANS model exhibits a phase transition for general p, whereas the NS model has a phase transition only for $p = 0$ [6,7]. The flux q generally takes its maximum value at the transition. (For small p, however, maximum flux occurs at a density above $\rho_c = 1/(v_{max} + 2)$, approaching $\rho = \frac{1}{v_{max}+1}$ for $p = 0$.) The low-density absorbing phase has $v_i = v_{max}$ and $d_i \geqslant v_{max} + 1$, $\forall i$; in this phase all drivers advance in a deterministic manner, with the flux given by $j = \rho v_{max}$. In the active state, by contrast, a nonzero fraction of vehicles have
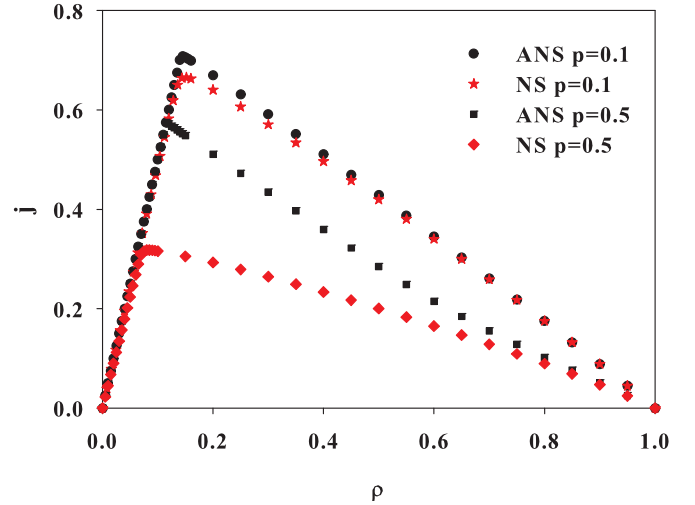

FIG. 1. Flux j versus density in the NS and ANS models for probabilities $p = 0.1$ (upper) and $p = 0.5$ (lower). System size $L = 10^5$; vehicles are distributed randomly at $t = 0$. Error bars are smaller than symbols.

$d_i \leqslant v_{max}$. For such vehicles, changes in velocity are possible, and the configuration is nonabsorbing. The stationary fluxes in the NS and ANS models differ significantly over a considerable interval of densities, especially for high values of p. Below the critical density ρ_c, this difference is due the existence of an absorbing phase in the ANS model. For densities slightly above ρ_c, most vehicles have velocity $v_i = v_{max}$ and $d_i = v_{max} + 1$, although there is no absorbing state. As the density approaches unity, the differences between the fluxes in the ANS and NS models become smaller.

For fixed deceleration probability p, the flux $j = \rho \bar{v}$ first grows, and then decreases as we increase the vehicle density ρ. An intriguing feature is the dependence of the density at maximum flux on the probability p: Fig. 2 shows that the density at maximum flux decreases with increasing p until reaching a minimum near $p = 0.5$, and subsequently increases with increasing p. This reflects the reentrant nature of the phase diagram, as discussed in Sec. III.

A. Special cases: $p = 0$ and $p = 1$

For the extreme values $p = 0$ and $p = 1$ the ANS model is deterministic; these two cases deserve comment. For completeness we mention the corresponding results pertaining to the NS model given in Ref. [18], which also includes a discussion of mean field theories. For $p = 0$, the NS and ANS models are identical. The system reaches an absorbing state, $v_i = v_{max}$, $\forall i$, for densities $\rho \leqslant 1/(v_{max} + 1)$. For higher densities we observe nonzero activity in the steady state. We note however that there are special configurations, in which $v_i = d_i$, $\forall i$, with some $v_i < v_{max}$, whose evolution corresponds to a rigid rotation of the pattern. [A simple example is $v_i = d_i = n$, $\forall i$, with $n = 1, 2, 3$, or 4, and density $\rho = 1/(n+1)$.] Since our interest here is in the model with $0 < p < 1$ we do not comment further on such configurations.

For the NS model with $p = 1$, from one step to the next, each velocity v_i is nonincreasing. (Of course $v_i \to v_i + 1$ at
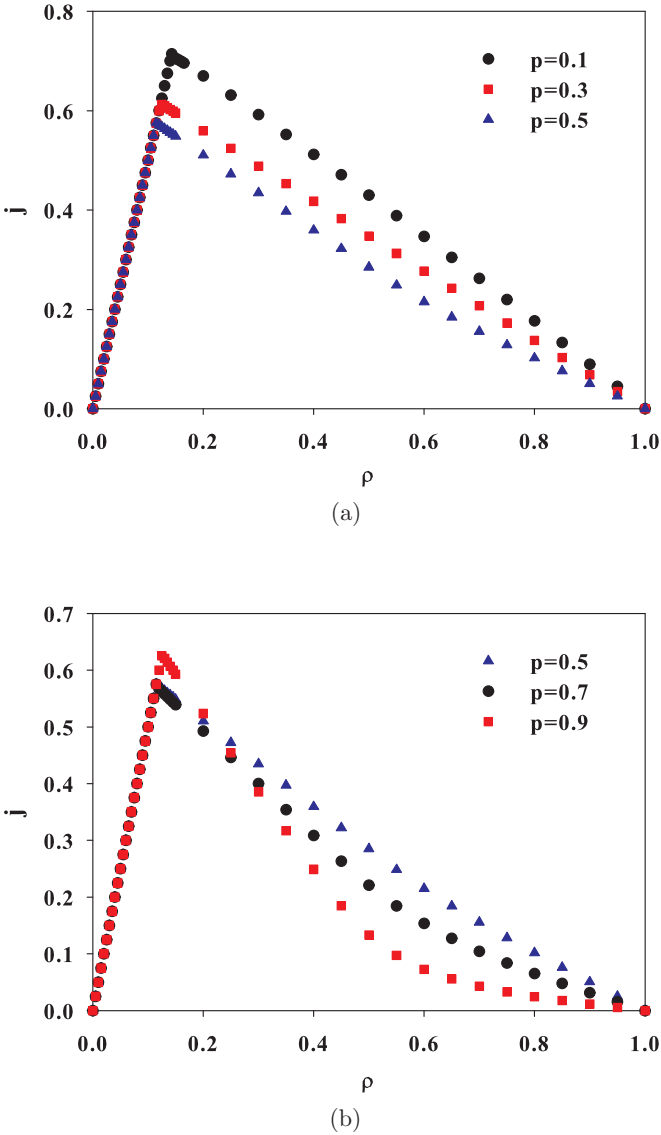
FIG. 2. Steady-state flux versus density in the ANS model for (a) $p = 0.1$, 0.3, and 0.5, and (b) $p = 0.5$, 0.7, and 0.9. Note that the density of maximum flux first decreases, and then increases, with increasing p; the minimum occurs near $p \simeq 0.5$. System size $L = 10^5$; vehicles are distributed randomly at $t = 0$. Error bars are smaller than symbols.

the acceleration substep, but this is immediately undone in the subsequent substeps.) Thus if the evolution leads to a state in which even one vehicle has velocity zero, all vehicles eventually stop. Such an event is inevitable for $\rho > 1/3$, since in this case $d_i \leqslant 1$ for at least one vehicle, which is obliged to have $v_i = 0$ after one step. For $\rho \leqslant \frac{1}{3}$, steady states with nonzero flux are possible, depending on the choice of initial condition. Such configurations are *metastable* in the sense that the stationary state depends on the initial distribution. In the ANS model with $p = 1$ the mean velocity in steady state is zero only for $\rho \geqslant 1/2$. For $\rho \leqslant 1/(v_{max} + 2)$, we find that the system always reaches an absorbing configuration with $\bar{v} = v_{max}$. In the remaining interval, $1/(v_{max} + 2) < \rho \leqslant 1/2$, we find $\bar{v} = 1 - 2\rho$.

III. PHASE DIAGRAM

A. Initial condition dependence

In studies of traffic, states are called *metastable* if they can be obtained from some, but not all initial conditions [12–16]; such states are an essential component of real traffic. Since the NS model is not capable of reproducing this feature, models with modified update rules have been investigated by several authors [12–14]. In the ANS model, by contrast, there is a region in the ρ-p plane in which, depending on the initial condition, the system may evolve to an active state or an absorbing one. Our results are consistent with the usual scenario for absorbing-state phase transitions [19–21]: activity in a finite system has a finite lifetime; in the active phase, however, the mean lifetime diverges as the system size tends to infinity. Properties of the active phase may be inferred from simulations that probe the *quasistationary regime* of large but finite systems [24].

To verify the existence of metastable states in the ANS model, we study its evolution starting from two very different classes of initial conditions (ICs): homogeneous and jammed. In a homogeneous IC, the headways d_i are initially are uniform as possible, given the density $\rho = 1/(1 + \bar{d})$, where $\bar{d}$ denotes the mean headway. In this case the initial velocity is v_{max} for all vehicles. In a jammed IC, N vehicles occupy N contiguous sites, while the remaining $N(\rho^{-1} - 1)$ sites are vacant; in this case $d_i = 0$ for $i = 1, \ldots, N - 1$, and only vehicle N has a nonzero initial velocity ($v_N = v_{max}$). Homogeneous ICs are much closer to an absorbing configuration than are jammed ICs. We note that random initial conditions lead to the same steady state as jammed ICs.

Figure 3 shows the fundamental diagram obtained using homogeneous and jammed ICs for $p = 0.1$; for this value of p the stationary state is the same, regardless of the IC, except near $\rho = \frac{1}{7}$ where, for the homogeneous ICs, an absorbing configuration is attained, having a greater steady-state flux than obtained using jammed ICs. For higher probabilities p, we find a larger interval of densities in which the stationary behavior depends in the choice of IC. In Fig. 4, for $p = 0.5$, this interval corresponds to $0.118 \leqslant \rho \leqslant 0.143$; higher fluxes (black points) are obtained using homogeneous ICs, and lower fluxes (red) using jammed ICs. Homogeneous ICs rapidly evolve to an absorbing configuration, while jammed ICs, which feature a large initial activity, do not fall into an absorbing configuration for the duration of the simulation ($t_{max} = 10^7$), for the system size ($L = 10^5$) used here. In Fig. 4, the flux obtained using jammed ICs (red stars) exhibits a discontinuous first derivative, signaling a continuous phase transition. The flux for homogeneous ICs (black circles), exhibits a downward jump at $\rho = 1/7$. While the latter might be interpreted as evidence of a discontinuous phase transition, we note that the absorbing state, to which homogenous ICs evolve for smaller densities, ceases to exist for $\rho > 1/7$. Thus $\rho = 1/7$ can be seen as the terminal line of the absorbing phase. As in sandpile models, the absorbing-state phase transition occurs at a smaller density (in the ANS model, that marking the discontinuity in the derivative of j), at which a nonabsorbing (active) phase first appears. For $0 < p < 1$, the properties of the active phase (obtained using either jammed or random ICs) are nonsingular at $\rho = 1/7$.
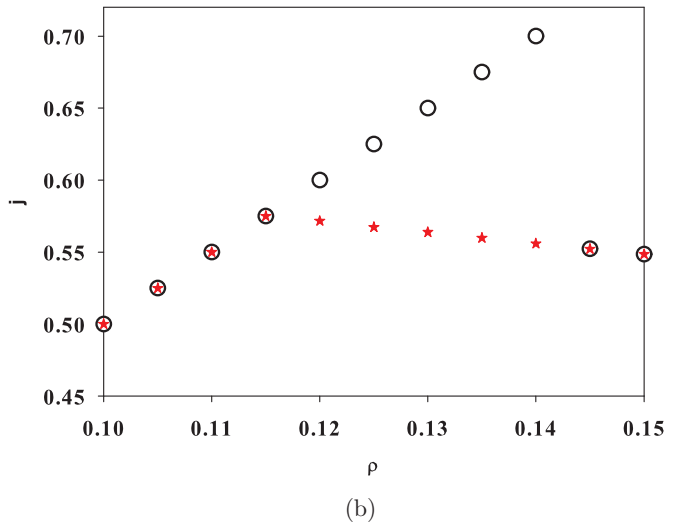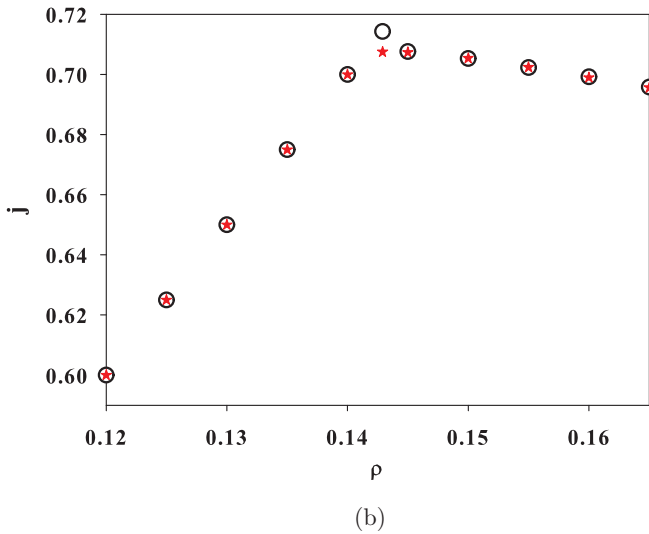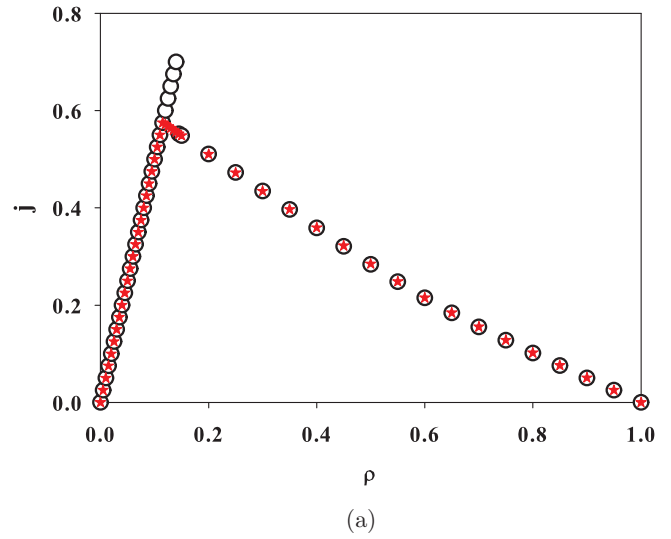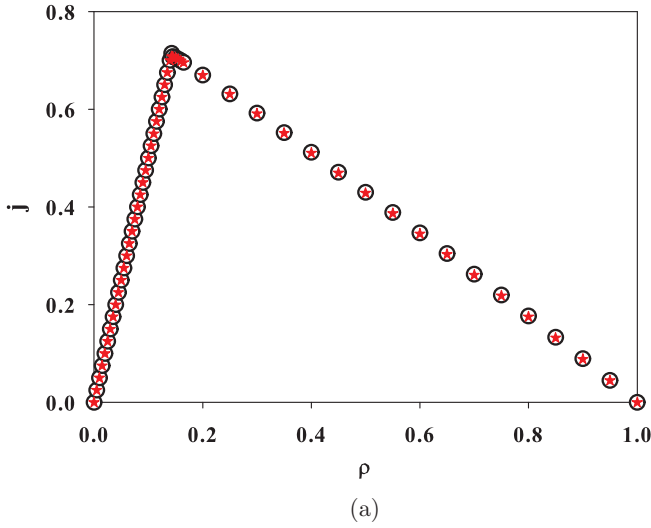
(a)

(b)

FIG. 3. Steady-state flux versus density for $p = 0.1$ and $L = 10^5$. Homogeneous (stars) and jammed (circles) ICs lead to identical stationary states [panel (a)] except for a small interval of densities near maximum flux highlighted in panel (b). Error bars are smaller than symbols.

Systematic investigation of the steady-state flux obtained using homogeneous and jammed ICs leads to the conclusion that the ρ-p plane can be divided into three regions. To begin, we recall that for $\rho > 1/(v_{\max} + 2)$ and $p > 0$, the mean velocity $\bar{v}$ must be smaller than $v_{\max}$. Thus the activity is nonzero and the configuration (i.e., the set of values v_i and d_i) changes with time. In this region, homogeneous and jammed ICs always lead to the same steady state.

For $\rho \leqslant 1/(v_{\max} + 2)$, absorbing configurations exist for any value of p. There is nevertheless a region with $\rho < 1/(v_{\max} + 2)$ in which activity is long-lived. In this region, which we call the *active phase*, the steady state depends on whether the IC has little activity (homogeneous) or much activity (jammed). For smaller densities, all ICs evolve to an absorbing configuration; we call this the *absorbing phase*. The boundary between the active and absorbing phases, determined via the criterion of different steady states for homogeneous

(a)

(b)

FIG. 4. Steady-state flux versus density as in Fig. 3, but for $p = 0.5$.

and jammed ICs, is shown in Fig. 5. We note that in Wang's model [10] there are only two regions: an absorbing phase for $\rho \leqslant 1/7$ and an active one for $\rho > 1/7$.

Our results are consistent with the following scenario, familiar from the study of phase transitions to an absorbing state [19–21]: for finite systems, all ICs with $\rho < 1/(v_{\max} + 2)$ and $p > 0$ eventually fall into an absorbing configuration. Within the active phase, however, the mean lifetime of activity grows exponentially with system size. The phase boundary represents a line of critical points, on which the lifetime grows as a power law of system size. (Further details on critical behavior are discussed in Sec. IV.) A surprising feature of the phase boundary is that it is *reentrant*: for a given density in the range $0.116 < \rho < 1/(v_{\max} + 2)$, the absorbing phase is observed for both small and large p values, and the active phase for intermediate values. The reason for this is discussed in Sec. III C. We denote the upper and lower branches of the phase boundary by $p_+(\rho)$ and $p_-(\rho)$, respectively; they meet at $\rho_{c,<} \simeq 0.116$.
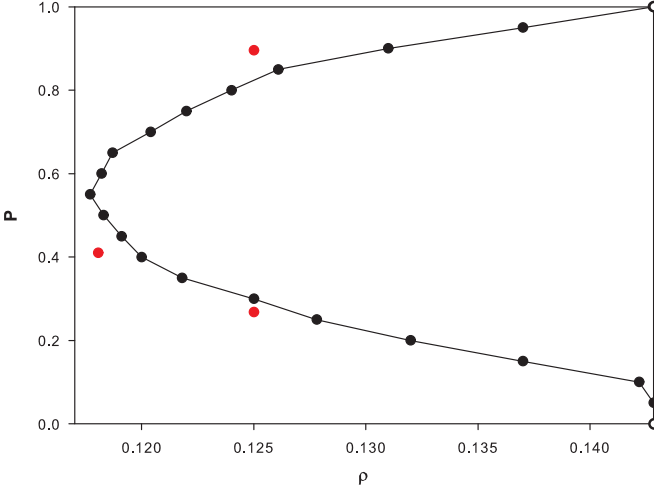
FIG. 5. Boundary between active and absorbing phases in the ρ-p plane. Black points joined by lines: preliminary estimates from initial-condition dependence as explained in text. Isolated red points: precise estimates obtained via finite-size scaling as described in Sec. IV. The open circle at $\rho = 1/7$, $p = 0$ is not part of the phase boundary: for $p = 0$ the transition occurs at $\rho = 1/6$. The open circle $\rho = 1/7$, $p = 1$ marks the other end of the phase boundary; we note however that at this point, all initial conditions evolve to the absorbing state.

The phase boundary is singular at its small-p limit. As p tends to zero from positive values, the critical density approaches $1/7$, but for $p = 0$ the transition occurs at $\rho = 1/6$. The phase diagram of the ANS model for $0 < p < 1$ is similar to that of a stochastic sandpile [22,23]. In the sandpile, there are no absorbing configurations for particle density $\rho > z_c - 1$, where z_c denotes the toppling threshold; nevertheless, the absorbing-state phase transition at a density strictly smaller than this value. Similarly, in the ANS model there are no absorbing configurations for $\rho > 1/7$, but the phase transition occurs at some smaller density, depending on the deceleration probability p. Further parallels between the ANS model and stochastic sandpiles are noted below.

The phase boundary shown in Fig. 5 represents a preliminary estimate, obtained using the following criterion. Points along the lower critical line $p_-(\rho)$ correspond to the smallest p value such that each of 200 arbitrary ICs remain active during a time of 10^7 steps, in a system of $L = 10^5$ sites. Similarly, $p_+(\rho)$ corresponds to the largest p value such that all 200 realizations remain active. For selected points, a precise determination was performed, as described in Sec. IV. We defer a more precise mapping of the overall phase diagram to future work.

The phase transitions at $p_-(\rho)$ and $p_+(\rho)$ appear to be continuous. Figure 6 shows the steady-state activity (defined below) versus p for density $\rho = 1/8$. In the vicinity of the transition, the curves become sharper with increasing system size, as expected at a continuous phase transition to an absorbing state.

B. Order parameter

Having identified a continuous absorbing-state phase transition in the ANS model, further analysis requires that we define an appropriate order parameter or activity density. Since the
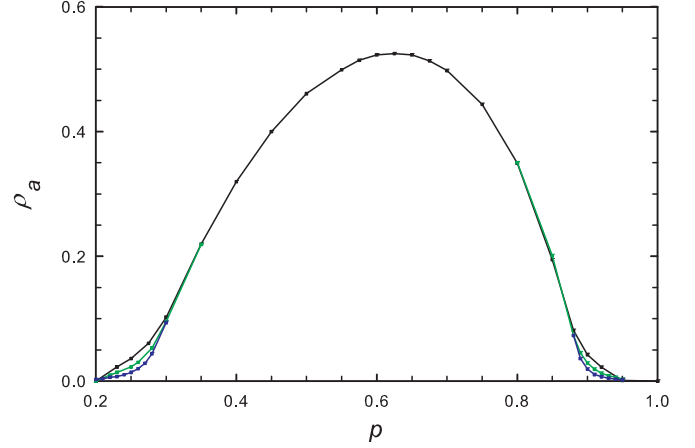

FIG. 6. Steady-state activity ρ_a versus p for vehicle density $\rho = 1/8$. System sizes (upper to lower curves) $N = 1000, 2000$, and 4000. Error bars smaller than symbols.

absorbing state is characterized by $v_i = v_{\max}, \forall i$, one might be inclined to define the activity density simply as $\rho_a = v_{\max} - \bar{v}$. The problem with this definition is that not all configurations with $v_i = v_{\max}, \forall i$ are absorbing: a vehicle with $d_i = v_{\max}$ may reduce its speed to $v_{\max} - 1$, yielding activity in the first sense. Since such a reduction occurs with probability p, it seems reasonable to define the activity density as

$$\rho_a = v_{\max} - \bar{v} + p\rho_{a,2} \equiv \rho_{a,1} + p\rho_{a,2}, \tag{1}$$

where $\rho_{a,2}$ denotes the fraction of vehicles with $v_i = d_i = v_{\max}$. According to this definition, the activity density is zero if and only if the configuration is absorbing, that is, if $v_i = v_{\max}$ and $d_i > v_{\max}$, $\forall i$. Studies of large systems near the critical point reveal that $\rho_{a,1} \gg \rho_{a,2}$, so that the latter can be neglected in scaling analyses. It is nonetheless essential to treat configurations with $\rho_{a,2} > 0$ as *active*, even if $\rho_{a,1} = 0$.

C. Reentrance

In this subsection we discuss the reason for reentrance, that is, why, for $\rho_{c,<} < \rho < \rho_c$, the system reaches the absorbing state for *large* p as well as small p. Since deceleration is associated with generation of activity (i.e., of speeds $< v_{\max}$), a reduction in activity as p tends to unity seems counterintuitive. The following intuitive argument helps to understand why this happens. For $p \simeq 0$, vehicles rarely decelerate if they have sufficient headway to avoid reaching the position of the car in front. This tends to increase the headway of the car behind, so that (for $\rho < \rho_c$), all headways attain values $\geqslant v_{\max} + 1$, which represents an absorbing configuration. For $p = 1$, a car with speed $v_i = d_i$ always decelerates, which tends to increase its own headway. In either case, $p = 0$ or $p = 1$, as reduced headway (i.e., inter-vehicle intervals with $d_i < v_{\max} + 1$) is transferred down the line, vehicles may be obliged to decelerate, until the reduced headway is transferred to an interval with headway d_i large enough that no reduction in velocity is required. [Intervals with $d_i > v_{\max} + 1$, which we call *troughs*, always exist for $\rho < \rho_c = 1/(v_{\max} + 2)$.] When all reduced headways are annihilated at troughs, the system attains an absorbing configuration.
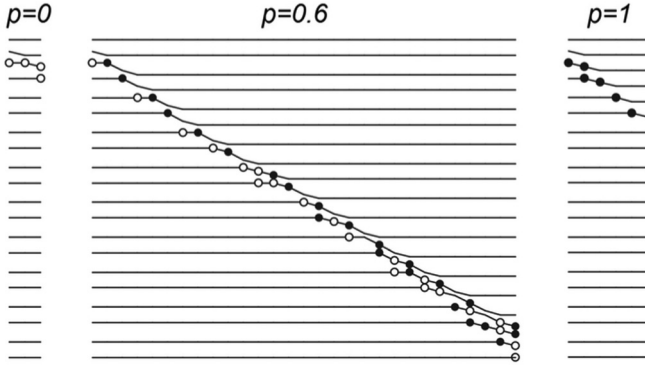
FIG. 7. Vehicle positions relative to the first (lowest) vehicle versus time t (horizontal) for $t \geqslant 2$, in a system with $N = 20$, $v_{\max} = 2$, and vehicle density $\rho = 2/9 < \rho_c = 0.25$. Initially, all vehicles have $v_i = v_{\max}$. The headways d_i initially alternate between three and four, except for $d_{19} = 0$ and $d_{20} = 7$. Filled (open) circles denote D (N) events, i.e., events in which a vehicle with speed $v(i) = d(i)$ decelerates (does not decelerate). In an absorbing configuration all velocities are equal, yielding a set of horizontal lines with spacings $\geqslant v_{\max} + 1$. Left panel: $p = 0$, system inactive for $t > 4$; right panel: $p = 1$, system inactive for $t > 7$; center panel: example of a realization with $p = 0.6$ in which activity persists until $t = 56$ (evolution for $t > 30$ not shown).

Call events in which a vehicle having $v_i = d_i$ decelerates D *events*, and those in which such a vehicle does not decelerate N *events*. For $\rho < \rho_c$, if only D events (or only N events) are allowed, the system attains an absorbing configuration via annihilation of reduced headways with troughs. Thus some alternation between D and N events is required to maintain activity, and the active phase corresponds to intermediate values of p.

These observations are illustrated in Fig. 7, for a system of twenty vehicles with $v_{\max} = 2$ and density $\rho = 2/9 < \rho_c = 0.25$. Initially, all vehicles have $v_i = v_{\max}$. The headways d_i initially alternate between three and four (the latter are troughs), except for $d_{19} = 0$ and $d_{20} = 7$. In the left panel, for $p = 0$, the system reaches an absorbing configuration after four time steps. Similarly, in the right panel, for $p = 1$, an absorbing configuration is reached after seven steps. For $p = 0.6$ (middle panel), the evolution is stochastic. Most realizations reach an absorbing configuration rapidly, but some remain active longer, as in the example shown here. From the distribution of D and N events, it appears that activity persists when vehicles first suffer an N event, reducing their own headway, and subsequently (one or two steps later) suffer a D event, reducing the headway of the preceding vehicle. Such an alternation of N and D events allows a region with reduced headways to generate more activity before reaching a trough [25].

IV. CRITICAL BEHAVIOR

We turn now to characterizing the phase transition along the lines $p_-(\rho)$ and $p_+(\rho)$. Since the transition is continuous, this requires that we determine the associated critical exponents, in order to identify the universality class of the ANS model. The analysis turns out to be complicated by strong finite-size effects: different from simple systems exhibiting an absorbing-state phase transition, such as the contact process, for which studies of systems with $L \leqslant 1000$ yield good estimates for critical exponents [19], here we require systems of up to 10^5 sites to obtain reliable results. We are nevertheless able to report precise results at several points along the phase boundary.

We use quasistationary (QS) simulations to probe the behavior at long times conditioned on survival of activity [24]. Since the deceleration probability p is continuous while the density ρ can only be varied in discrete steps, we keep the latter fixed and vary the former in each series of studies. As in other studies of QS behavior at absorbing-state phase transitions, we focus on the finite-size scaling (FSS) of the activity density, ρ_a, the lifetime, τ, and the moment ratio $m = \langle \rho_a^2 \rangle / \rho_a^2$, as functions of system size, N [19,24]. At a critical point, these variables are expected to exhibit scale-free (power-law) dependence on N, that is, $\rho_a \sim N^{-\beta/\nu_\perp}$ and $\tau \sim N^z$, where β is the order-parameter exponent and $\nu_\perp$ the exponent that governs the divergence of the correlation length as one approaches the critical point. In the active phase, ρ_a approaches a nonzero constant value, while τ grows exponentially as $N \to \infty$. In the absorbing phase, $\rho_a \sim 1/N$ while τ grows more slowly than a power law as $N \to \infty$. At the critical point, the moment ratio is expected to converge to a nontrivial limiting value, $m = m_\infty + \mathcal{O}(N^{-\lambda})$, with $\lambda > 0$. In the active (inactive) phase, m curves sharply downward (upward) when plotted versus $1/N$. These are the criteria we employ to determine the critical point, $p_c(\rho)$. The distance from the critical point can be estimated from the curvature of log-log plots of ρ_a and τ versus N.

As noted in Sec. III B, the order parameter is the sum of two contributions: $\rho_a = \rho_{a,1} + p\rho_{a,2}$. In simulations, we therefore determine $\rho_{a,1}$ and $\rho_{a,2}$ separately. In the vicinity of the critical point we find $\rho_{a,1} \sim N^{-0.5}$ and $\rho_{a,2} \sim N^{-0.9}$, showing that the fraction $\rho_{a,2}$ of vehicles with $v_i = d_i = v_{\max}$ decays more rapidly than $\rho_{a,1} = v_{\max} - \bar{v}$, so that it makes a negligible contribution to the activity density for large N. We therefore adopt $\rho_{a,1}$ as the order parameter for purposes of scaling analysis. Configurations $\rho_{a,1} = 0$ and $\rho_{a,2} > 0$ are nevertheless considered to be active; only configurations with $v_i = v_{\max}$ and $d_i > v_{\max}$, $\forall i$, are treated as absorbing.

We study rings of 1000, 2000, 5000, 10 000, 20 000, 50 000, and 100 000 sites, calculating averages over a set of 20 to 160 realizations. Even for the largest systems studied, the activity density reaches a stationary value within 10^6 time steps. We perform averages over the subsequent 10^8 steps. As detailed in Ref. [24], the QS simulation method probes the quasistationary probability distribution by restarting the evolution in a randomly chosen active configuration whenever the absorbing state is reached. A list of N_c such configurations, sampled from the evolution, is maintained; this list is renewed by exchanging one of the saved configurations with the current one at rate p_r. Here we use $N_c = 1000$, and $p_r = 20/N$. During the relaxation phase, we use a value of p_r that is ten times greater, to eliminate the vestiges of the initial configuration from the list. The lifetime τ is taken as the mean time between attempts to visit an absorbing configuration, in the QS regime.

Initial configurations are prepared by placing vehicles as uniformly as possible (for example, for density $\rho = 1/8$, we
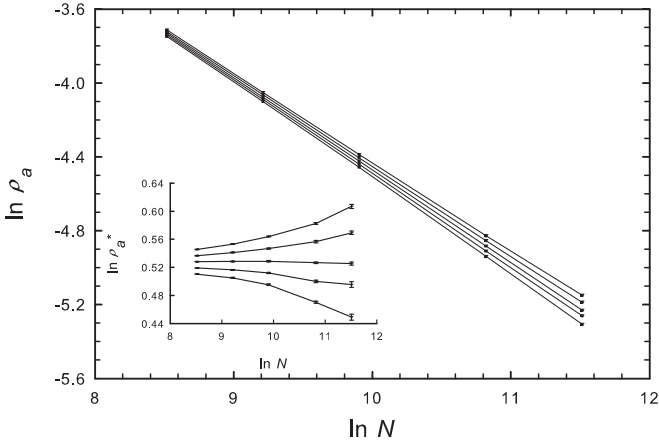
FIG. 8. Activity density versus number of vehicles for density $1/8$ and (lower to upper) $p = 0.2679, 0.2681, 0.2683, 0.2685$, and 0.2687. Error bars are smaller than symbols. Inset: scaled activity density $\rho_a^* = N^{0.5}\rho_a$ versus number of vehicles.
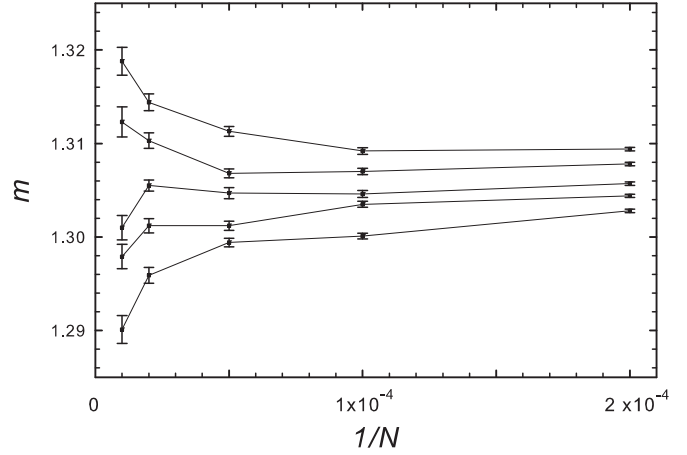

FIG. 10. Moment ratio m versus reciprocal system size for density $1/8$ and (upper to lower) $p = 0.2679, 0.2681, 0.2683, 0.2685$, and 0.2687.

set $d_i = 7$, $\forall i$), and then exchanging distances randomly. In such an exchange a site j is chosen at random and the changes $d_j \rightarrow d_j - 1$ and $d_{j+1} \rightarrow d_{j+1} + 1$ are performed, respecting the periodic boundary condition, $d_{N+1} \equiv d_1$. The random exchange is repeated N_e times (in practice we use $N_e = 2N$), avoiding, naturally, negative values of d_j. Since headways $d_j < v_m$ are generated in this process, at the first iteration of the dynamics, velocities $v_j < v_{\max}$ arise, leading to a relatively large, statistically uniform initial activity density.

We performed detailed studies for densities $\rho = 1/8$, on both the upper and lower critical lines, and for density $17/144 = 0.1180\bar{5}$, on the lower line. Figures 8–10 show, respectively, the dependence of the order parameter, lifetime and moment ratio m on system size for density $1/8$ and p values in the vicinity of the lower critical line. In the insets of Figs. 8 and 9 the values of ρ_a and τ are divided by the overall trend to yield $\rho_a^* \equiv N^{0.5}\rho_a$ and $\tau^* = \tau/N$. These plots make

evident subtle curvatures hidden in the main graphs, leading to the conclusion that $p_c(\rho = 1/8)$ is very near 0.2683.

A more systematic analysis involves the curvatures of these quantities: we fit quadratic polynomials,

$$\ln \rho_a = \text{const} + a \ln N + b(\ln N)^2, \qquad (2)$$

and similarly for $\ln \tau$, to the data for the four largest system sizes. The coefficient of the quadratic term, which should be zero at the critical point, is plotted versus p in Fig. 11. Linear interpolation to $b = 0$ yields the estimates $p_c = 0.26830(3)$ (data for activity density) and $p_c = 0.26829(2)$ (data for lifetime); we adopt $p_c = 0.26829(3)$ as our final estimate. (Figures in parentheses denote statistical uncertainties.) The data for m, although more scattered, are consistent with this estimate: from Fig. 10 it is evident that p_c lies between 0.2681 and 0.2683.
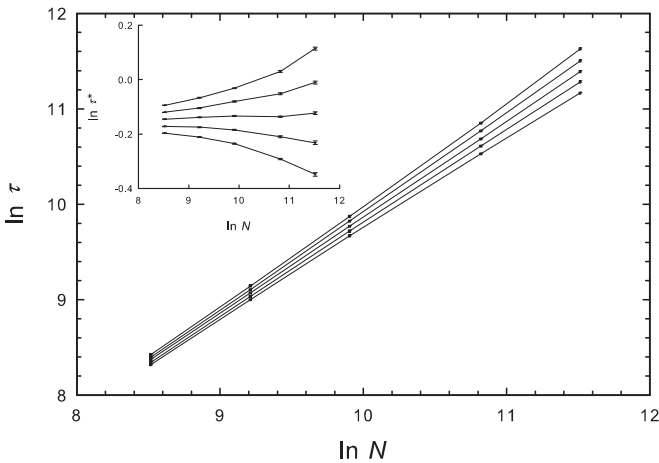

FIG. 9. Lifetime versus number of vehicles for density $1/8$ and (lower to upper) $p = 0.2679, 0.2681, 0.2683, 0.2685$, and 0.2687. Error bars are smaller than symbols. Inset: scaled lifetime $\tau^* = N^{-1.0}\tau$ versus number of vehicles.
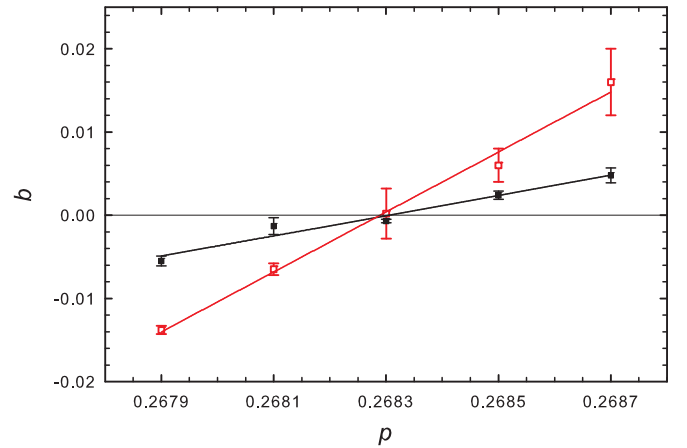

FIG. 11. Curvature of $\ln \rho_a$ (filled symbols) and $\ln \tau$ (open symbols) as functions of $\ln N$, as measured by the coefficient b of the quadratic term in least-squares quadratic fits to the data in Figs. 8 and 9. Straight lines are least-squares linear fits to b versus deceleration probability p, for vehicle density $\rho = 1/8$. Intercepts with the line $b = 0$ furnish estimates of p_c.
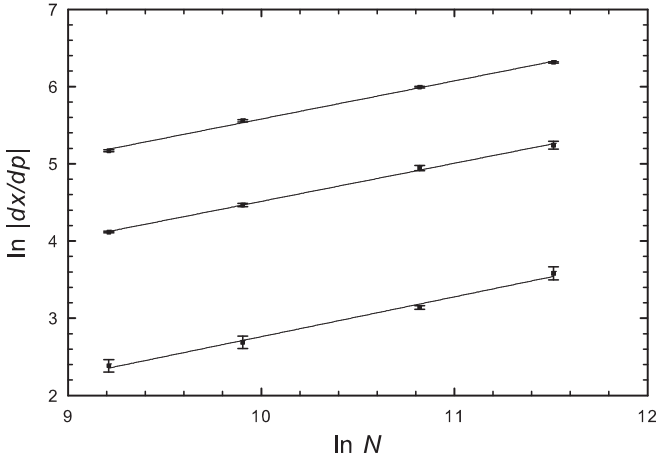
FIG. 12. Derivatives of (lower to upper) m, $\ln \rho_a$ and $\ln \tau$ with respect to p in the vicinity of p_c, versus N for vehicle density $\rho = 1/8$. Lines are least-squares linear fits to the data.

To estimate the critical exponents $\beta/\nu_\perp$ and z we perform linear fits to the data for $\ln \rho_a$ and $\ln \tau$ versus $\ln N$ (again restricted to the four largest N values), and consider the slopes as functions of p. Interpolation to p_c yields the estimates: $\beta/\nu_\perp = 0.500(3)$ and $z = 1.006(8)$. A similar analysis yields $m_c = 1.306(6)$. The principal source of uncertainty in these estimates is the uncertainty in p_c.

Using the data for ρ_a, τ, and m we also estimate the critical exponent $\nu_\perp$. Finite-size scaling implies that the derivatives $|dm/dp|$, $d \ln \tau/dp$, and $d \ln \rho_a/dp$, evaluated at the critical point, all grow $\propto L^{1/\nu_\perp}$. We estimate the derivatives via least-squares linear fits to the data on an interval that includes p_c. (The intervals are small enough that the graphs show no significant curvature.) Power-law dependence of the derivatives on system size is verified in Fig. 12. Linear fits to the data for the four largest sizes, for $\ln \rho_p$, $\ln \tau$, and m yield $1/\nu_\perp = 0.494(15)$, $0.495(15)$, and $0.516(29)$, respectively, leading to the estimate $\nu_\perp = 2.00(5)$. Repeating the above analysis for simulations at vehicle density $\rho = 17/144$, we find $p_-(17/144) = 0.4096(1)$, $\beta/\nu_\perp = 0.503(6)$, $z = 1.011(15)$, $m = 1.302(2)$, and $\nu_\perp = 2.02(2)$.

Thus, for the two points studied on the lower critical line, the results are consistent with a simple set of exponent values, namely, $z = 1$, $\nu_\perp = 2$, and $\beta = 1$. The same set of critical exponents appears in a system of activated random walkers (ARW) on a ring, when the walkers hop in one direction only [26]. The critical moment ratio for ARW is $m_c = 1.298(4)$, quite near present estimates. We suggest that these values characterize a universality class of absorbing-state phase transitions in systems with a conserved density (of

walkers in ARW, and of vehicles in the present instance), and anisotropic movement. The ARW with *symmetric* hopping is known to belong to the universality class of conserved directed percolation [27], which also includes conserved stochastic sandpiles [22,23].

A study on the upper critical line for vehicle density $\rho = 1/8$ yields results that are similar but slightly different. Repeating the procedure described above, we find $p_+(1/8) = 0.89590(5)$, $\beta/\nu_\perp = 0.487(8)$, $z = 1.021(15)$, $\nu_\perp = 1.98(6)$, and $m_c = 1.315(5)$. The exponent values are sufficiently near those obtained on the lower critical line that one might attribute the differences to finite-size effects. We defer to future work more detailed analyses, to determine whether scaling properties along the upper and lower critical lines differ in any respect.

V. SUMMARY

We consider a version of the Nagel-Schreckenberg model in which probabilistic deceleration is possible only for vehicles whose velocity is equal to the headway, $v_i = d_i$. In the resulting ANS model, a free-flow configuration, $v_i = v_{\max}$ and $d_i > v_{\max}$, $\forall i$, is *absorbing* for any value of the deceleration probability p. The phase transition in the original NS model at deceleration probability $p = 0$ is identified with the absorbing-state transition in the ANS model: the two models are identical for $p = 0$. In the original model, a nonzero deceleration probability corresponds to a spontaneous source of activity which eliminates the absorbing state, and along with it, the phase transition.

The ANS model, by contrast, exhibits a line of absorbing-state phase transitions in the ρ-p plane; the phase diagram is reentrant. We present preliminary estimates for the phase boundary and several critical exponents. The latter appear to be associated with a universality class of absorbing-state phase transitions in systems with a conserved density and asymmetric hopping, such as activated random walkers (ARWs) with particle transfer only in one direction [26]. In this context it is worth noting that in traffic models, as well as in sandpiles and ARW, activity is associated with a local excess of density: in sandpiles, activity requires sites with an above-threshold number of particles; in ARW, it requires an active particle jumping to a site occupied by an inactive one; and in the ANS model, it requires headways d smaller than $v_{\max} + 1$. One may hope that the connection with stochastic sandpiles will lead to a better understanding of traffic models, and perhaps of observed traffic patterns.

[1] K. Nagel and M. Schreckenberg, A cellular automaton model for freeway traffic, J. Phys. I (France) **2**, 2221 (1992).

[2] G. Csányi and J. Kertész, Scaling behavior in discrete traffic models, J. Phys. A **28**, L427 (1995).

[3] B. Eisenblätter, L. Santen, A. Schadschneider, and M. Schreckenberg, Jamming transition in a cellular automaton model for traffic flow, Phys. Rev. E **57**, 1309 (1998).

[4] M. Gerwinski and J. Krug, Analytic approach to the critical density in cellular automata for traffic flow, Phys. Rev. E **60**, 188 (1999).

[5] A. M. C. Souza and L. C. Q. Vilar, Traffic-flow cellular automaton: Order parameter and its conjugated field, Phys. Rev. E **80**, 021105 (2009).

[6] L. Roters, S. Lübeck, and K. D. Usadel, Critical behavior of a traffic flow model, Phys. Rev. E **59**, 2672 (1999).

[7] D. Chowdhury, J. Kertész, K. Nagel, L. Santen, and A. Schadschneider, Comment on "Critical behavior of a traffic flow model," Phys. Rev. E **61**, 3270 (2000).

[8] L. Roters, S. Lübeck, and K. D. Usadel, Reply to "Comment on 'Critical behavior of a traffic flow model,' " Phys. Rev. E **61**, 3272 (2000).

[9] K. Nagel and M. Paczuski, Emergent traffic jams, Phys. Rev. E **51**, 2909 (1995).

[10] L. Wang, B. H. Wang, and B. Hu, Cellular automaton traffic flow model between the Fukui-Ishibashi and Nagel-Schreckenber models, Phys. Rev. E **63**, 056117 (2001).

[11] S. Krauss, P. Wagner, and C. Gawron, Continuous limit of the Nagel-Schreckenberg model, Phys. Rev. E **54**, 3707 (1996).

[12] M. Takayasu and H. Takayasu, 1/f noise in a traffic model, Fractals **01**, 860 (1993).

[13] S. C. Benjamin and N. F. Johnson, Cellular automata models of traffic flow along a highway containing a junction, J. Phys. A **29**, 3119 (1996).

[14] R. Barlovic, L. Santen, A. Schadschneider, and M. Schreckenberg, Metastable states in cellular automata for traffic flow, Eur. Phys. J. B **5**, 793 (1998).

[15] S. Krauss, P. Wagner, and C. Gawron, Metastable states in a microscopic model of traffic flow, Phys. Rev. E **55**, 5597 (1997).

[16] X. Li, Q. Wu, and R. Jiang, Cellular automaton model considering the velocity effect of a car on the sucessive car, Phys. Rev. E **64**, 066128 (2001).

[17] A. Schadschneider, D. Chowdhury, and K. Nishinari, *Stochastic Transport in Complex Systems from Molecules to Vehicles* (Elsevier, Oxford, 2011).

[18] A. Schadschneider, The Nagel-Schreckenberg model revisited, Eur. Phys. J. B **10**, 573 (1999).

[19] J. Marro and R. Dickman, *Nonequilibrium Phase Transitions in Lattice Models* (Cambridge University Press, Cambridge, 1999).

[20] G. Ódor, *Universality in Nonequilibrium Lattice Systems: Theoretical Foundations* (World Scientific, Singapore, 2007).

[21] M. Henkel, H. Hinrichsen, and S. Lubeck, *Non-Equilibrium Phase Transitions Volume I: Absorbing Phase Transitions* (Springer-Verlag, The Netherlands, 2008).

[22] M. A. Muñoz, R. Dickman, R. Pastor-Satorras, A. Vespignani, and S. Zapperi, in Sandpiles and absorbing-state phase transitions: Recent results and open problems, in *Modeling Complex Systems*, Proceedings of the 6th Granada Seminar on Computational Physics, edited by J. Marro and P. L. Garrido, AIP Conf. Proc. No. 574 (AIP, New York, 2001), p. 102.

[23] G. Pruessner, *Self-Organised Criticality* (Cambridge University Press, Cambridge, 2012).

[24] M. M. de Oliveira and R. Dickman, How to simulate the quasistationary state, Phys. Rev. E **71**, 016129 (2005).

[25] J. M. Carlson, J. T. Chayes, E. R. Grannan, and G. H. Swindle, Self-organized criticality in sandpiles: Nature of the critical phenomenon, Phys. Rev. A **42**, 2467(R) (1990).

[26] R. Dickman, L. T. Rolla, and V. Sidoravicius, Activated random walkers: Facts, conjectures and challenges, J. Stat. Phys. **138**, 126 (2010).

[27] J. C. Mansur Filho and R. Dickman, Conserved directed percolation: exact quasistationary distribution of small systems and Monte Carlo simulations, J. Stat. Mech. (2011) P05029.